UNIVERSITÀ DEGLI STUDI DI TRIESTE

XXXI CICLO DEL DOTTORATO DI RICERCA IN BIOMEDICINA MOLECOLARE

Functional characterization of the biofilm exopolysaccharide produced by *Burkholderia multivorans* C1576

Settore scientifico-disciplinare: **BIO/10**

DOTTORANDO
MARCO DISTEFANO

COORDINATORE
PROF. GERMANA MERONI

SUPERVISORE
DR. PAOLA CESCUTTI

CO-TUTOR
PROF. DANIELE SBLATTERO

ANNO ACCADEMICO 2017/2018

UNIVERSITÀ DEGLI STUDI DI TRIESTE

XXXI CICLO DEL DOTTORATO DI RICERCA IN BIOMEDICINA MOLECOLARE

Functional characterization of the biofilm exopolysaccharide produced by *Burkholderia multivorans* C1576

Settore scientifico-disciplinare: **BIO/10**

DOTTORANDO
MARCO DISTEFANO

COORDINATORE
PROF. GERMANA MERONI

SUPERVISORE
DR. PAOLA CESCUTTI

CO-TUTOR
PROF. DANIELE SBLATTERO

ANNO ACCADEMICO 2017/2018

Abstract

Biofilms are polymicrobial aggregates in which bacterial cells are embedded in a self-produced matrix consisting of highly hydrated biopolymers referred to as extracellular polymeric substances (EPS). EPS are mainly polysaccharides, proteins, nucleic acids and lipids which form the 3D scaffold of the biofilm matrix. Among EPS, exopolysaccharides (Epols) are generally the most abundant component. Bacterial biofilms are widely exploited in industry and environmental biotechnology. However, they also represent a serious health concern as they are found associated with chronic infections which are difficult to eradicate due to biofilms enhanced tolerance and resistance to antimicrobial agents. Epols are recognized to confer mechanical stability to biofilms, but they also protect bacterial cells toward antibiotics and the host immune system, thus allowing infections to persist. The aim of this research project was to elucidate the structural and functional role played by the exopolysaccharide known as EpolC1576 in the biofilm matrix of *B. multivorans* C1576 which is a Gram-negative opportunistic pathogen that causes severe lung infections in cystic fibrosis (CF) patients. EpolC1576 consists of the following tetrasaccharide repeating unit which is made up of mannose and rhamnose, both present in equimolar amount:

$$[2)\text{-}\alpha\text{-D-Man}p\text{-}(1\rightarrow 2)\text{-}\alpha\text{-D-Rha}p\text{-}(1\rightarrow 3)\text{-}\alpha\text{-D-Rha}p\text{-}(1\rightarrow 3)\text{-}\alpha\text{-D-Man}p\text{-}(1\rightarrow]_n$$
$$\begin{array}{c} 3 \\ | \\ OCH_3\ (50\%) \end{array}$$

The presence of clusters of rhamnose, a 6-deoxy sugar with nonpolar features, together with the presence of a methoxy substituent (-OCH_3) on carbon 3 of 50% of the 2-linked rhamnose, confer to EpolC1576 an amphiphilic character that is “uncommon” among polysaccharides. The presence of less polar domains along its chain might be crucial for biofilm maintenance and stabilization, but also might enable EpolC1576 to interact with hydrophobic biologically active compounds, thus favoring their trafficking through the biofilm matrix. The first part of the research project investigated the ability of EpolC1576 to interact with smallnonpolar compounds such as the aromatic fluorescent probes ANS and TNS. Fluorescence spectroscopy data showed that the two aromatic probes interact significantly with EpolC1576, whereas no interaction was detected with the polysaccharide dextran which is a glucan polymer lacking methyl groups on its chain. The presence of relevant interaction between EpolC1576 and both ANS and TNS was confirmed by nuclear magnetic resonance (NMR) spectroscopy analyses. These results led to investigate the possible interaction of EpolC1576 with the nonpolar

quorum sensing molecule cis-11-methyl-2-dodecenoic acid (11-Me-C12:Δ^2) of *B. multivorans* by means of NMR. Spectroscopic data showed that EpolC1576 increases the solubility of the nonpolar signaling molecule in aqueous solution, thus suggesting that the polymer may favor the diffusion of the signaling molecule through the highly hydrated environment of the matrix. To characterize in more detail the hydrodynamics of EpolC1576 in aqueous solution and the mechanisms by which the polymer interacts with hydrophobic molecules, molecular modeling simulations of the EpolC1576 (tetramer) in the presence of nonpolar guest molecules (hexane and 11-Me-C12:Δ^2) were carried out. It was found that in aqueous environment EpolC1576 displays a high flexibility that allows the carbohydrate chain to dynamically bend and straighten. Simulations with both hexane and the signaling molecule 11-Me-C12:Δ^2 showed that EpolC1576 has frequent dynamic interactions with both nonpolar molecules that can also be encapsulated in transient hydrophobic pockets that form along the polymer chain. With the aim of mapping the binding site (epitope) of both ANS and TNS to EpolC1576, saturation transfer difference NMR (STD NMR) experiments were carried out. This technique revealed those aromatic regions/atoms on both fluorescent probes mainly involved in the binding event to EpolC1576. STD NMR was also chosen to investigate a possible interaction between EpolC1576 and the aminoglycoside antibiotic Kanamycin. Interestingly, STD NMR data showed that EpolC1576-Kanamycin interaction occurs, with distinct atoms on the pyranose rings of the antibiotic more involved than others in the binding event. A further confirmation of EpolC1576 ability to bind hydrophobic molecules came from a surface plasmon resonance (SPR) investigation in which increasing concentrations of the polymer were observed to bind with a good affinity to aliphatic chain immobilized on a gold surface. To help in understating how EpolC1576 chains may organize to set up the 3D carbohydrate scaffold of the biofilm matrix, atomic force microscopy (AFM) imaging of the polymer was performed. EpolC1576 molecules were observed as spherical objects that organize themselves in single units or in densely-packed aggregates at low and high concentrations, respectively.

During the second part of the research project, efforts were made to characterize the macromolecules that build up the biofilm matrix of *B. multivorans* C1576. It was found that in biofilm-forming conditions, *B. multivorans* C1576 produces only EpolC1576 as exopolysaccharide once seeded on cellulose membranes deposited on the synthetic cystic fibrosis (SCFM) and on Muller Hinton (MH) media. The morphological aspect and macromolecular composition of *B. multivorans* C1576 biofilms developed in three different media were investigated by means of confocal laser scanning microscopy (CLSM) imaging.

CLSM data revealed that media composition influences both the biofilm structure and the relative abundance of the macromolecules that made up the biofilm matrix. To further characterize its composition, the biofilm matrix was ultra-centrifuged to pellet potential outer membrane vesicles (OMVs), spherical bilayered structures that gemmate from the outer membrane of various Gram-negative bacterial species. Transmission electron microscopy (TEM) imaging of the pellet produced after biofilm matrix ultracentrifugation of *B. multivorans* C1576 revealed the presence of OMVs. The identity of proteins associated with OMVs and the biofilm matrix was later revealed by means of mass spectrometry. As observed for other bacterial species forming biofilms, the matrix was found to be particularly enriched in intracellular proteins involved in metabolic pathways, translation and protein folding. About 10% of the matrix-associated proteins are in common with OMVs whose protein content is mainly represented by outer membrane proteins. Various enzymes involved in detoxification of reactive oxygen species (ROS) were found in both the matrix and OMVs, thus suggesting a possible role for these proteins in protecting bacteria from ROS produced by cells of the immune system. Other identified proteins may behave as virulence factors. With the aim of identifying proteins of *B. multivorans* C1576 able to interact with EpolC1576, a phage library of all genomic DNA sequences (gDNAs) of *B. multivorans* C1576 was built-up. The library consists of phage particles that display on their surface a copy of each protein of *B. multivorans* C1576. The phage library was incubated in the presence of EpolC1576 immobilized on a solid support. The immobilization of EpolC1576 was accomplished after an optimization process in which fragments of EpolC1576 were covalently coupled to BSA, a protein well-known to absorb on plastic surfaces. After three rounds of selections to enrich the library for phages that had high affinity for EpolC1576, selected phage particles were subjected to ELISA assays to test individually their binding affinity for EpolC1576 fragments immobilized on the surface of microplates as carbohydrate-BSA conjugate. It was observed that the selected phages bound to EpolC1576 fragments coupled to BSA with an affinity comparable or an even lower if compared to that showed toward BSA alone, thus suggesting the library was enriched for phages displaying cross-reactivity to BSA. Unfortunately, time constraints did not allow a second trial of the phage library; future plans are to screen the phage library against EpolC1576 fragments coupled directly to the plastic surface, in order to avoid the non-specific interference of BSA.

Table of contents

1 INTRODUCTION

1.1 Bacterial Biofilms

1.1.1 The biofilm lifestyle

Nowadays there is a growing awareness that bacterial cells do not predominantly live a solitary existence [1]. They rather organize themselves in densely populated microbial communities called biofilms in which cell-to-cell communication is a common phenomenon [2]. Biofilms consist of aggregates of microbial cells encased in a self-produced matrix made up of highly hydrated extracellular polymeric substances (EPS) [3]. EPS are generally represented by polysaccharides, proteins, lipids and extracellular DNA (eDNA) [4]. They can virtually form and develop on whatever biotic and abiotic surface [1]. Biofilm cells show remarkable spatial organization, coordinated activities and integrated metabolism [1]. This sessile lifestyle allows for social and physical interactions that are not conceivable for free-living planktonic bacteria [1]. Cooperation within biofilms increases microbial cells fitness and improves biofilm performances [5]. However, biofilm formation is not crucial for bacterial cell survival; it is rather a way of life that increases cells chances of survival, metabolism and reproductive success despite fluctuating and/or extreme environmental conditions [5]. Biofilms provide microorganisms a highly stable microenvironment that resists to external insults and quickly adapts to new environmental conditions [5]. They are practically present in every habitat on Earth [5]. They have been found in deep-sea hydrothermal vents where bacterial cells thrive in sharp gradients of temperature, pressure, pH and metals. Biofilms cells can also adapt to the high levels of salinity characterizing hypersaline lakes [5] and flourish in environments with extremely acidic conditions and nutrients scarcity. Biofilms actively participate in biogeochemical cycles of most elements in sediment, aqueous and soil environments [6] as well as in underground stores of fresh water [7]. They are exploited in many biotechnological applications such as drinking water production, wastewater and solid waste treatment, but also as catalysts in various industrial procedures such as manufacturing of fine chemicals, bulk and fuels from organic materials [8]. However, biofilms can represent a threat for plants, animals and humans since they are able to efficiently colonize biotic surfaces [9], an event that can lead to the establishment of chronic infections [10]. Biofilms are also responsible for colonization of prostheses and medical devices [11], biological fouling, contamination of

water used in industrial processes and facilities [12], reducing the hygienic quality of potable water [13] and promoting bio-corrosion [14]. Biofilms usually host various bacterial species and are densely populated communities: about one gram of wet weight can count up to one hundred billion of microbial cells [15,16]. The different physiological activities performed by biofilm cells contribute to producing sharp gradients of oxidizing and reducing agents, but also of pH, signaling molecules and metabolism by-products [3]. A high degree of phenotypic heterogeneity can characterize even biofilms containing a single species: oscillation of gene expression with time and between different cells may produce many phenotypical variants among the same species [3]. Formation of mature biofilms usually requires various stages (Fig. 1).

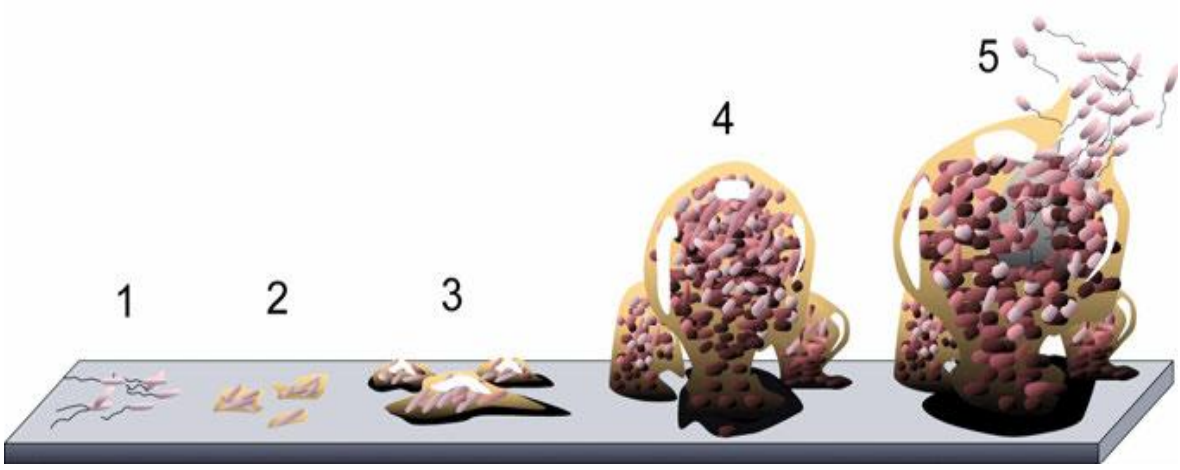

Figure 1. Stages of biofilm formation. Biofilm formation begins with adhesion of free-living bacteria to biotic or inanimate surfaces (1). Bacterial cells divide to produce micro-colonies, but also synthesize and secrete extracellular polymeric substances making the attachment irreversible (2). Cell division and EPS production lead to the formation of a multi-layered microbial community (3). The biofilm development continues with the formation of complex 3D-structures (4). Eventually, biofilm maturation can be followed by bacterial cells dispersal (5). Figure adapted from D. Monroe [17] under the creative commons license. Image credit: D. Davis.

1.1.2 The biofilm matrix

Biofilm cells surround themselves with a matrix consisting of hydrated biopolymers known as extracellular polymeric substances (EPS) [18]. EPS are polysaccharides, proteins, lipids and extracellular DNA molecules mainly and actively produced by microbial cells [18]. Generally, about nine tenths of a biofilm dry mass is represented by EPS while the rest consists of microbial cells [18]. Biofilm cells are usually organized in clusters whose spatial architecture depends on EPS production, which is mostly responsible for the continuous remodeling of the biofilm structure [19]. The biofilm

matrix acts as a physical interface connecting the biofilm to the surrounding environment and determining biofilm internal activities and exchanges with the environment [18]. In biofilms, polymers in the EPS interact with each other, thus fostering the formation of a three-dimensional structure that is crucial for biofilm adhesion to surfaces and stabilization [18]. EPS provide biofilm cells with a broad range of beneficial properties almost exclusive of this sessile lifestyle [18]. They transiently prevent biofilms cells from diffusing away, thus promoting a physical closeness that is fundamental for social interactions [18]. Furthermore, through voids and tunnels in the biofilm matrix or directly from surfaces on which biofilms develop, nutrients dissolved in the aqueous phase can easily reach microbial cells [3]. Biofilm cells exhibit greatly enhanced ability to capture nutrients compared to planktonic cells [3]. Owing to EPS, the matrix acts as a passively absorbing sponge which is then globally involved in exchanging any sort of compounds between biofilms and the external environment [20]. Biofilms have different ways of resource capture with binding sites localized in the matrix, but also in both the cytosol and the wall of microbial cells [3]. Binding sites can be either positively or negatively charged molecules that enable biofilm cells to sequester and amass highly diverse compounds, potentially exploitable as carbon and energy source [21], no matter how concentrated they are. In this way, the matrix allows biofilm communities to thrive in environments with scarcity of nutrients [22]. The ability of biofilms to capture molecules is not substance-specific, thus implying that also potentially harmful compounds can be trapped and accumulated [3]. In fact, although being a highly hydrophilic environment, the matrix can also trap very hydrophobic molecules such as benzene, toluene and xylene [23]. The biofilm matrix with its high proportion of hydrated EPS molecules make microbial cells tolerant to water shortage [3]. Some bacterial species react to water stress by actively synthesizing EPS with high water-retention capabilities, thus allowing the biofilm matrix to behave like an aqueous gel-like structure [24]. Beside protecting microbial cells from desiccation, the biofilm matrix also enhances tolerance and resistance of microorganisms towards antimicrobial compounds and host immune defenses [3]. Some information on matrix components occurring in the biofilm matrix is hereafter given, while more detailed information on matrix polysaccharides is reported in paragraph 1.1.3.

Proteins. Structural proteins of the biofilm matrix, both extracellular carbohydrate-binding proteins (lectins) and those anchored to the microbial cell surface, support the

formation of the carbohydrates scaffold of the matrix reinforcing its architecture and act as a bridge between EPS and the cellular surface [18]. For example, LecA and LecB lectins of *Pseudomonas aeruginosa*, exhibiting specificity for galactose and fucose residues respectively, are necessary matrix components for biofilm formation [25], [26]. In *Staphylococcus aureus*, the biofilm matrix protein Bap stimulates biofilm formation and allows the Gram-positive bacterium to adhere to and cluster on various types of epithelia [27,28]. Bacterial surface appendages such as flagella, fimbriae and pili also give structure to the biofilm matrix through their interactions with other EPS matrix components [18]. Type IV pili expressed on the surface of *P. aeruginosa* was found to strongly interact with DNA, thus foreseeing an important role in biofilm formation [29]. *Escherichia coli* and *Salmonella* Typhimurim produce a stiff and strongly hydrophobic extracellular mesh upon co-synthesizing thin aggregative fimbriae and cellulose, while the absence of one of these two components results in highly weakened extracellular matrix [30], highlighting the role of this type of appendages for matrix mechanical stability. Thanks to the presence of extracellular enzymatic proteins, the biofilm matrix also acts similarly to a digestive system that decomposes EPS into monomers readily to be internalized by biofilm cells and exploited as carbon and energy reservoirs [18]. Extracellular enzymes also break down EPS having structural roles, allowing bacterial cells to leave the biofilm community [18] and disperse to form new microbial communities [31,32]. Some enzymes act as virulence factors that take active part during infectious diseases [18]. Finally, extracellular enzymes are trapped by biofilm matrix polysaccharides that prevent them from diffusing away [33] and improve their stability against high temperatures and proteolytic cleavages [34].

Extracellular DNA (eDNA). eDNA was shown to be a common constituent of biofilms matrix in which it can represent a crucial structural element [18]. eDNA molecules are released after microbial cell lysis, but they can also be actively secreted [35]. In *P. aeruginosa,* eDNA serves as intercellular connector and is necessary for biofilm formation since DNase treatment prevents bacterial cells from organizing into biofilm communities [36,37]. eDNA of *S. aureus* binds positively charged moonlighting proteins associated with the bacterial cell surface, thus sticking bacteria to each other [38] and assists the assembly of small matrix peptides, known as phenol soluble modulins (PSMs), into amyloid fibrils that promote biofilm stabilization [39]. Interestingly,

Bacillus cereus attachment to surfaces, prelude to biofilm formation, is mediated by eDNA [40].

Lipids. Even though the biofilm matrix is a highly hydrated environment, in the EPS hydrophobic constituents are also present [18], and lipids have been recovered from the biofilm matrix of various microorganisms [41]. For example, *Thiobacillus ferroxidans* adheres to the mineral pyrite via lipopolysaccharides [42], while *Serratia marcescens* secretes lipids, named "serrawettins", able to lower the surface tension in aqueous systems (biosurfactants) [43]. Another biosurfactant with surface-active properties, known as viscosin, is partly responsible for biofilm dispersal of *Pseudomonas fluorescence* [44]. Viscosin can also emulsify nonpolar compounds, thus enhancing their bioavailability [18]. Other than biofilm spreading, biosurfactants produced by *P. aeruginosa* promote bacterial migration along surfaces, initial microcolony establishment, development of multicellular mushroom-like structures and maintenance of water channels among mushroom-like structures [45].

Outer membrane vesicles. Besides secreted and surface-attached biopolymers, the biofilm matrix of many Gram-negative bacteria can also contain the so-called Outer Membrane Vesicles (OMVs) [46]. They are small (20-500 nm diameter), spherical, vesicular structures gemmating from the outer membrane of both pathogenic and non-pathogenic Gram negative bacterial species [47]. OMVs usually are made of lipopolysaccharides (LPS), phospholipids, outer membrane proteins (OMPs), proteins of cytoplasmic and periplasmic origin, nucleic acids, ions and signaling compounds. OMVs characterize different physiological and pathological properties of bacteria, but they generally increase bacterial nutrients uptake, cells ability to cope with stresses and overcome the host immune system thanks to their cargo of adhesins, toxins and other virulence factors [46].

1.1.3 Biofilm exopolysaccharides

Bacteria produce extracellular polysaccharides which fall into two distinct categories: capsular polysaccharides (CPSs) and exopolysaccharides (Epols) [48]. CPSs are tightly linked to the bacterial cell surface creating a capsule, while Epols are actively secreted by bacteria in their surroundings, frequently making up a slime [49]. Epols are thought to perform many biological functions, but most of them remain elusive [49]. Among EPS molecules, Epols are the predominant component of biofilms matrix [50]. They are

usually high molecular mass polymers, linear or branched, whose molecular weight ranges from half million Daltons to few millions Daltons [18]. Some of them consist of a monosaccharide unit repeated many times (homopolysaccharides): examples are Epols containing glucose or fructose residues produced by streptococci in oral biofilms, but also cellulose synthesized by species that belong to the Enterobacteriaceae [30] and Pseudomonadaceae families [50]. However, the majority of Epols are heteropolymers as the repeating unit is composed of different monosaccharides, which can be neutral or charged [18]. Physical and biological features of Epols are also dictated by the presence of inorganic and/or organic functionalities [18]. Several Epols are polyanionic as they consist of uronic acids, and less frequently they can carry pyruvate or sulfate substituents [18]. The most-studied negatively charged Epols are alginate, colanic acid and xanthan [18]. However, positively charged Epols are not unusual [18]. The polycationic intercellular adhesin (PIA), which is a partly deacetylated polymer of β-1,6-linked N-acetylglucosamine [18], was first found in biofilms of *S. aureus* and *S. epidermis*, and later in other bacterial species [30]. Bacterial strains of the same species can produce different Epols [18]. *P. aeruginosa*, which represents a model microorganism for biofilm studies, synthesizes no fewer than three different exopolysaccharides (alginate, Psl and Pel) that are involved in biofilm formation and structure [51]. Alginate is a high-molecular mass linear heteropolymer made up of 1-4-linked residues of β-D-mannuronate and L-D-guluronate [18]. Alginate participates in micro-colonies formation, laying the foundations for biofilm development, but also stabilizes the structure of later stages biofilms [18]. Psl contains D-mannose, D-glucose and L-rhamnose assembled in pentasaccharide repeating units [52], while Pel is a polycationic heteropolysaccaride of 1-4-linked residues of N-acetylgalactosamine and N-acetylglucosamine [53]. Unlike alginate, Pel and Psl are responsible for biofilm formation in non-mucoid wild type strains [18]. For several bacterial species, biofilm production is closely linked to presence of Epols since mutants unable to synthesize Epols cannot adopt the biofilm lifestyle at all or form mature biofilms [31] Epols confer many benefits to biofilm cells such as adhesion, shelter and structure [54]. Epols make it easier for biofilm cells to colonize either biotic or abiotic surfaces, thus preventing bacteria from being removed by physical stresses, for example those exerted by flowing fluids [54]. Epols act as a shield against external insults such as desiccation (high level of hydration due to hydroxyl groups), immune cells, and attacks perpetrated by

phagocytes and amoebae [54]. Even though biofilms matrix is not an insurmountable barrier to cross for antimicrobials, Epols might slow their diffusion allowing either bacterial cells to express genes involved in tolerance mechanisms [55] or stabilize extracellular enzymes that inactivate antimicrobials before reaching cell targets [56]. Epols also impart structure to microbial communities providing biofilms with stratification and promoting the formation of gradients of nutrients and by-products [54]. In this light, Epols participate in the development of heterogeneous populations, thus enabling biofilm communities to resist to external insults caused by sudden environmental changes that bacteria usually experience [54].

1.1.4 Social interactions within biofilms

The peculiar structure of biofilms, which relies on the EPS matrix production, allows bacterial cells to be very close to each other, thus promoting intimate physical and social contacts [3]. The biofilm lifestyle makes possible a type of cell-cell communication referred to as Quorum Sensing (QS) [1]. It was described for the first time in the bioluminescent marine bacterial species *Vibrio fischeri* [57]. In this process, biofilm cells continuously synthesize, release and detect extracellular signaling molecules (autoinducers) which are informative about cell density [1]. Once autoinducers concentration goes beyond a certain threshold, biofilm cells start regulating the expression of specific sets of genes [58]. In this light, QS allows high cell densities bacterial communities to benefit from various collective behaviors such as biofilm synthesis, production of virulence factors, lytic enzymes and siderophores, which would be rather expensive and ineffective for single cells or at low cell densities [59]. Other phenomena under QS control are sporulation, production of bacteriocins, bioluminescence and the ability to take up high molecular mass eDNA (genetic competence) [60]. Communication within biofilms usually occurs among cells of the same species, but it can also involve cells of different species and result in either competitive or cooperative behaviors [61]. The restricted environment characterizing biofilms allows signaling molecules to concentrate which may partly explain the efficiency of cell-cell communication in biofilms with respect to planktonic free-living cells [3]. The ability of bacterial cells to perceive sufficiently high concentrations of signaling molecules depends on different parameters and features, some of which are inherent to biofilms: high cell density that assures high levels of autoinducers,

physicochemical properties of the matrix which affect the rate of diffusion and flow velocity, opportunities for bacteria to cluster thereby reducing the gap for signaling molecules to fill [62]. Biofilm cells speak different chemical languages depending on the type of signaling molecule produced: Gram-negative bacteria generally communicate by the employment of acyl-homoserine lactones (AHLs), whereas social interactions among Gram-positive bacteria mainly rely on short peptides (Fig. 2) [1]. It has also been demonstrated that some Gram-negative species make use of unsaturated fatty acids as signaling molecules [63]. Gram-positive bacteria generally synthesize signaling peptides that are cleaved or chemically modified in their active form (autoinducing peptides or AIP) which are then transferred outside cells via dedicated membrane transport proteins [1]. Signaling peptides are usually perceived by membrane bound sensor kinases that pass the information to transcription factors in the cytoplasm, thus causing gene expression modifications [64]. Otherwise, peptides can cross bacterial membranes through transporter systems and reach the cytoplasm where they bind cognate receptors, thus altering the expression of specific genes [65]. Unlike signaling peptides, AHLs freely cross Gram-negative bacterial membranes [64]. The cytosolic enzyme LuxI-type synthase uses S-adenosylmethionine (SAM) to produce AHLs that successively bind to receptors (LuxR-like receptor) either located in the inner membrane or in the cytoplasm [64]. This event leads to DNA transcription changes that can involve up to hundreds of genes controlling different biological phenomena [64].

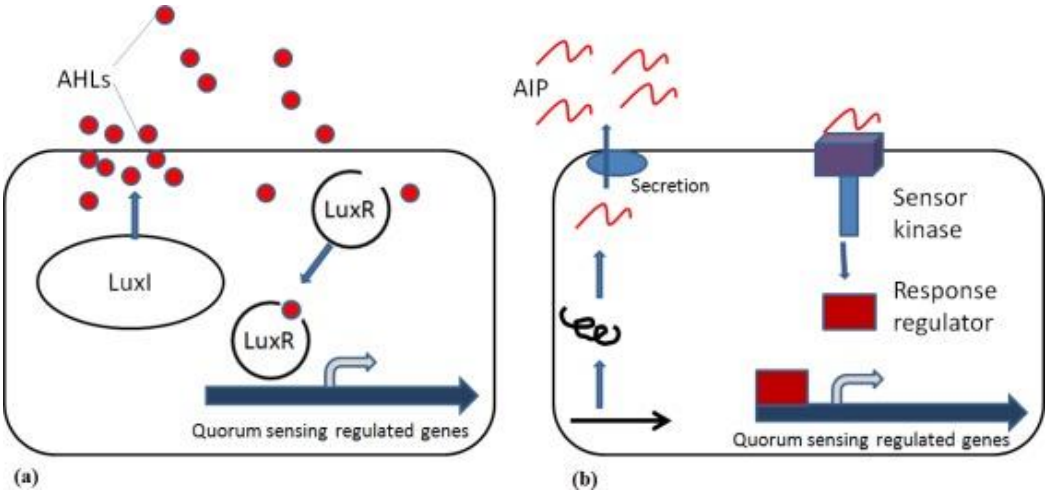

Figure 2. Schematic representation of how bacterial quorum sensing systems work. (**a**) Gram-negative bacteria: once AHLs (red circles) are synthesized by the LuxI-type synthase they bind to the cognate LuxR receptor. The AHL-LuxR complex recognizes DNA elements in the promoter region of specific genes whose expression is then regulated (**b**) Gram-positive bacteria produce AIP (curvy lines) that undergo post-translational modification before being secreted. Upon detection of AIP by a specific two-component signal transduction system, a response regulator protein becomes phosphorylated and then able to bind to DNA promoter sequences, thus modifying the expression of QS-regulated genes. Figure adapted from Wai-Fong Y. [66] under creative commons attribution license.

Since biofilm communities often enclose different bacterial species, it is not surprising that a universal chemical language for inter-species communication has been discovered [67]. This cross-species QS system is based on a signaling molecule known as autoinducer-2 (AI-2) and it has been found in both Gram-positive and Gram-negative bacteria [67].

1.1.5 Biofilms as virulence factor

Biofilms and establishment of chronic infections are usually strictly linked [68]. Owing to the presence of the matrix, biofilm cells are much more resistant and/or tolerant to antimicrobial compounds with respect to planktonic bacteria [3]. The biofilm lifestyle enables microbial cells to resist and tolerate concentrations of toxic substances that prove fatal to planktonic susceptible organisms [3]. Biofilms can raise the level of bacterial tolerance to antibiotics from 100 to 1000 times with respect to their planktonic counterparts [69]. Conventional antibiotic therapies usually decrease the number of biofilm cells but are not able to totally eliminate bacterial pathogens, thus allowing the infection to come back [1]. Tolerance is a property that bacterial cells acquire once they start living within these sessile matrix-encased communities [70,71] and that they lose

after bacterial cells disperse from biofilms [72,73]. Tolerance to antimicrobial compounds can be strictly linked to the specific biofilm-forming species, but different mechanisms also account for the increased tolerance characterizing biofilm cells [1]. EPS matrix can shelter biofilm cells from antibiotics by functioning as a shield that limits antibiotics penetration across biofilms [74,75]. EPS can decrease antibiotics diffusion through biofilms by either forming stable complexes with them or by acting as a physical barrier [1]. For example, negatively charged EPS molecules can complex positively charged antimicrobial peptides, cationic antibiotics such as aminoglycosides and toxic heavy metals cations [76]. However, also neutral exopolysaccharides have been demonstrated to efficiently interact with cationic antimicrobial peptides, thus reducing their bactericidal activity [77]. Generally, antibiotics kills bacterial cells dwelling the outermost layers of biofilms, but fail to reach those ones localized in the deeper layers, thus letting them survive [1]. However, the low efficiency of antimicrobials in the treatment of bacterial biofilm infections cannot be ascribed only to the physicochemical shield represented by the matrix [3]. Some antibiotics have been proved to easily penetrate biofilms without interacting with EPS molecules [78]. EPS can decrease activity and bioavailability of antimicrobials that cross the matrix also via enzymatic inactivation or chemical modifications [78]. In addition, biofilm cells survive antimicrobial compounds either via reducing growth rates or entering a dormant state [79]. Since they are usually provided with low levels of oxygen and nutrients, bacterial cells that inhabit deep inside the biofilm are characterized by slow growth rates [1]. Most antibiotics are useful at killing fast-growing bacteria as they generally target microbial processes such as DNA replication, DNA transcription and protein synthesis [1]. By decreasing their metabolism, primary targets of antimicrobials are not active, thus making microbial cells of deeper biofilm layers less susceptible to these compounds, thus enabling biofilm infections to persist [1]. Biofilm cells can also adopt a non-sporulating dormant state referred to as persisters [3]. Persister cells usually represent a small amount of both free-living bacteria in stationary growth phase and biofilm communities of several species [1]. Their tolerance to antibiotics is not due to acquired genetic mutations but rather a trait that randomly appears among a very small part of genetically identical populations of wild type bacteria [80]. Similarly to slow-growing cells, persisters survive antibiotic treatment because expression of antimicrobial compounds targets is switched off [1]. Unlike tolerance, resistance to antimicrobial

compounds is genetically transmitted [80]. Higher rates of mutation characterizing biofilm cells with respect to their clonal free-living counterpart [81] and frequently occurring events of horizontal gene transfer within biofilms [82] contribute to increase the resistance of biofilm cells to antibiotics [83]. These physiological processes are inherent to biofilm nature and can account for multi-drug resistance shown by biofilm cells towards structurally unrelated antibiotics such as fluoroquinolones, aminoglycosides and beta-lactam antibiotics [56]. In this light, microbial cells that inhabit biofilm communities can simultaneously express enzymatic proteins that make antibiotics harmless, targets that show low affinity for antibiotics and upregulate efflux pumps that help biofilm cells to extrude a wide range of compounds [56]. For example, some CF isolates of *P. aeruginosa* show increased resistance to beta-lactam antibiotics due to the combined effect of overexpression of the chromosomally-coded AmpC β-lactamase and MexAB-OprM efflux pump [56]. The biofilm matrix also acts as a reservoir of eDNA [84]. Uptake of eDNA, among which are genes coding for antibiotics resistances, is favored by high cell density, higher genetic competence and the huge amount of mobile genetic elements present within the biofilm community [83]. Direct transfer of DNA plasmids from one cell to another (conjugation) is one of the most frequent mechanisms by which horizontal gene transfer occurs [3]. Interestingly, conjugal plasmid of *S. aureus* is transferred through conjugation when microbial cells are organized in biofilm communities, while no transfer was detected for cultured planktonic cells [85], thus highlighting the importance of both the physical closeness and stable environment provided by biofilms.

1.2 The *Burkholderia cepacia* complex (Bcc)

1.2.1 Taxonomy and genomics of the Bcc

The *Burkholderia cepacia* complex (Bcc) is a group of closely-related bacterial species [86], highly versatile and widely distributed in soil, water and plant rhizosphere [87]. Bcc species display a high sequence similarity for the genes coding 16S rRNA (98-100%) and the recA protein (94-95%), and a moderate extent (30-50%) of DNA-DNA hybridization [88]. Bcc species have uncommon large genomes (4-9 Mb) usually organized in multiple chromosomes (from two to four) [87]. The Bcc assembles important plant pathogens, strains causing hospital-acquired infections, but also strains capable of degrading contaminants or providing plants with defenses against diseases

[87]. Bacterial species belonging to the Bcc were found for the first time in the 1940s by Walter Burkholder who discovered they were the causative agent of "sour skin", a disease affecting the bulbs of onion [89]. Burkholder suggested the name of *Pseudomonas cepacia* for the seven isolates recovered from decomposing onion bulbs [89]. Later, in 1992, *P. cepacia* together with other six bacterial species previously classified as *Pseudomonas* rRNA group II [90] were moved from the genus *Pseudomonas* to the new-born genus *Burkholderia* [91] to acknowledge W. Burkholder's fundamental contribution. In Canada, from 1970s to 1980s, *P. cepacia* was increasingly found associated with CF lung infections that led many patients to develop a fulminant and fatal pneumonia [92]. In the early 90's, investigations conducted after 16 CF American young adults had attended the same educational program undoubtedly demonstrated for the first time person-to-person transmissibility of a Bcc species [93], which was discovered years later to be a *B. dolosa* strain [94]. The best studied and prominent CF isolate of Bcc is *B. cenocepacia* J2315/CF5610 [95]. It is an epidemic strain of the intercontinental lineage known as ET 12 (Edinburgh/Toronto or electrophoretic type 12) that produced devastating outbreaks in CF populations of Canada, United Kingdom and others European countries because of its high transmissibility through social contacts [96]. The severe consequences of Bcc infections in CF patients has stimulated intense research in the last two decades that has produced a huge quantity of taxonomic data [97]. Nowadays, scientists identify and categorize Bcc species resorting to polyphasic, multilocus and genomic approaches that have taken the place of classical methodologies such as DNA-DNA hybridization for species differentiation and 16S rRNA sequence studies for phylogenetic tree construction [97]. To date, Bcc comprises 21 species: *B. ambifaria, B. anthina, B. arboris, B. cenocepacia, B. cepacia, B. contaminans, B. diffusa, B. dolosa, B. latens, B. lata, B. metallica, B. multivorans, B. pyrrocinia, B. seminalis, B. stabilis, B. ubonensis, B. vietnamiensis* [93–96]*, B. pseudomultiovorans* [102]*, B. stagnalis, B. territorii* [103] and *B. puraquae* [104].

1.2.2 The Bcc as opportunistic human pathogens in Cystic Fibrosis

Cystic fibrosis (CF) is a disorder with autosomal recessive mode of inheritance caused by mutations of the gene coding for the cystic fibrosis transmembrane conductance regulator (CFTR) [105]. The CFTR protein is an ion channel regulating chloride flux [106] and its malfunction leads to the development of a multi-organ disease that can

compromise proper functioning of airways, liver, pancreas, small intestine, reproductive system and sudoriferous glands [106]. The most frequently occurring mutation (70% of cystic fibrosis patients) is a deletion affecting codon 508 which specifies the amino acid phenylalanine (phe508del or ΔF508) [107]. Overall, more than 2000 genetic mutations of the CFTR gene, whose alleles are located on chromosomes 7, have been identified so far [106]. The disease affects to one infant out of 2000, with Caucasians being the most affected worldwide (70,000 people) [106]. CF patients properly treated have usually a life expectancy higher than 35 years, but in some centers it can exceed 50 years [106]. Lungs of CF patients are characterized by the accumulation of a thick and sticky mucus that decreases the ability of pulmonary cilia to keep airways clear from inhaled bacteria [108]. Consequently, CF people are prone to develop persistent pulmonary infections [108]. As mucociliary clearance is impaired, polymorphonuclear leukocytes (PMN) and antibodies are recruited to the site of infection causing chronic inflammation [106]. *P. aeruginosa* is the most common bacterial pathogen associated with persistent infections of CF lungs as well as the main cause of fatal outcome among CF people [106]. Starting from the 80s, Bcc species have been recognized as important pathogens of CF patients [69]. Bcc bacteria are particularly problematic since they easily spread from one individual to another and intrinsically multi-drug resistant, and they cause infections whose outcome cannot be predicted. In fact, CF patients can either experience no symptoms at all (asymptomatic carriage) or develop a fatal necrotizing pneumonia (cepacia syndrome) followed by septicemia [69]. Even though all members of Bcc might infect CF patients, *B. cenocepacia* and *B. multivorans* are the most represented bacterial species [109]. Epidemiological investigations conducted in several nations indicated that among Bcc species *B. multivorans* is the most predominant opportunistic pathogen in cystic fibrosis (CF) infections [110–116]. It is probable that the natural environment represents the major reservoir of pathogenic *B. multivorans* strains for CF people. The ability of Bcc species to form biofilms is thought to favor the establishment of chronic infections (mainly in CF patients) and decrease bacterial cells susceptibility to antimicrobial agents with respect to single free-living cells [117–121]. *B. cenocepacia* and *B. multivorans* were shown to produce more abundant biofilms *in vitro* compared to *B. cepacia*, *B. stabilis* and *B. vientamiensis* [122]. The ability of Bcc species to form biofilms on abiotic surfaces, but also to invade lung epithelial cells *in vitro*, suggest that their coexistence *in vivo* might explain the difficulties in eradicating Bcc bacteria from

CF infected lung [96]. The presence of bacterial biofilms in CF airways was demonstrated for *P. aeruginosa* which was found forming unattached microbial communities [123,124]. However, the ability of Bcc species to form biofilms *in vivo* is still debatable and unclear [109]. Investigations conducted on CF airways revealed that Bcc species existed mainly as single-cellular entities (both intracellularly located and not) or at least as small clusters, but they were not found organized in structured communities resembling biofilms [125,126]. On the contrary, staining of sputum coming from a CF individual affected from persistent infection revealed the presence of biofilm-like structures populated by *B. multivorans* cells, thus indicating that Bcc species can adopt the biofilm lifestyle *in vivo* [106]. It must be taken into account that the high complexity and heterogeneity of human respiratory system prevent airways from being thoroughly sampled, thus making it difficult to definitively claim that Bcc species form biofilms *in vivo* or not [127].

1.2.3 Extracellular polysaccharides produced by members of Bcc

To understand how biofilm cells interact with the surroundings, either the environment or the site of an infection, it is necessary to acquire detailed structural knowledge of extracellular polysaccharides, both CPSs and Epols, since they are usually the most represented EPS molecules fraction within the matrix [49]. Less than thirty years ago, an Epol biosynthesized by a bacterial species belonging to the Bcc was identified for the first time [128]. That Epol, later named Cepacian (**CEP**), was found to be made up of a heptasaccharide repeating unit containing glucose, mannose, glucuronic acid, rhamnose and three galactoses [129] with or bearing from 1 to 3 O-acetyl substituents [130]. **CEP** is a highly branched polymer as the backbone consists of just a trisaccharide repeated along the polymer backbone chain (Fig. 3) [48]. Several Bcc species generally biosynthesize **CEP** as the main extracellular polysaccharide, particularly when they are seeded on yeast extract mannitol agar under non-biofilm conditions [129,131]. Other than **CEP**, additional Epols produced in biofilm and non-biofilm conditions by Bcc species have been structurally characterized (Fig. 3):

PS-I: a linear Epol consisting of glucose and 4,6-O-(1'-carboxyethylidene)-galactose [131,132].

Dextran: homopolymer of 1→6 linked glucose produced by some Bcc species [132].

Levan: homopolymer made up of 2→6 fructose residues [133].

GAL-KDO: a polyanionic linear polymer consisting of a tetra-saccharide repeating unit made up of three galactoses and one residue of 3-deoxy-D-manno-oct-2-ulsonic acid (Kdo) [133].

BV-EP: an Epol consisting of fucose, glucose and glucuronic acid organized in hexa-saccharide repeating units and found to be synthesized by a clinical strain of *B. vietnamiensis* [134].

CO-CEP: an Epol consisting of t-Gal, 6-Gal and 1,2,4-GlcA produced by eight Bcc species out of ten grown on solid YEM under non-biofilm conditions [49].

Epol C1576: neutral linear polymer synthesized by *B. multivorans* C1576 and made up of a tetrasaccharide repeating unit containing equimolar amounts of 2-Rha, 3-Rha, 2-Man and 3-Man with 50% of 2-linked rhamnose having a methoxy substituent on carbon 3 [135].

Many Epols synthesized by Bcc species are usually negatively charged polymers, mainly because of uronic acids presence, and share a high molecular mass, often exceeding 10^6 Daltons [49]. Bcc species usually produce mixtures of Epols, with **CEP** being the most represented extracellular polysaccharide when YEM medium is utilized both in biofilm and non-biofilm conditions [49]. Furthermore, the type of Epol produced depends not only on the medium composition, but it is also function of the nature of a solid support [49].

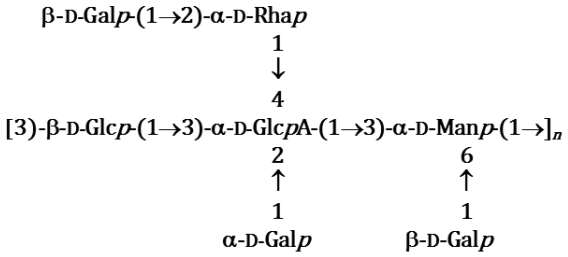

CEP

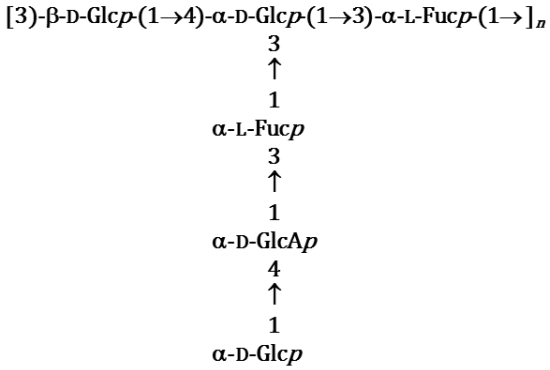

BV-EP

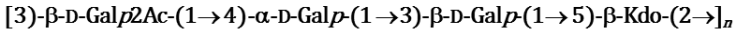

GAL-KDO

PS1

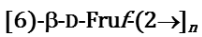

Levan

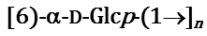

Dextran

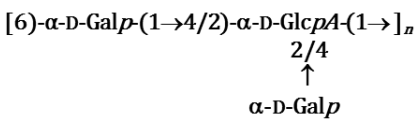

CO-CEP

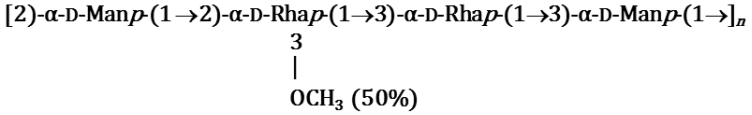

EpolC1576

Figure 3. The structure of the saccharide repeating unit of eight different Epols synthesized by Bcc species.

1.2.4 Antimicrobial tolerance and resistance in Bcc biofilms

Bcc species show remarkable tolerance and resistance to many structurally unrelated antibiotics, chemicals for disinfection and additives used to lower the risk of foodborne infections [136]. Many features contribute to the enhanced resistance of Bcc bacteria: coexistence of distinct multi-drug efflux pumps, decreased outer membrane permeability, structural diversity of surface lipopolysaccharides, inducible expression of chromosomally-encoded lytic enzymes targeting β-lactam antibiotics and modifications of drug targets (i.e. modified penicillin-binding proteins) [96,136]. However, some mechanisms of tolerance seem to be intrinsic to the biofilm lifestyle: delayed diffusion of antibiotics through the biofilm, phenotypic heterogeneity among biofilm populations, the constant presence of a small fractions of "persister cells" and biofilm ability to react adaptively to external insults [137–139]. The degree of diffusion of antimicrobial compounds through biofilms is a crucial parameter since it can influence the dose bacteria are exposed to; on the contrary, planktonic bacterial cells in a well-mixed liquid suspension are not affected by diffusion "problems" as they quickly experience the dose of antimicrobial in its entirety [140–143]. The rate of diffusion of an antimicrobial agent across a biofilm can be delayed with respect to that characterizing a liquid culture of bacteria. In this light, biofilms can provide microbial cells with enough time to organize an effective response towards the antimicrobial compound [140]. Theoretical models suggest that biofilms would not be able to decrease the rate of diffusion of several antibiotics [142,143], whereas experimental work indicates that antibiotic-delayed diffusion is function of the specific physicochemical properties of a given chemical agent and/or biofilm. For example, it was demonstrated that degradation of cepacian upon treatment of Bcc biofilms with NaClO caused an increase in the bactericidal activity of tobramycin, thus suggesting that biofilm Epol can affect antibiotics rate of penetration [144]. Furthermore, the highly negative Epol alginate present in *P. aeruginosa* biofilms probably delays the rate of diffusion of positively charged aminoglycosides such as tobramycin and gentamicin with respect to β-lactam antibiotics [145–147]. In addition, extracellular lytic enzymes can be also responsible for decreasing the rate of diffusion of antibiotics; EPS associated with the matrix of mucoid Bcc biofilms have been shown to be protective towards antimicrobial compounds as well as the host immune defenses [144]. For example, Epols synthesized by *B. cenocepacia* repress neutrophils chemotaxis and lower the amount of reactive-

oxygen species (ROS) produced by neutrophils [148]. Cepacian, the most common Epol among Bcc bacteria, shows protection toward hypochlorite (ClO^-), a ROS released by neutrophils and particularly effective at killing bacteria. ROS-scavenging ability of cepacian causes the Epol to lose acetyl-groups and later to undergo degradation of the backbone [149]. Furthermore, upon treatment with reactive-oxygen species (H_2O_2 and NaOCl), *B. cenocepacia* biofilm cells were shown to up- and down-regulate the expression of hundreds of genes. Among those positively transcribed were genes that specify for factors underlying ROS scavenging, but also for proteins implicated in repairing damages caused by ROS [150].

1.2.5 Quorum sensing in the Bcc

Bcc species share the QS system based on LuxI-type synthase and LuxR-like regulator, which are homologous of LuxI and LuxR proteins first described in *Vibrio fischeri* [151]. LuxI is an enzyme responsible to produce AHL signaling molecules while LuxR is a receptor protein that, upon binding AHL molecules, recognizes a promoter consensus sequence, the *lux* box, thus up- or down-regulating the expression of specific genes [151]. AHLs synthesized by Bcc members have acyl side chains of different length which can also carry various substituents [151]. Frequently, the LuxR bound to AHL molecules activates expression of *luxI* gene, thus promoting a positive feedback loop that increases the concentration of the signaling molecule [152]. The AHL-dependent QS system known as CepIR is highly conserved among Bcc species [153] and function thanks to the production and detection of N-octanoyl-homoserine lactone (C8-HSL), and to a little extent of N-hexanoyl-homoserine lactone (C6-HSL) [154]. Another Bcc QS system, named CciIR, is based on the synthesis and perception of C6-HSL, even though CciIR produces also small quantities of C8-HSL [63]. This supplementary QS system is coded by genes of the *cci* pathogenicity island and was found in strains of the *B. cenocepacia* ET12 epidemic lineage [155]. CepIR and CciIR systems are interlinked, since CepR upregulates *cciIR* genes whereas CciR represses *cepI* transcription [156]. QS systems allow several determinants of virulence to be expressed and play a prominent role in the ability of microbial cells to cause a disease [157]. CepIR QS system of *B. cenocepacia* was found to promote the expression of zinc metalloproteases (ZmpA and ZmpB), chitin degrading enzymes, a protein killing nematodes (AidA), but also to be involved in flagellum-dependent swarming motility, biofilm maturation and synthesis of

siderophores (ornibactin) [158,159]. By using lytic enzymes targeting AHL signaling molecules, the involvement of QS system CepIR in biofilm production was proven for many Bcc strains investigated [160]. The compromised ability to form canonical biofilms was firstly demonstrated for *B. cenocepacia* H111 [161]. Mutants defective in the expression of either CepI or CepR were unable to form mature biofilms, thus showing lower biomass with respect to wild-type *B. cenocepacia* H111 [161]. Furthermore, CepIR QS system governs the synthesis of the Biofilm Associated Protein (Bap) in *B. cenocepacia* H111 [162]. Bap is a large surface protein generally transferred outside the cell thanks to a Type I secretion system and thought to be weakly attached to bacterial membranes [163,164]. Large surface proteins were demonstrated to take active part in biofilm development in various bacterial species [63]. Indeed, in *bapA* mutants of *B. cenocepacia* H111 the ability to form biofilm on inanimate surfaces is severely impaired, affecting both biofilm structure and biomass [162]. Other genes found to be regulated by a AHL-dependent QS system are organized in the *bclABC* cluster and encode for three carbohydrate-binding proteins or lectins: BclA, BclB and BclC [162]. It was shown that mutations in lectin-coding genes affect the proper structural development of biofilms, thus resulting in biofilms with unusual architectures [162]. Epols are also common components of the biofilm matrix and were proven to be involved in cellular adhesion and biofilms stabilization [63]. However, there is still lack of evidence about the link between QS systems based on AHLs molecules and Epols biosynthesis for Bcc species [165]. Many strains of *B. cenocepacia* were also found to use a fatty acid as signaling molecule [166]. *B. cenocepacia* J2315 strain synthesizes the cis-2-dodecenoic acid, also known as *Burkholderia* Diffusible Signal Factor (BDSF) [63], that has a structure almost identical to the Diffusible Signal Factor (DSF) produced by the plant pathogen *Xanthomonas campestris* pv *campestris* [167]. In *X. campestris*, DSF, which is a cis-11-methyl-2-dodecenoic acid, promotes the activation of RpfCG, a two component system that causes intracellular c-di-GMP levels to decrease, thus stimulating the transcription of genes coding for virulence determinants and biofilm spreading [168,169]. Enzymes of *X. campestris* and *B. cenocepacia* producing DSF and BDSF share a high degree of homology (RpfF and $RpfF_{Bc}$ respectively) [166,170]. *B. cenocepacia* perceives BDSF signaling molecules produced by $RpfF_{Bc}$ via the RpfR receptor protein [171]. The latter has three distinct domains: PAS, GGDEF and EAL. GGDEF and EAL, which are evolutionarily well-conserved and function as diguanylate cyclase and

phosphodiesterase respectively, thus fine-tuning c-di-GMP intracellular levels [172]. When BDSF binds to the PAS domain, RpfR undergoes a change in conformation that leads the phosphodiesterase domain to hydrolyze c-di-GMP, thus decreasing c-di-GMP levels. This intracellular second messenger is widely used among bacteria and known to promote the switch from the planktonic to the biofilm way of life [63]. High concentrations of c-di-GMP usually stimulate bacteria to form biofilm [172]. Fazli *et al* demonstrated that upon binding to c-di GMP, the transcription factor BCAM1349 orchestrates the expression of a 12-gene cluster coding for enzymes responsible to produce an Epol [173]. This structurally uncharacterized Epol was found to improve stability of *B. cenocepacia* H111 biofilms developed in flow-cell system [173].

1.3 Phage display technology

1.3.1 Phage display: how it functions

Phage display is a molecular technique that allows for selection of proteins with desired binding properties by analyzing the interaction of proteins displayed on the surface of a bacteriophage with potential targets [174]. This technique was first described by George P. Smith in 1985, who managed to display peptides on the surface of a filamentous bacteriophage [175]. Bacteriophages or phages are virus that infects bacterial cells. They can be categorized in filamentous, lambda and T7 phages. M13 belongs to the filamentous phage family and is commonly used for phage display [176]. M13 is a non-lytic bacteriophage that exploits the F-pilus to attach to and enter host bacteria. The infected host amplifies the phage genome and synthesizes all the coat and packaging proteins necessary for assembly and replication of phage particles. A simplified illustration of the life cycle of a filamentous phage is shown in Fig. 4 [177].

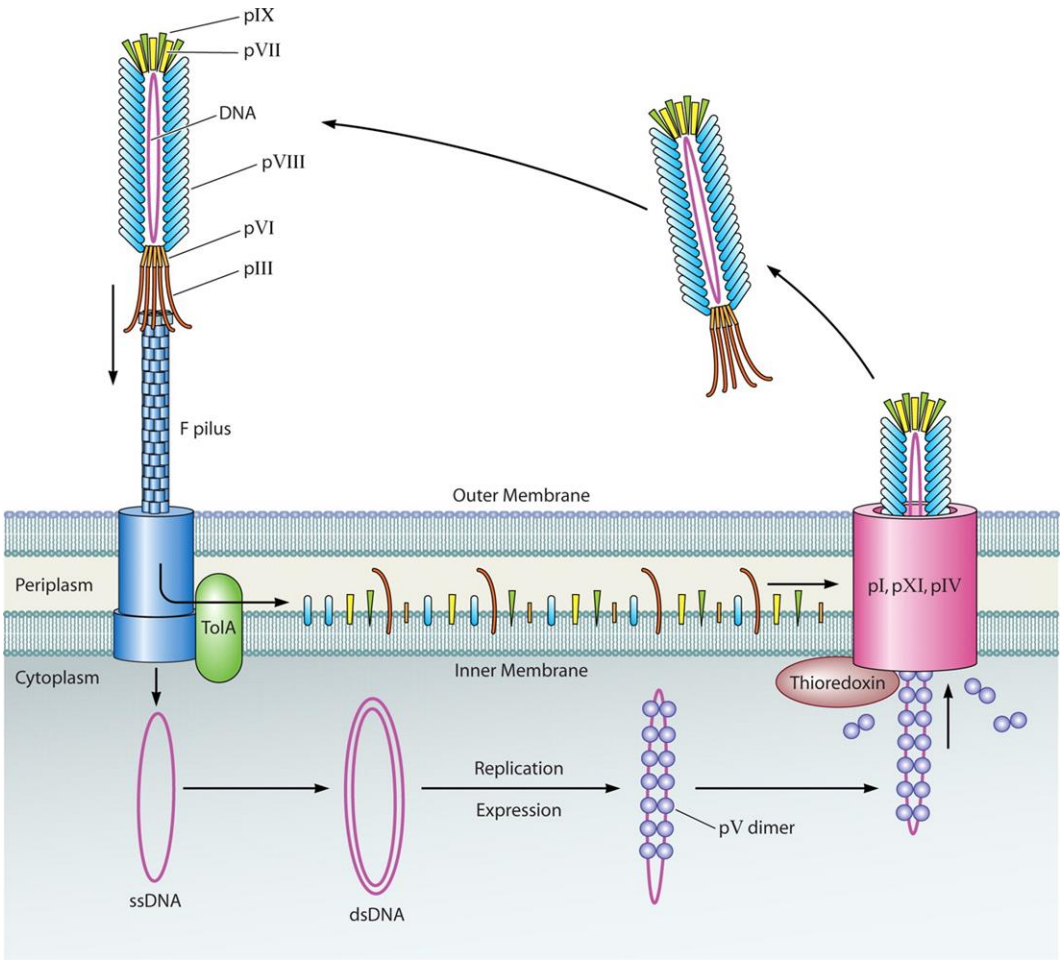

Figure 4. Life cycle of filamentous phages. The filamentous bacteriophage binds to the F-pilus of an *E. coli* cell via the coat protein pIII. A bacterial protein (TolA) depolymerizes the phage coat protein that remains outside to be reused. The ssDNA of the phage reaches the cytosol where it is converted into double-stranded DNA (dsDNA), replicated and expressed thanks to the host enzymes. ssDNA and dimers of pV protein assemble to give rise to precursors of mature phage particles. Later, within the channel generated by phage proteins pI, pXI, pIV and host thioredoxin pV is substituted by pVIII. The life cycle ends with complete virus particles that abandon the host cell. Figure adapted from Johnny X. Huang [178] under creative commons attribution license.

M13 contains a circular single-stranded DNA molecule which is surrounded by approximately 2700 copies of the major coat protein pVIII and capped on the ends with 5 copies of minor coat proteins pIX, pVII, pVI and pIII. The latter is the one involved in the recognition of the F-pilus of the host *E. coli* [179]. For phage display purposes, the most suitable coat proteins are pIII and pVIII, even though pVI can be exploited. DNA fragments to be investigated are generally cloned upstream the gene that specifies for pIII or pVIII proteins, thus allowing the expression of 3-5 or 2700 copies of recombinant proteins, respectively. Since the major coat protein pVIII is relatively small (50 amino

acids) and does not tolerate large insertions, pIII phage display systems are usually chosen.

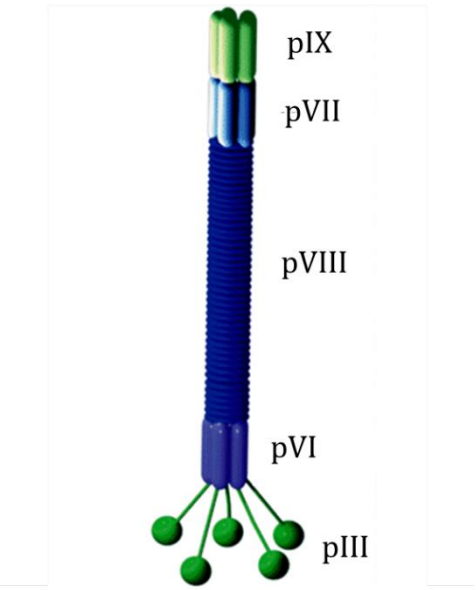

Figure 5. Structure of M13 bacteriophage: pIII, pVI, pVII, pVIII and pIX are coat proteins. Exogenous displayed proteins are generally fused to coat proteins pIII or pVIII. Figure adapted from M. Arap [180] under creative commons attribution license.

Since phage particles carry the genetic sequence coding for the protein displayed on their surface, the phage constitutes a direct link between the genotype and phenotype. The phage display technology allows for selection of proteins among the library that binds to specific targets with relative ease. The enrichment of the library for clones displaying proteins that bind to the target can be rapidly accomplished by incubating the library with the target, washing away the unbound phage particles and amplifying in the host bacteria those phages that bound to the target (Fig. 6). The opportunity to carry out consecutive rounds of selection (panning) allows the isolation of proteins present in very low amount in a library composed of billions of phage particles. Generally, a good enrichment of the library for target-specific proteins can be obtained after three to five rounds of selection. The identity of selected proteins is inferred by sequencing the corresponding coding DNA. In this way, highly diverse phage libraries containing up to 10^{11} distinct DNA inserts [181] can be produced, amplified, stored and analyzed for the presence of proteins that bind specific targets.

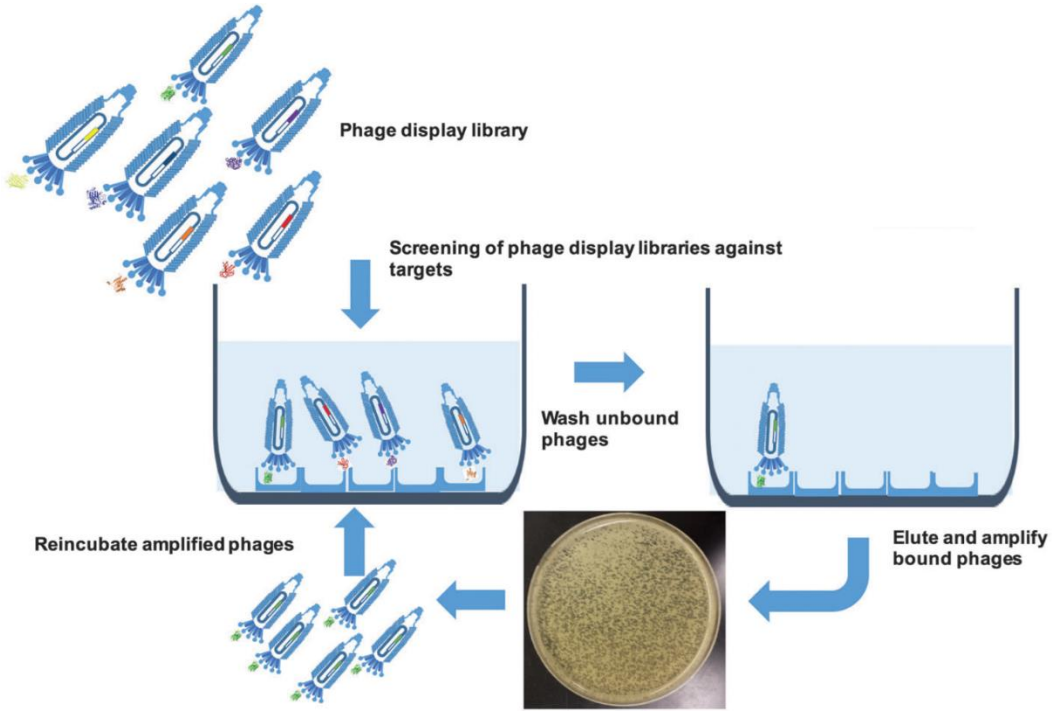

Figure 6. Phage display selection. It starts with the phage library screening in the presence of the immobilized target. Successively, unbound phages are washed away and bound phages are eluted using bacterial cells. Infected bacteria are later amplified and selected phages can be recovered for a second round of selection. Figure adapted from A. Galán [182] under creative commons attribution license.

Since phage genomes are not easy to work with, phagemid vectors have been developed. The type of protein display in phage libraries can be either polyvalent or monovalent. In the polyvalent version, each copy of the coat protein (pIII or pVIII) displays the protein encoded by the DNA insert. Phage particles used for polyvalent display contains vectors derived from phage genome that are equipped with all the genes coding for phage replication and packaging. This type of phage display is well suited for peptides display, since large DNA inserts affect the function of coat proteins, thus compromising the ability of phage to infect the host bacteria. For large inserts that code for high molecular mass proteins, monovalent display is usually chosen as it allows pIII to keep its function. In the monovalent display, the phagemid vector expresses the coat protein fusion, whereas a helper phage provides all the wild-type coat proteins [183,184]. The helper phage (a phage with a signal for packaging that does not work or less efficient than that of the phagemid vector) is meant to supply all the proteins needed for phagemid replication, ssDNA synthesis and packaging. In this way, phage particles of the library are functional since the recombinant protein represents a small fraction of the entire

coat protein (more than 99% of phage particles have either one or no copy of the recombinant protein), thus allowing to display proteins with high molecular weight (up to 100 kDa).

Display of both coding (cDNAs) and genomic (gDNAs) DNA sequences by means of phage libraries has been difficult because DNA inserts must be in frame with the gene coding for the phage coat protein selected for the display. Different methods have been developed to eliminate non-expressed out-of-frame DNA inserts [185–187], but also to make sure that displayed proteins coded by in-frame DNA inserts are soluble. These methods are based on the presence of a reporter gene, for example a gene coding β-lactamase, downstream the DNA insert for the protein to display but upstream the phage coat gene chosen for the display. Only DNA inserts in-frame coding for displayed proteins that fold correctly confer a selectable phenotype [188], thus allowing to remove all phage particles containing non-coding DNA inserts and those displaying insoluble and/or misfolded proteins.

2 AIM OF THE RESEARCH

Biofilms are polymicrobial aggregates in which bacterial cells are encased in a self-produced and highly hydrated matrix consisting of polysaccharides, proteins, nucleic acids and lipids that form the 3D network of the biofilm matrix. Among these macromolecules, exopolysaccharides (Epols) are usually the most abundant component. Biofilms are frequently found associated with chronic infections which are difficult to treat due to enhanced tolerance and resistance to antimicrobial agents. Epols are believed to be mainly involved in the maintenance and mechanical stability of biofilms, but they might also protect bacterial cells toward antibiotics and the host immune system, thus allowing infections to persist. The exopolysaccharide known as EpolC1576 purified from the biofilm matrix of *B. multivorans* C1576, a Gram-negative opportunistic pathogen that causes severe lung infections in cystic fibrosis (CF) patients, shows an interesting peculiar chemistry. Indeed, it consists of a tetrasaccharide repeating unit made up of equimolar amounts of mannose and rhamnose, with the latter being a 6-deoxy sugar with nonpolar features.

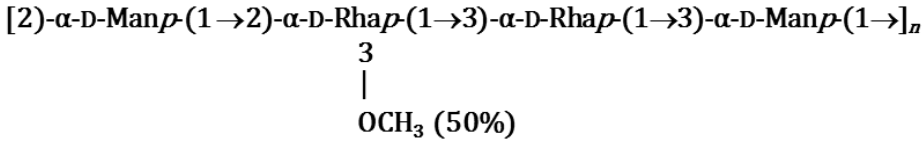

EpolC1576 tetrasaccharide repeating unit.

The presence of clusters of rhamnose together with a methoxy substituent on carbon 3 of 50% of the 2-linked rhamnose, confers to EpolC1576 an amphiphilic character that is quite "uncommon" among polysaccharides.

The goals of this research are:

a) investigating the ability of EpolC1576 to interact with hydrophobic molecules to understand whether the polysaccharide can have a role in the modulation and diffusion of non-polar biologically active molecules such as signaling compounds of quorum sensing and antibiotics through the highly hydrated environment of the biofilm matrix;

b) analyzing the conformational behavior of EpolC1576 and its ability to form aggregates to gain insight into EpolC1576 molecules self-organization in the 3D scaffold of the matrix;
c) studying the morphology of *B. multivorans* C1576 biofilm and characterizing the macromolecular components of the matrix with an interest in the proteinaceous fraction to help in understanding the possible biological roles of the matrix.

3 PART I - Investigation of the role of EpolC1576 hydrophobic domains in the interaction with nonpolar small molecules and in biofilm formation and maintenance

3.1 INTRODUCTION

As stated in chapter 1, Epols usually represent the major component among the extracellular polymeric substances building-up the biofilm matrix [54]. However, the physicochemical properties of most of bacterial Epols are unknown, thus making it challenging to elucidate the relationships between the structural and functional roles they actually play [189]. It is supposed that the 3D network of the biofilm matrix is fostered by non-covalent bonds involving hydrophilic and hydrophobic domains characterizing the extracellular polymeric substances actively produced by bacterial cells; however, the precise details of molecular interactions occurring among these matrix biopolymers are still elusive [190]. Even though the biofilm matrix is a highly hydrated environment, hydrophobic or apolar interactions might participate in biofilm structural and mechanical stabilization and in retaining useful less polar compounds [189]. Bcc species were shown to synthesize several structurally diverse Epols, singularly or in mixture, when seeded on different solid culture media [49]. Moreover, experimental culture conditions might influence the type of Epols produced [49]. Under biofilm conditions, *B. multivorans* C1576 grown on cellulose membranes deposited on Petri dishes containing solid yeast extract mannitol (YEM) medium produces almost only cepacian as Epol [191], whereas in the same growth conditions but using Müller-Hinton (MH) as culture medium, bacteria biosynthesize an exopolysaccharide whose tetrasaccharide repeating unit (Fig. 7) contains equimolar amounts of α-D-mannose and α-D-rhamnose [135]. About 50% of the 2-linked rhamnose carries a methoxy substituent (-OCH_3) on the sugar ring carbon 3.

$$[2)\text{-}\alpha\text{-D-Man}p\text{-}(1\rightarrow2)\text{-}\alpha\text{-D-Rha}p\text{-}(1\rightarrow3)\text{-}\alpha\text{-D-Rha}p\text{-}(1\rightarrow3)\text{-}\alpha\text{-D-Man}p\text{-}(1\rightarrow]_n$$
$$\begin{array}{c} 3 \\ | \\ OCH_3\ (50\%) \end{array}$$

Figure 7. Tetrasaccharide repeating unit of EpolC1576.

This rhamno-mannan exopolysaccharide, hereafter named EpolC1576, is particularly interesting due to the hydrophobicity conferred to the polymer by the presence of clusters of α-D-rhamnose, a 6-deoxy-sugar. Indeed, rhamnoses lack a hydroxyl function (-OH) on C6 which thus is a methyl group. Also, the presence of a methyl ether substituent on C3 on about half of the 2-linked rhamnose residues decreases the number of hydroxyl groups, thus reducing EpolC1576 hydrophilicity if compared to other bacterial Epols which are commonly made up of more hydrophilic monosaccharides [189]. Even though carbohydrates are commonly considered highly hydrophilic molecules due to the high proportion of hydroxyl groups, some of them showed the ability to complex hydrophobic molecules [189]. Specifically, cyclodextrins adopt a toroid configuration that allow them to host aliphatic and aromatic compounds into their cavity since it lacks hydroxyl groups. For example, Rizzo *et al.* studied the complexation properties of cyclodextrins with two aromatic fluorescent probes (Fig. 8): 1-anilino-8-naphthalene sulfonate (ANS) and 2-(p-toluidinyl)-6-naphthalene sulfonate (TNS) [192]; these two hydrophobic molecules were also employed for identification of hydrophobic pockets in proteins [193,194].

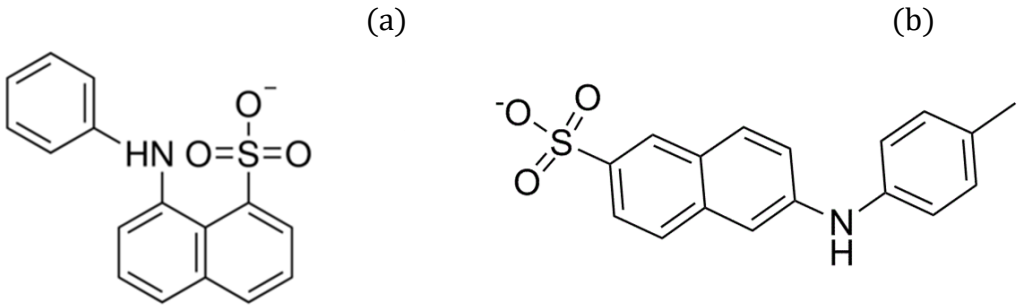

Figure 8. Structures of hydrophobic fluorescent probes ANS (a) and TNS (b).

Here, it is suggested that the hydrophobic chain segments of EpolC1576 might be involved in both self- and non-self-intermolecular interactions within the biofilm matrix,

thus enhancing biofilm stabilization in highly hydrated environments [189]. Furthermore, EpolC1576 hydrophobic domains might transiently bind and retain small nonpolar compounds which may play a biological role, thus making EpolC1576 capable of modulating their activity in the aqueous environment of the biofilm matrix. Bacteria make use of a communication system named quorum sensing that coordinates the expression of genes underling phenomena such as biofilm production and maturation, synthesis of proteases and swarming motility [195]. Interestingly, *B. multivorans* C1576 utilizes fatty acids as quorum sensing signaling molecules [196] which have also been demonstrated to play a role in the expression of determinants of virulence and biofilm synthesis in several pathogens [168]. In this light, the conformation of EpolC1576 under different experimental conditions as well as its ability to interact with hydrophobic molecules has been investigated resorting to various instrumental techniques, and also by means of molecular modeling calculations.

3.2 MATERIAL AND METHODS

3.2.1 Biofilm production by *B. multivorans* C1576 on semipermeable cellulose membranes and EpolC1576 purification

B. multivorans C1576 (LMG 16660) is a reference strain that belongs to the panel of *B. cepacia* complex strains (EP1), and it was purchased from the BCCM™ bacteria collection. The biofilm was developed on cellulose membranes (Sigma, cut-off 12.400 Da) that were prepared as follows: they were cut in circles to fit the Petri dish, boiled in 5% Na_2CO_3 solution for 15 min and then boiled in water for 15 min, subjected to autoclave sterilization and laid on Petri dishes containing MH agar medium. Membranes extended all over the plate and surplus of water was let evaporate under the hood. An overnight liquid culture of *B. multivorans* C1576 was diluted to obtain a cell suspension having 0.13 OD at 600 nm and three aliquots of 10 µL of the cell dilution were transferred on the membranes. It was used the same liquid medium for the overnight culture of *B. multivorans* C1576 and for Petri dishes filling. After 7 days of incubation at 30°C, the biofilm on the membranes was recovered with sterile 0.9% NaCl, the cell suspension was added with NaOH to reach a final concentration of 0.1 M, incubated at room temperature, with shaking for 3 hours to dismantle the biofilm. The cell suspension was then centrifuged at 40,000 g at 4 °C for 30 min and the supernatant, containing soluble EpolC1576, was recovered and dialyzed against distilled water using 12–14 kDa molecular weight cut-off (MWCO) membrane for 72 hours at 25 °C. The solution recovered from dialysis tube was cooled in ice and added with trichloroacetic acid (20% w/v final concentration) to precipitate proteins and nucleic acids. After 30 minutes of incubation, the solution was centrifuged 40,000 g for 30 minutes at 4 °C, the supernatant was collected and dialyzed against distilled water using 12–14 kDa molecular weight cut-off (MWCO) membrane for 72 hours at 25 °C. The dialysate was cooled in ice, added with 4 volumes of 96% cold ethanol and the mixture was placed at -20 °C for 24 hours to precipitate the polysaccharide from lipids. The solution was then centrifuged at 40,000 g for 30 minutes at 4 °C and the pellet consisting of polysaccharide was resuspended in Milli-Q water and dialyzed against the same for 72 hours at 4 °C using a 12–14 kDa MWCO membrane. The remaining retentate was taken to neutral pH, filtered through a 0.22 µm pore size filter (KX Sterile Syringe Filter, Kinesis) and lyophilized. The purity EpolC1576 was verified by NMR. ^1H NMR spectrum was recorded on a 500-MHz

Varian spectrometer operating at 50 °C. EpolC1576 was subsequently exchanged three times with 99.9 % D_2O by lyophilization and finally dissolved in 0.6 mL of 99.9% D_2O before recording the NMR spectra.

3.2.2 Fluorescence spectroscopy experiments

The fluorescent probes 1-anilino-8-naphthalene sulfonate sodium salt (Na^+ ANS^-) and 2-(p-toluidinyl)-6-naphthalene sulfonate potassium salt (K^+ TNS^-) were purchased from Sigma. Solubilization of EpolC1576 was performed in water to reach a final concentration of octasaccharide repeating unit (4 Rha, 4 Man, 1 *O*-Me; molecular mass, 1246 Da) of 2 x 10^{-4} M. ANS and TNS were resuspended in water and aliquots of each solution were transferred to the EpolC1576 solution to reach the desired final concentration in the range of 0–7·10^{-4} M. Fluorescence spectra were recorded on a PerkinElmer Life Sciences LS50B spectrofluorimeter thermostated at 25 °C and using 10-mm path length quartz cells. For ANS, the excitation wavelength was 365 nm, and emission was detected from 300 to 650 nm. The behavior of fluorescence intensity as a function of ANS concentration was reported at 460 and 510 nm, after ANS self-absorption correction [193]. For TNS, the excitation wavelength was 287 nm, and emission was detected from 300 to 650 nm. The behavior of fluorescence intensity as a function of TNS concentration was reported at 425 nm, after TNS self-absorption correction. For comparison purposes, the same experiments were also performed in the presence of the polysaccharide dextran, since it does not possess non-polar moieties along its chain. The dextran concentration was fixed in the same manner as for EpolC1576. Values of fluorescence intensity of both ANS and TNS were corrected for dye self-absorption as stated in [193].

3.2.3 NMR experiments

^1H NMR spectra were recorded on a 500 MHz Varian spectrometer operating at 25 °C. All samples were successively exchanged three times with 99.9% D_2O by lyophilization and finally solubilized in 0.6 mL of 99.99% D_2O. For the experiments performed to study interactions with each aromatic fluorescent probe, the concentration of EpolC1576 was 5.7 x 10^{-4} M, whereas concentrations of ANS and TNS were 1.5·10^{-3} M and 2.3·10^{-3} M, respectively. For comparison purposes, NMR investigations were also performed with dextran utilizing the same concentrations of polysaccharide and aromatic dyes.

3.2.4 Interactions of EpolC1576 with *cis*-11-methyl-2-dodecenoic acid

The procedure employed consisted of resuspending the same amount of *cis*-11-methyl-2-dodecenoic acid with a polysaccharide aqueous solution of either EpolC1576 or dextran. The fatty acid was first solubilized in CH_3Cl, then an equal amount of the solution was transferred into two glass vials and dried under a nitrogen flux. An aliquot of EpolC1576 and dextran both containing 0.4 μmoles (calculated for an octasaccharide repeating unit) were exchanged three times with 99.9 % D_2O by lyophilization, solubilized in 0.6 mL of 99.9 % D_2O, and added to the two vials, each containing 9.4 μmoles of *cis*-11-methyl-2-dodecenoic acid. The two vials were gently mixed on a rotary shaker at room temperature for about 7 h, centrifuged at 14,500 g for 10 min at room temperature to pellet insoluble particles, and the supernatant transferred in NMR tubes. ^1H NMR spectra were processed using MestreNova software. Chemical shifts are expressed in parts per million and referred to the HOD signal, set as 4.768 ppm [197].

3.2.5 Molecular simulations

Molecular simulations were carried out by Prof. Michelle Kuttel at the Dept. of Computer Science, University of Cape Town (South Africa) [189]. Molecular simulations using all-atom molecular dynamics were employed, modeling a tetramer (4 repeating units for a total of 16 monosaccharides of EpolC1576, having one 3-*O*-methyl Rha every second repeating unit) with guest species in water considering also the presence of counterions to neutralize the charges. Hexane and *cis*-11-methyl-2-dodecenoic acid were used as guest species.

3.2.6 Saturation-Transfer Difference NMR experiments

Saturation-Transfer Difference NMR experiments were carried out at the University of East Anglia (Norwich, United Kingdom) in collaboration with prof. Jesus Angulo (School of Pharmacy). They were performed to study interactions between EpolC1576 and the following compounds: ANS, TNS and Kanamycin. STD NMR is a technique based on the transfer of magnetization from a macromolecule to small ligands [198]. STD NMR investigation typically starts with the registration of a one-dimensional (1D) ^1H NMR spectrum in thermal equilibrium of a solution composed of a low-concentrated macromolecule and a high-concentrated small ligand (*off resonance* experiment). Successively, another ^1H NMR analysis is run (*on resonance* experiment), which consists in the irradiation of distinct protons of the macromolecule with impulses having low

power radiofrequency for a fixed number of seconds (*saturation time*). If the solution is properly irradiated, then protons of the macromolecule are selectively and effectively saturated, whereas the ones carried by the small ligand are not. Transfer of saturation from the macromolecule to the bound ligand, which is based on the intermolecular Nuclear Overhauser Effect (NOE), occurs only if two conditions are simultaneously satisfied: 1) distance between protons of both species is less than 6 Å; 2) the ligand interacts "transiently" with the macromolecule. In this way, magnetization of bound ligands is transferred to free ligand molecules, thus causing saturation to quickly accumulate over the course of the irradiation in the bulk solution and only protons of the ligand to produce signals. The difference between the intensity of ligand signals produced in the *off resonance* (I_0) and *on resonance* experiments (I_{sat}) gives rise to the "difference spectrum". Since not all protons of the ligand receive the same amount of magnetization, STD NMR allows also for mapping those regions of the ligand more involved in the interaction with the macromolecule [198].

3.2.7 EpolC1576 fragments preparation and characterization

In order to obtain saccharide fragments of suitable molecular weight, native EpolC1576 (800 kDa) was hydrolyzed with 0.5 M trifluoroacetic acid (TFA) for 2 hours at 80 °C. High performance size exclusion chromatography (HP-SEC) analysis of hydrolysis products was performed on an Agilent Technologies 1200 series HPLC equipped with three TSKgel columns (Tosoh Bioscience) in series: G3000PW (< 50,000 Da), G5000PW (< 1 x 10^6 Da) and G6000PW (< 8 x 10^6 Da), with internal diameter of 7.5 mm, length of 30 cm and kept at 40 °C in a thermostatted column compartment (Agilent Technologies). Calibration of the chromatographic system was done resorting to pullulan standards (Polymer Laboratories, Germany and Sigma for pullulan with MM=1.6 x 10^6). Elution was performed with 0.15 M NaCl, using a flow rate of 0.5 mL/min and monitored using a refractive index detector (Knauer, Labservice Analytica), interfaced with a computer via Agilent software. Since EpolC1576 fragments produced a distribution of molecular masses, the chromatographic peak was divided into high (H), medium (M) and low (L) molecular weight fragments. Successively, HP-SEC analysis was repeated to establish the apparent molecular weight of each pool of fragments. EpolC1576 fragments were also analyzed by NMR. An aliquot of each pool of fragments together with native EpolC1576 were subsequently exchanged three times with 99.9 % D_2O, lyophilized and finally

dissolved in 0.6 mL 99.9 % D_2O before NMR analysis. Spectra were recorded on a 500 MHz VARIAN spectrometer operating at 50°C.

3.2.8 Surface Plasmon Resonance experiments

Surface plasmon resonance experiments were carried out by Dr Milena Guida at the University of Trieste (Dept. of Life Sciences). The ability of EpolC1576 to interact with hydrophobic molecules was further investigated via Surface Plasmon Resonance experiments by taking advantage of the HPA chip that consists of a flat hydrophobic surface of long alkyl chain molecules attached directly to a gold film. The experiment was performed on a Biacore X100 instrument (GE Lifesciences). Solutions with increasing concentrations (from 5.2 to 167 μM) of both medium molecular weight fragments of EpolC1576 (M-EpolC1576, molecular mass 12 kDa) and dextran (12 kDa analytical standard for GPC, Fluka) were injected in sequence, at a constant flow rate of 10 μL/min for a contact time of 540 sec, followed by a dissociation time (washing) of 1200 sec with water as running buffer. Binding events result in a local variation of the refractive index, leading to altered resonance properties that allows real-time monitoring of the interaction. This is reported as a variation in "resonance units" (RU), so that 1 RU = 1 pg of analyte binding per mm^2 of surface [199] . At the end of each run, the flow cell was regenerated with n-octyl glucopyranoside (OGP) 40 mM and NaOH 50 mM. Sensorgrams of binding were obtained using BIAevaluation software v 1.1 and then elaborated using GraphPad v 6.04. The best fit for binding curves was obtained with the "Affinity-Steady State" mathematical model in the BIAevaluation software. The affinity is reported as an equilibrium dissociation constant (K_D) value which is the inverse of the association constant (K_A). Biacore Assay Handbook 29-0194-00 Edition AA (page 64) [200].

3.2.9 Atomic Force Microscopy (AFM) imaging of EpolC1576

The AFM images were obtained in tapping mode using a Multimode™ AFM (Veeco Metrology) equipped with a HQ:NSC19/AL BS tip (MikroMasch, radius 8 nm) and a Nanoscope V controller (Digital Instruments, Veeco Metrology Group). Images were captured with 274-275 KHz drive frequency, and 250-300 mV drive amplitude. Aqueous solutions of 5 and 30 μg/mL of EpolC1576 were filtered using 0.22 μm pore-size membranes (GP Millex, Millipore) and subsequently sprayed onto a freshly cleaved mica

surface, dried at 30 °C under vacuum for 16 h prior AFM imaging. To process the data, it was used using program Nanoscope V7.30.

3.3 RESULTS AND DISCUSSION

3.3.1 Interaction of nonpolar fluorescent dyes with EpolC1576

The behavior of the aromatic fluorescent probe TNS in the presence of EpolC1576 and dextran is depicted in Fig. 9 a and 9 b, respectively.

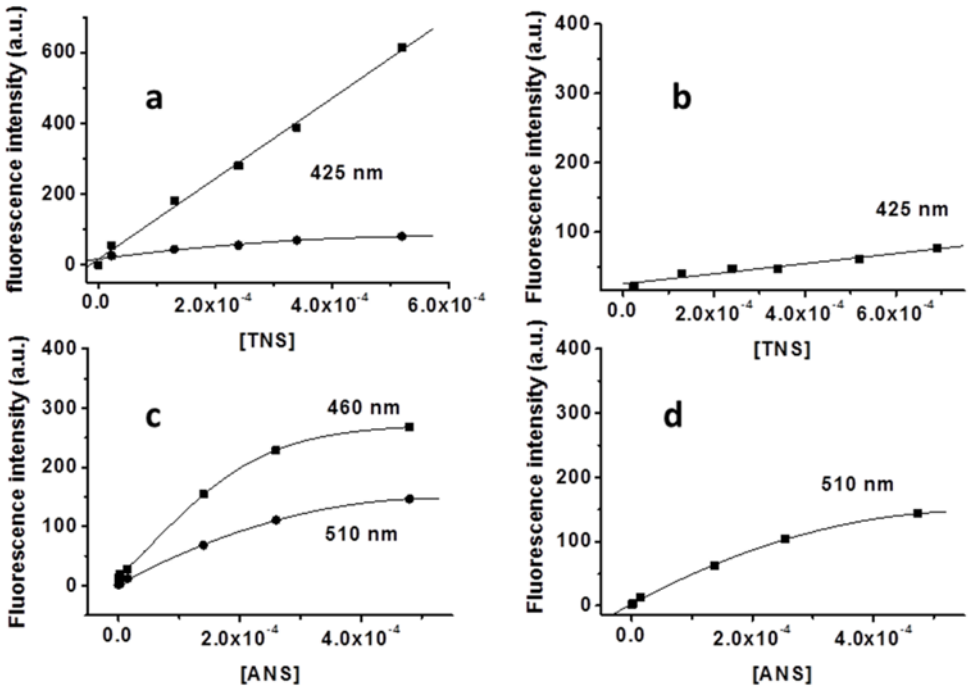

Figure 9. Fluorescence emission intensity of TNS and ANS in the presence of EpolC1576 (a and c) and dextran (b and d). ■, fluorescent aromatic probes in the presence of polysaccharides; ●, fluorescent aromatic probes in water. a.u., arbitrary units.

As proven for cyclodextrins, the encapsulation of TNS within hydrophobic pockets formed by EpolC1576 chain causes an enhancement in fluorescence emission intensity due to the decreased number of molecular collisions with water that acts as a quencher solvent molecule. Spectroscopic data clearly shows that the fluorescence emission intensity of TNS alone in water and with dextran is nearly identical and considerably lower with respect to that produced in the presence of EpolC1576. Once corrected for TNS self-absorption, the addition of EpolC1576 causes the fluorescence intensity of TNS to increase consistently (Fig. 9 a). A quite similar behavior can be seen for ANS in the presence of EpolC1576 and dextran (Fig. 9 c and 9 d). The addition of increasing concentrations of ANS to the solution containing EpolC1576 produces a marked increase in fluorescence emission intensity of the aromatic probe, but also causes a blue shift,

from 510 to 450 nm, which is a further evidence of ANS binding to EpolC1576. Indeed, as seen for tryptophan in proteins [201], fluorescence emission properties of chromophores are affected by the polarity of the surrounding environment that then may alter their emission maximum. It can be speculated that the ANS-EpolC1576 interaction promotes those solution conformations of the polymer that produce a suitable binding site that limits the solvent (water) interaction with the aromatic dyes. The slight difference in fluorescence behavior of the two aromatic probes can be attributed to their structural differences (Fig. 8 a and b).

3.3.2 NMR investigation of the interaction between aromatic dyes and EpolC1576

NMR spectroscopy analysis provided with independent evidence for ANS and TNS interaction with EpolC1576, thus suggesting different dynamics for the two hydrophobic fluorescent probes in the presence of EpolC1576 and dextran, respectively. In Fig. 10 ^{1}H NMR spectra of both TNS and ANS aromatic region obtained in the presence of EpolC1576 are compared with that recorded in the presence of dextran.

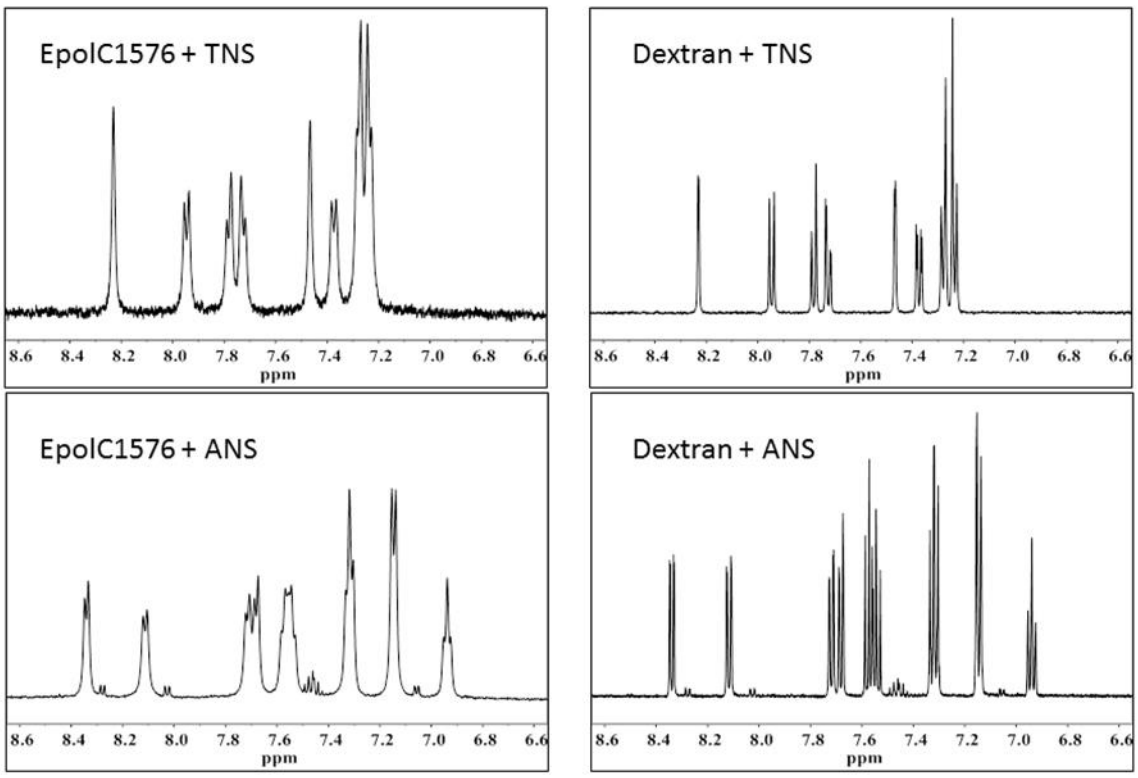

Figure 10. The ^{1}H NMR aromatic region of the spectra of fluorescent dyes TNS and ANS with EpolC1576 and dextran.

The spectra of both hydrophobic probes in the presence of EpolC1576 are characterized by a broadening of the line width of the aromatic resonance signals (Fig. 10, left panels), which are different when compared with the very sharp resonance peaks obtained for both dyes alone in solution and in the presence of dextran (Fig. 10, right panels). The broadening of resonance peaks suggest that molecular dynamics of TNS and ANS decrease, a phenomenon that can be ascribed to interactions with the hydrophobic segments of the EpolC1576 [202]. The data shown in Fig. 10 indicates that the presence of Rha and 3-*O* methylated Rha residues in the tetrasaccharide repeating unit of EpolC1576 produces domains that enable the polysaccharide to interact with hydrophobic moieties. Indeed, when compared with ^{1}H NMR spectra obtained in the presence of dextran, which displays a "common" highly hydrophilic saccharide chemistry, the interactions obtained with EpolC1576 can be seen as "supported" by the hydrophobic groups of the polysaccharide backbone. This peculiar feature of EpolC1576 may aid in disclosing the interactions necessary for the establishment and maintenance of the biofilm macromolecular matrix, but also the potential molecular mechanisms on which the biological activities of the matrix are based on. In this light, the role of quorum-sensing molecules is particularly important for their involvement in biofilm synthesis and bacterial pathogenicity. These signaling molecules often display a hydrophobic character, and interactions with EpolC1576 may regulate their activity.

3.3.3 NMR investigation of the interaction between *cis*-11-methyl-2-dodecenoic acid and EpolC1576

Once the ability of EpolC1576 to interact with hydrophobic compounds was proven, the potential interaction of *cis*-11-methyl-2-dodecenoic acid (11-Me-C12:Δ^2) with EpolC1576 was analyzed using NMR spectroscopy. Due to the very poor water solubility of the quorum-sensing molecule, a fixed amount of 11-Me-C12:Δ^2 was resuspended with an aqueous solution of either EpolC1576 or dextran to evaluate the transfer of the signaling molecule to the water phase promoted by interactions with the two polysaccharides.

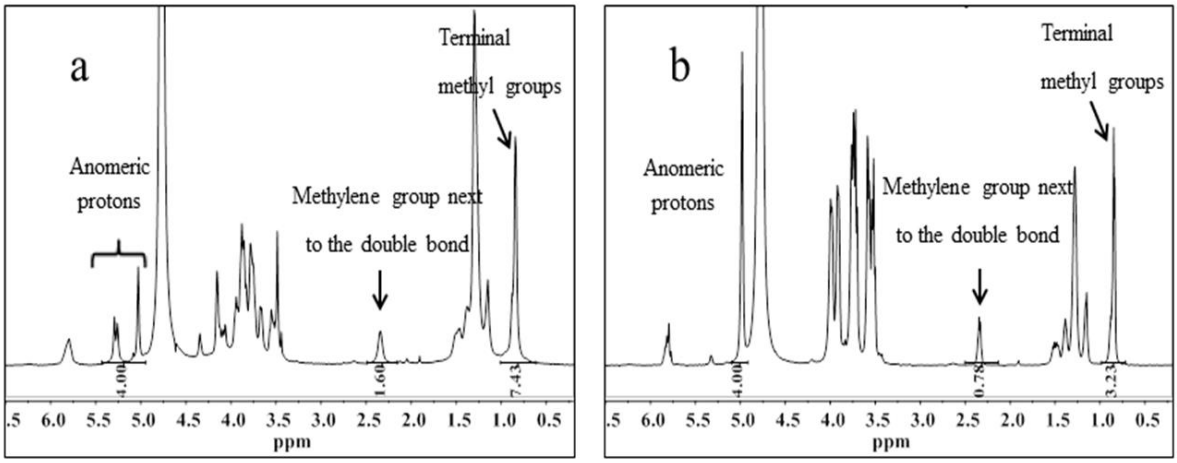

Figure 11. ^{1}H NMR spectra of the quorum-sensing molecule 11-Me-C12:Δ^2 in the presence of EpolC1576 (a) and dextran (b). Integration values of the H-1 anomeric proton signals and selected signals of the signaling molecule are shown below the spectra.

Once H-1 resonance signals of both polysaccharides were integrated with respect to distinct peaks of the signaling compound (-CH_2- at 2.3 ppm and -CH_3 at 1.0 ppm), it was noted that in the presence of EpolC1576 the solubilization of 11-Me- C12:Δ^2 in water was twofold higher (Fig. 11 a) (-CH_2-/H-1 peak area ratio = 0.40 and -CH_3/H-1 peak area ratio = 1.86) than that in the presence of dextran (-CH_2-/H-1 = 0.20 and -CH_3/H-1 = 0.81) (Fig. 11 b). This very interesting behavior of the signaling molecule in the presence of EpolC1576 led to study in more detail the nature of interaction between EpolC1576 and 11-Me-C12:Δ^2 molecule via molecular modeling simulation.

3.3.4 Modeling of hydrodynamic behavior of EpolC1576

Molecular dynamics simulations of the EpolC1576 tetramer (4 tetrasaccharide repeating units) in the presence of hydrophobic guest compounds and explicit water molecules show that in aqueous solution EpolC1576 behaves as a dynamic polymer chain having a high flexibility (Fig. 12).

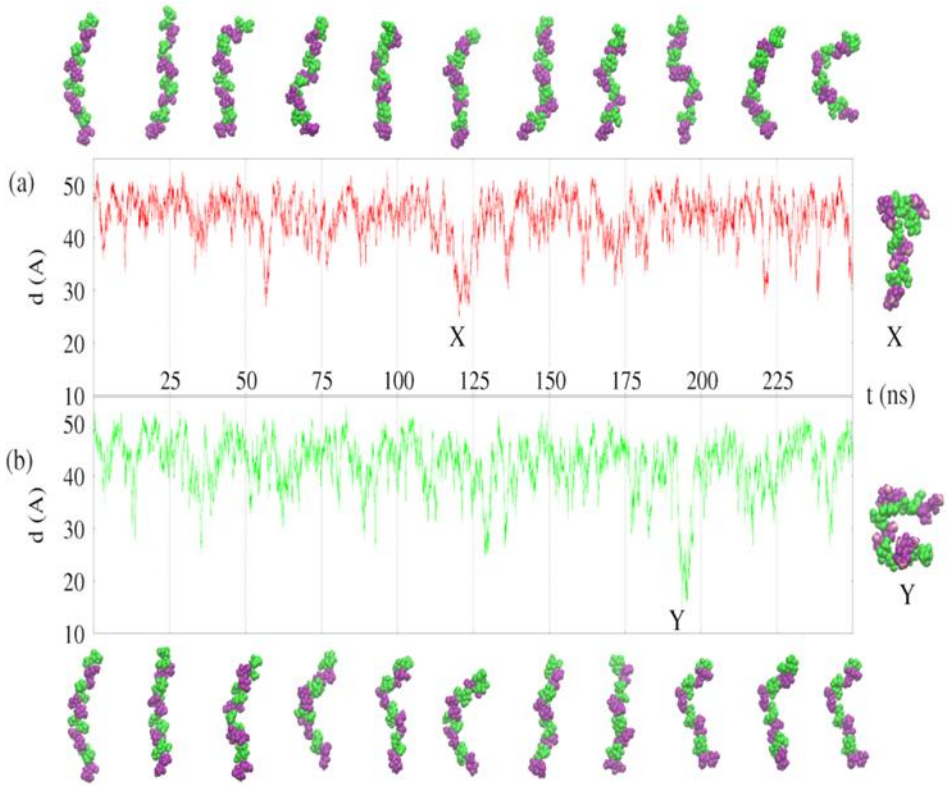

Figure 12. EpolC1576 dynamics in aqueous solution. a and b, the end-to-end molecular distance in angstroms (d(A)) during the simulation with three hexane molecules (a, red) and the simulation with the quorum sensing molecule (b, green). The conformational snapshots of the EpolC1576 tetramer are comparable for the simulations with hexane (a) and 11-Me-C12:Δ^2 (b). Mannose residues are colored green and rhamnose purple. Guest molecules, waters, and counterions are not shown. Snapshots of the most compressed conformations at X and Y are depicted on the right.

In both aqueous simulations, it was observed that EpolC1576 mainly adopts a quite elongated conformation characterized by regular and frequently occurring conformational changes, as shown in Fig. 12 a and Fig. 12 b by the end-to-end distance plots of the 250-ns simulation with hexane and 11-Me-C12:Δ^2 as guest molecules, respectively. Over the course of both simulations, the EpolC1576 chain shows to bend and straighten very rapidly, with the saccharide tetramer that does not maintain a regular structure, as can be observed from the snapshots taken from the simulation with hexane (Fig. 12 a) and the simulation with the quorum-sensing molecule (Fig. 12 b). Sporadically, EpolC1576 adopts more compact conformations favored by intramolecular interactions, as depicted by the examples X and Y in Fig. 12, a and b, respectively. However, these more compressed conformational structures do not exist for long periods of time in aqueous solution. Therefore, EpolC1576 is a carbohydrate

chain characterized by a high degree of flexibility that enables the polymer to undergo rapid conformational modifications in response to environmental changes.

3.3.5 Modeling of interactions of EpolC1576 with nonpolar guest compounds

Over the course of the 250-ns simulation, the three guest molecules of hexane have frequent interactions with EpolC1576. The plot of carbon-carbon contacts less than 5 Angstrom Å for EpolC1576-hexane in the last 50 ns (Fig. 13) is an accurate approximation of the entire 250-ns simulation: close interactions between EpolC1576 (host) and hexane molecules (guest) take place very frequently.

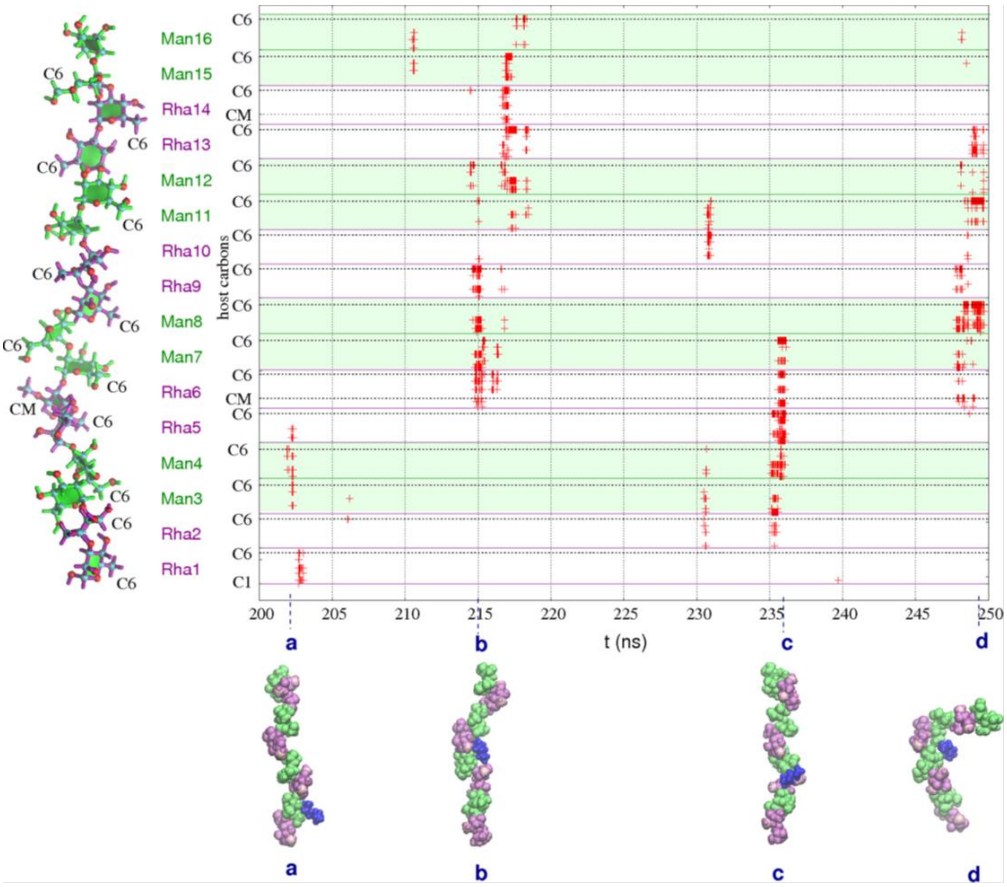

Figure 13. EpolC1576-hexane atomic contacts. It is shown a time series plot of the host-guest carbon-carbon contacts less than 5 Å for the last 50 ns of the simulation of EpolC1576 with three hexane guest molecules. Carbons are numbered consecutively along the y axis, from C1 in the Rha1 residue (bottom) to C6 in the Man16 residue (top). The specific localizations of the C6 and CM (3-O-methyl substituent) atoms are illustrated on the y axis. Interactions to which mannose residues participate are differentiated from those relative to rhamnose with background green shading. Representative snapshots of host-guest conformations are shown in a–d. Mannose residues are green, rhamnose purple, and O-methyl carbons pink.

The EpolC1576-hexane host-guest interaction shows to be very dynamic; even though two pairs of consecutive mannose/rhamnose residues participate to the interactions with hexane, the site of the non-bonded contact changes continuously. At least one rhamnose methyl atom (either C6 or the 3-*O*-methyl substituent, as indicated on the y axis in Fig. 13) usually participates to the interaction. Contacts of the hexane molecule with more than one carbon atom on a single monosaccharide residue are not infrequent and suggest that the guest aliphatic molecule orients itself to face the plane of the pyranose ring, as for Rha6 in the interaction marked b in Fig. 13. Where the guest molecule interacts at the same time with four or more host monosaccharide residues, the EpolC1576 chain has produced a pocket to accommodate a hexane guest molecule, as can be seen from snapshots taken at 215 ns (Fig. 13 b) and 235 ns (Fig. 13 c). The contiguous rhamnose residues with partial *O*-methyl substitutions mainly participate in the formation of these cavities, whereas mannose residues edge the cavities with the hydrophobic plane of their pyranose ring. When these pockets are produced, prolonged host-guest interaction that last for up to 2 ns may occur. Contacts of the guest hydrocarbon molecule with EpolC1576 are more frequent when compared to those involving 11-Me-C12:Δ^2, with 10% vs 8% of simulation time occupied by close host-guests interaction. This is not surprisingly, since there are more guest molecules in the simulation with hexane, and they diffuse faster than 11-Me-C12:Δ^2. However, the fact that the signaling molecule has a longer aliphatic chain and/or an amphipathic nature allows for prolonged interactions with respect to hexane, as can be observed by comparing the plots of guest-host carbon-carbon distances less than 5 Å for EpolC1576/hexane (Fig. 13) and EpolC1576/11-Me-C12:Δ^2 (Fig. 14).

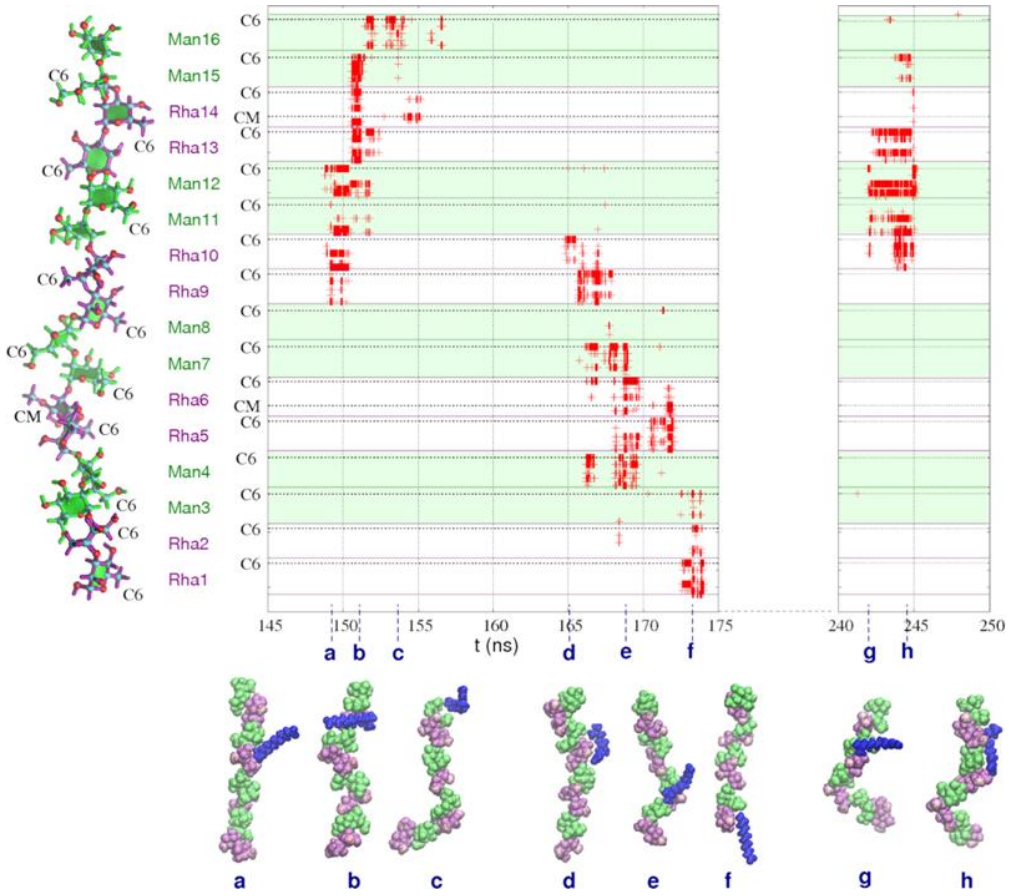

Figure 14. EpolC1576-11-Me-C12:Δ² atomic contacts. It is shown a time series graph of carbon-carbon contacts less than 5Å for the three-long host-guest interactions in the simulation of EpolC1576 and the signaling guest molecule 11-Me-C12:Δ². The specific locations of the C6 and CM (3-O-methyl substituent) atoms are indicated on the y axis. Interactions involving mannose residues are distinguished from rhamnose with background green shading. Representative snapshots of host-guest conformations are shown in a–h. Mannose residues are green, rhamnose purple, and O-methyl carbons pink.

The simulation performed with EpolC1576 and 11-Me-C12:Δ² is characterized by three long periods with recurring close host-guest contacts: from 148.6 to 155.5 ns (lasted 6.9 ns), from 164.7 to 174.4 ns (9.7 ns), and from 241.9 to 245.6 ns (3.7 ns). Longer contact with the rhamnose methyl carbons (either C6 or the 3-*O*-methyl substituent, as indicated on the y axis in Fig. 14) are a clear feature of these prolonged interactions. In the first-long interaction, from 148.6 to 155.5 ns, the EpolC1576 chain forms a pocket that involves a pair of central recessed rhamnose residues to enclose the signaling guest molecule (Fig. 14 b). The high flexibility of its chain potentially enables EpolC1576 to produce deep nonpolar cavities. In addition, during the temporal window going from 164.7 to 174.4 ns, interactions of 11-Me-C12:Δ² with EpolC1576 are very dynamic. The

continuous change of the site of non-bonded contacts is distinctly evident in the plot shown in Fig. 14: the signaling molecule "walks" down the EpolC1576 chain during the 9 ns of the second-long interaction (look at the snapshots in Fig. 14, d–f). In this light, the signaling molecule 11-Me-C12:Δ^2 may quickly move across the carbohydrate scaffold of the biofilm matrix. Moreover, the signaling molecule may act as a bridge between distinct EpolC1576 strands. The second-long host-guest interaction also shows the formation of a hydrophobic pocket at around 169 ns, illustrated in the snapshot in Fig. 10 e. During the third-long interaction (from 241.9 to 245.6 ns) the guest molecule interacts in its entirety with six successive monosaccharide residues of the EpolC1576 tetramer (Fig. 14 h). This is a further indication of the multiple modes of possible interactions between EpolC1576 and the quorum sensing molecule 11-Me-C12:Δ^2.

3.3.6 Saturation-Transfer Difference NMR analysis of the interaction between EpolC1576 and three small ligands (ANS, TNS and Kanamycin)

Saturation-Transfer Difference NMR (STD NMR) experiments were kindly performed by Prof. Jesus Angulo's research group at the University of East Anglia (Norwich, United Kingdom). Beside fluorescence spectroscopy results, the broadening of ^{1}H NMR resonance lines of both ANS and TNS in the presence of EpolC1576 was the second experimental evidence that the two hydrophobic fluorescent probes complex with the polymer. Interactions between EpolC1576 and both ANS and TNS were further demonstrated by use of STD NMR. The STD-NMR spectra of both hydrophobic fluorescent probes showed intense STD signals (data not shown), thus suggesting that ANS and TNS actively interact with EpolC1576. Structural details of the binding epitopes of ANS and TNS were obtained under two different EpolC1576 irradiations: (i) at 1.22 ppm, i.e. irradiating the -CH_3 groups of the Rha residues in the polysaccharide, and (ii) at 3.77 ppm, i.e. irradiating mostly the C-H carbohydrate region. Interestingly, the level of saturation received by both hydrophobic fluorescent probes was lower when the C-H protons at 3.77 ppm were irradiated (Fig. 15 a and 16 a).

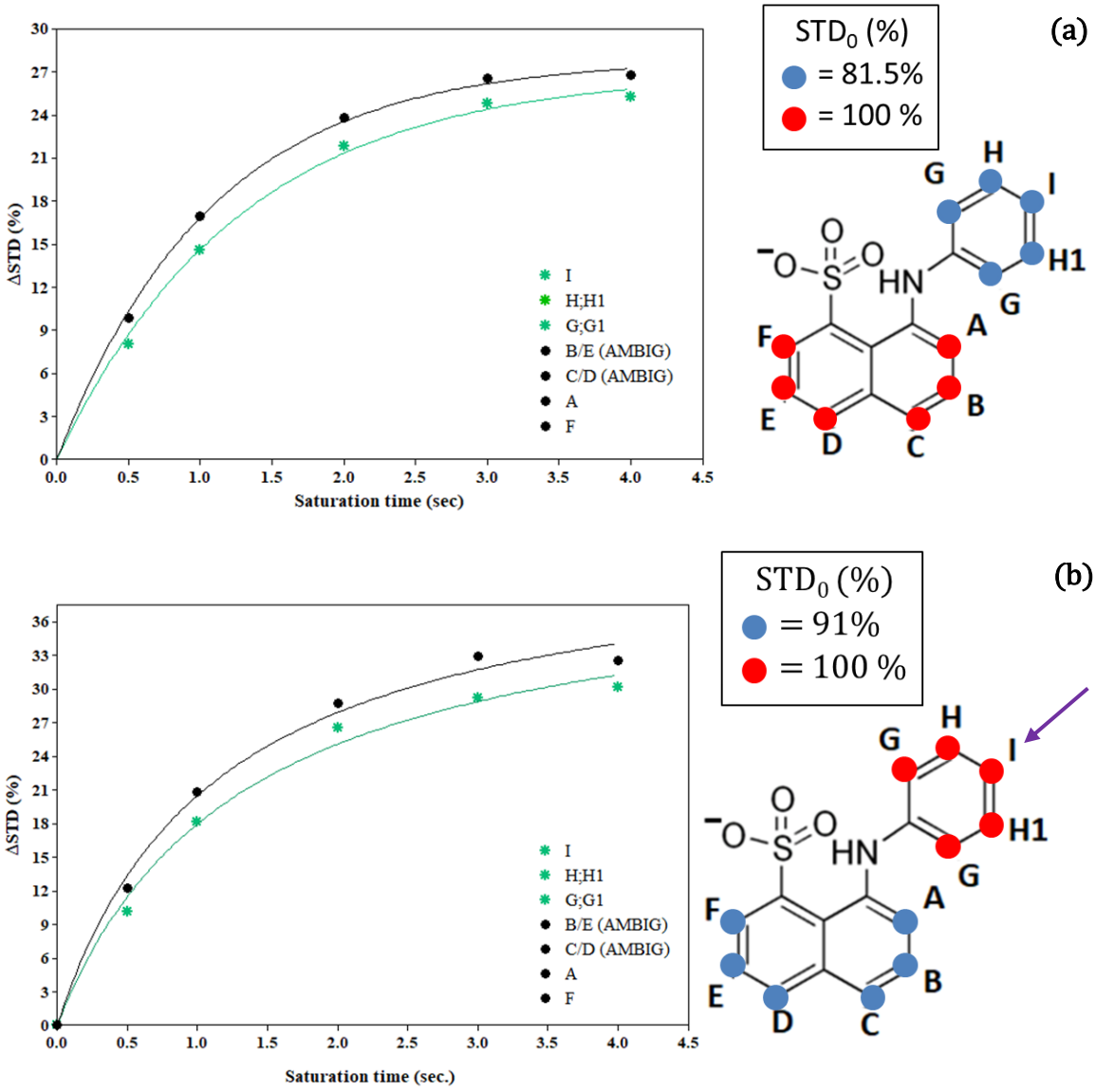

Figure 15. Epitope mapping for ANS and STD growth curves as a function of saturation time. The relative degrees of saturation of the individual protons expressed in % are mapped onto the structure (red and blue dots) and normalized to those of protons showing the most intense STD effect (thus they were arbitrarily set to 100%) for both irradiation conditions. The protons of ANS receiving the highest saturation are A-F (red dots, a) at 3.77 ppm irradiation, whereas protons G, G1, H, H1, I (red dots, b) at 1.22 pm irradiation showed the most intense magnetization. STD growth curves show the degree of involvement of ANS protons in the binding to EpolC1576 as a function of saturation time.

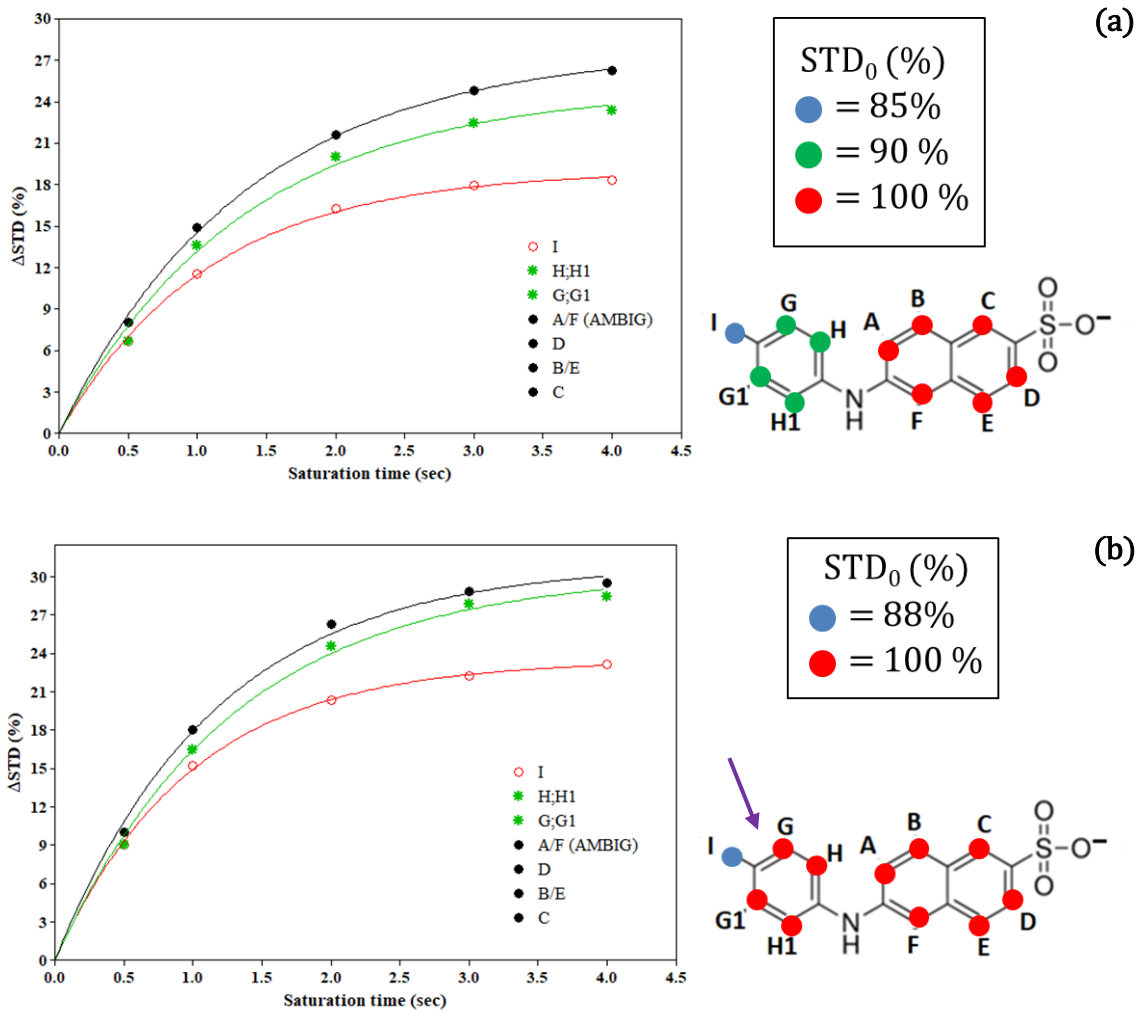

Figure 16. Epitope mapping for TNS and STD growth curves as a function of saturation time. The relative degrees of saturation of the individual protons expressed in % are mapped onto the structure (red and blue dots) and normalized to those of protons showing the most intense STD effect (thus they were arbitrarily set to 100%) for both irradiation conditions. The protons of TNS receiving the highest saturation are A-F (red dots, a) at 3.77 ppm irradiation, whereas protons A-H, G1 and H1 (red dots, b) at 1.22 pm irradiation are the most intensely in involved in the interaction with the polymer. STD growth curves showing the degree of involvement of TNS protons in the binding to EpolC1576 as a function of saturation time.

Considering that in that case not only the rhamno-pyranose rings, but also the manno-pyranose ones were irradiated, this result indicates that both ANS and TNS seems to spend more time around the -CH_3 groups producing higher saturation when irradiating at 1.22 ppm. Moreover, when -CH_3 groups of EpolC1576 were saturated rather than the C-H carbohydrate region to map the binding epitopes, some specific aromatic ring (Fig. 15 b and 16 b, purple arrows) of the molecules show increased saturation. This key information can be interpreted as if this particular ring is in close contact to the -CH_3 group, most likely involved in a CH-pi stacking interaction.

Biofilm formation is thought to play a role in bacteria tolerance to antimicrobial agents as distinct EPS molecules can decrease the rate of penetration of specific compounds by interacting with them [145]. To disclose a potential involvement of EpolC1576 in tolerance of *B. multivorans* C1576 to antibiotics, the nature of the interaction between EpolC1576 and the aminoglycoside antibiotic Kanamycin was monitored by STD NMR. Fortunately, Kanamycin was shown to "transiently" interact with EpolC1576, thus allowing an STD NMR experiment to be performed. Unlike ANS and TNS, Kanamycin contains pyranose rings whose resonances cover the region 4.5-3.2 ppm, thus making saturation of EpolC1576 rhamno- and manno-pyranoses not possible at 3.77 ppm. For this reason, two other resonances were used for the saturation pulse, 1.2 and -1.0 ppm. Respectively, these resonances are specific for methyl groups (-CH_3) and -CH moiety (very general) of the core of the EpolC1576. Fig. 17 and 18 show the analyses of the epitopes derived by the two different saturation frequencies used.

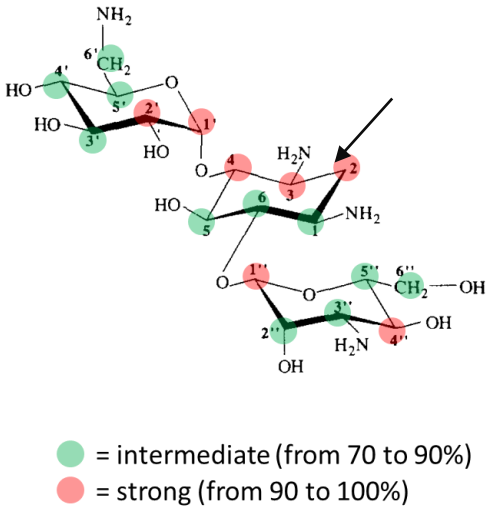

Protons position	Normalized STD intensities	STD growth curve
1’	99,9	A
1”	99,8	B
5’	85,3	C
2”	82,2	D
5" 3’ 5 6"	78,9	E
4 2’ 4"	94,9	F
6 4’ 3" 1 6’	85,9	G
3	98,2	H
2e	95,1	I
2a	100	K

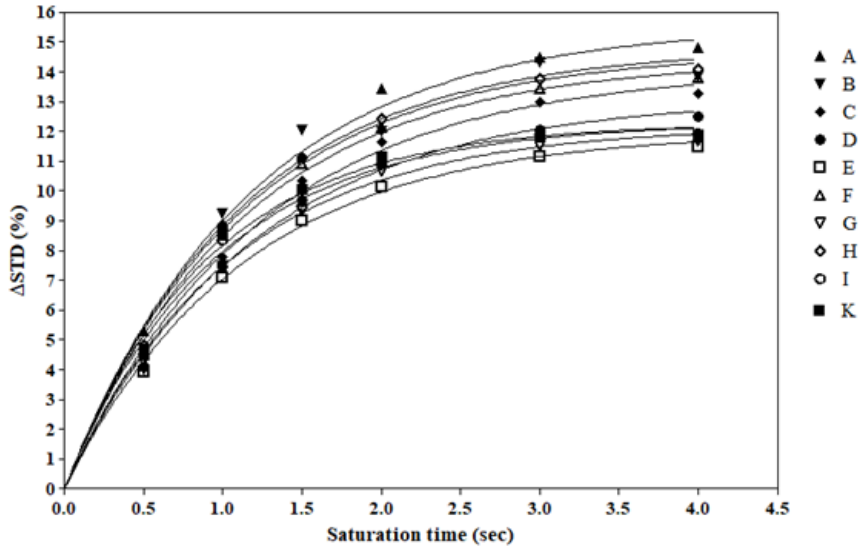

Figure 17. Epitope mapping for Kanamycin after irradiation of EpolC1576 -CH moieties at -1 ppm and STD growth curves as a function of saturation time. The relative degrees of saturation of the individual protons expressed in % and normalized to that of proton 2 (black arrow), which showed the most intense STD effect (thus it was arbitrarily set to 100%), are mapped onto the antibiotic structure (red and blue dots) and reported in the table. Axial proton at position 2 (2a, Table) received the most intense saturation. STD growth curves showing the degree of involvement of Kanamycin protons in the binding to EpolC1576 as a function of saturation time.

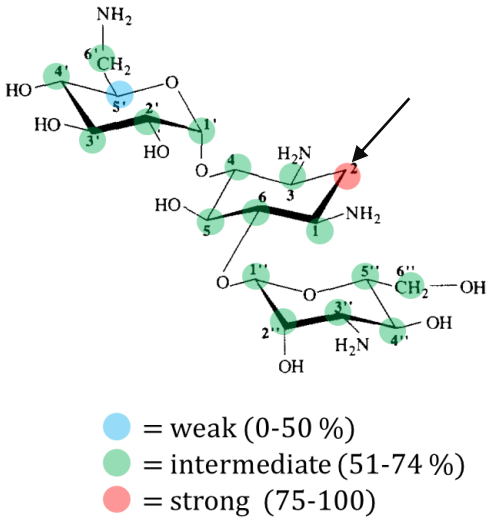

Protons position	Normalized STD intensities	STD growth curve
1’	53,346	A
1”	57,555	B
5’	50,417	C
2”	54,179	D
5" 3’ 5 6"	51,060	E
4 2’ 4"	53,278	F
6 4’ 3" 1 6’	67,546	G
3	51,808	H
2e	74,452	I
2a	100	K

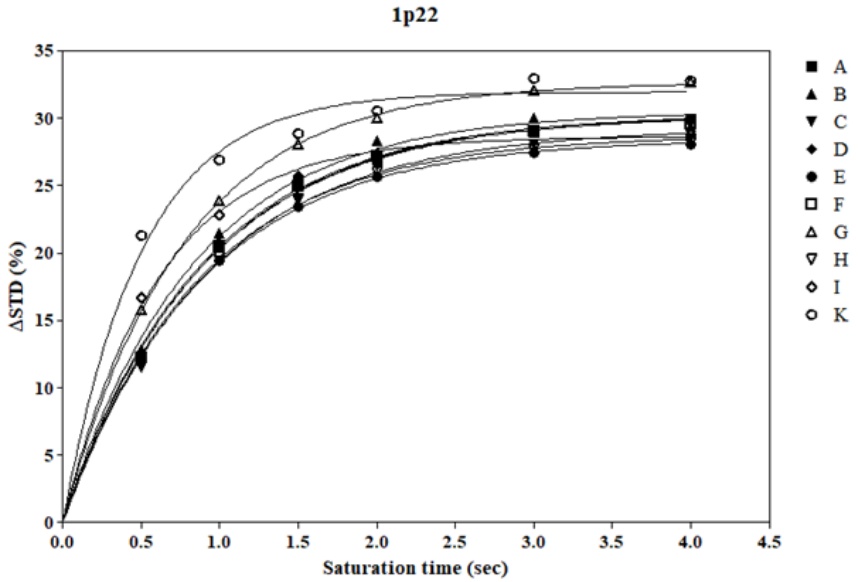

Figure 18. Epitope mapping for Kanamycin after irradiation of EpolC1576 methyl groups at 1.22 ppm and STD growth curves as a function of saturation time. The relative degrees of saturation of the individual protons expressed in % and normalized to that of proton 2 (black arrow), which showed the most intense STD effect (thus it was arbitrarily set to 100%), are mapped onto the antibiotic structure (red and blue dots) and reported in the table. As for irradiation at -1 ppm, axial proton at position 2 (2a, Table) revealed to be most intensely saturated proton. STD growth curves showing the degree of involvement of Kanamycin protons in the binding to EpolC1576 as a function of saturation time.

They indicate that position 2 (black arrow) on the Kanamycin structure is always found as the site that received the highest transfer of magnetization. This suggests that, in the case of Kanamycin, this region is in direct contact with the polysaccharide and should be found at the interface of the binding. However, it does not mean that other

regions of the Kanamycin molecule may also be involved in the binding as they show an intermediate (green dots) to strong (red dots) transfer of saturation which may be due to several binding sites participating in the interaction.

To further and better evaluate the epitope, an STD-HSQC experiment was performed. The HSQC (Heteronuclear Single Quantum Coherence) experiment determines proton-carbon single bond correlations. Using this technique, it was possible to derive the epitope only by saturating at 1.22 ppm due to the low concentration of Kanamycin used and to the fact that the experiment was performed in ^{13}C natural abundance. In fact, positioning the saturation pulse at -1 ppm the transfer of saturation was less efficient and no STD HSQC spectra could be detected. Anyway, it is interesting to note that also from this technique the position 2 of Kanamycin (Fig. 19) is found to be involved in the interface of binding.

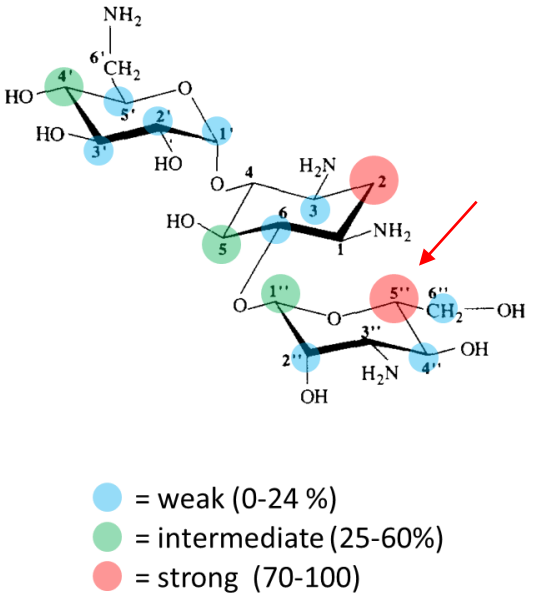

Carbons-Protons position	Normalized STD intensities
1’	45,8
1”	18,5
6	13,3
5”	100
2"	3,1
3’	18,3
2’	10,8
4’	29,4
5’	0,71
5	26,9
4”	19,6
6”	1,64
3	11,22
6’	3,28
2	82,47

Figure 19. Epitope mapping for Kanamycin after irradiation of EpolC1576 at 1.22 ppm over the course of an STD HSQC experiment. The relative degrees of saturation of the individual protons expressed in % and normalized to that of proton 5”, which showed the most intense STD effect (thus it was arbitrarily set to 100%), are mapped onto the antibiotic structure (red and blue dots) and reported in the table. STD HSQC signals are low due to the low concentration of Kanamycin and the fact that the experiment is based on the natural abundance of ^{13}C isotope. Interestingly, position 5” showed to receive the most intense magnetization.

Moreover, position 5" of Kanamycin (Fig. 19, red arrow) is also involved in the interface of the binding site while other possible sites this time show degrees of saturation from weak (Fog. 19, light blue dots) to intermediate (Fig. 19, green dots). Reassuming, during the interaction of Kanamycin with EpolC1576, site 2 is always found at the interface of binding even in the presence of a multisite model as presumed for this antibiotic. Since Kanamycin is a pseudo-trisaccharide molecule carrying four amino groups, STD NMR analysis of the interaction between EpolC1576 and Kanamycin suggests that carbohydrate-carbohydrate interactions occur and that they might have important biological implications for the modulation of aminoglycoside antibiotics activity, for example.

3.3.7 HPSEC and NMR analyses of EpolC1576 fragments

The products of chemical hydrolysis of native EpolC1576 with 0.5 M TFA for 2 hours at 80 °C were first analyzed by High Pressure Size Exclusion Chromatography (HP-SEC). The chromatogram of the reaction products (Fig. 20) indicates that hydrolysis of EpolC1576 was only partial and produced a distribution of molecular weights of saccharide fragments.

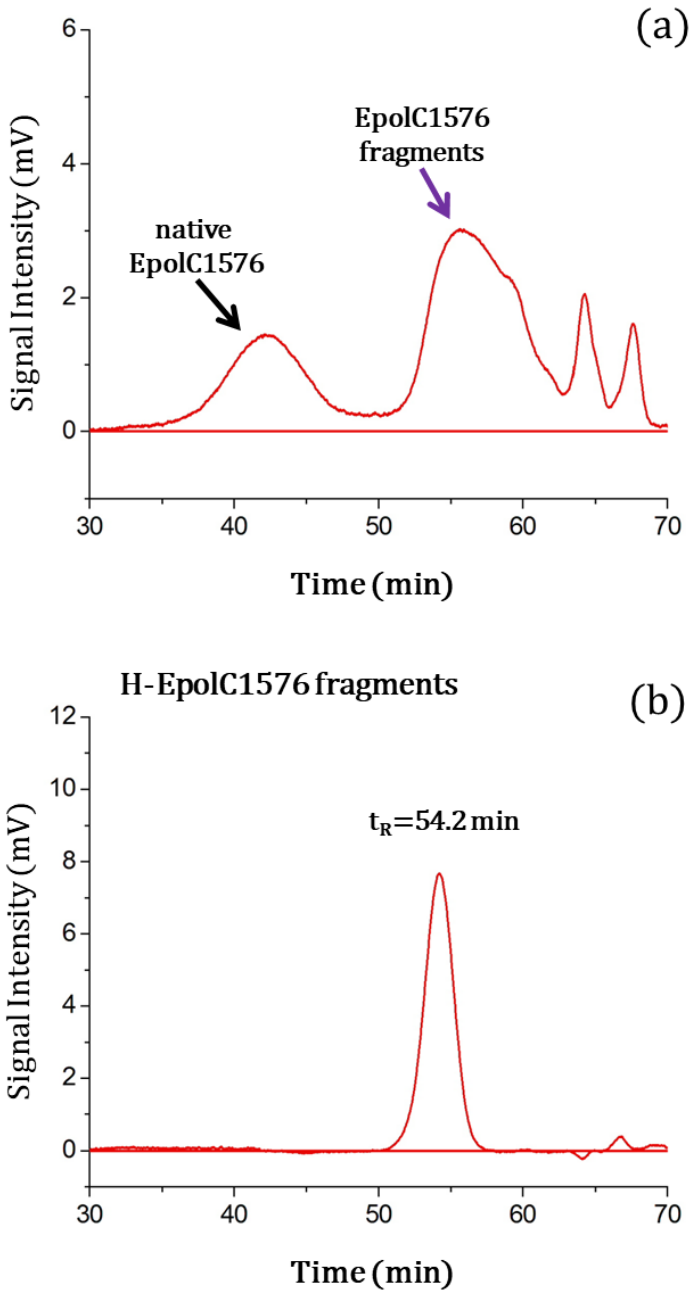

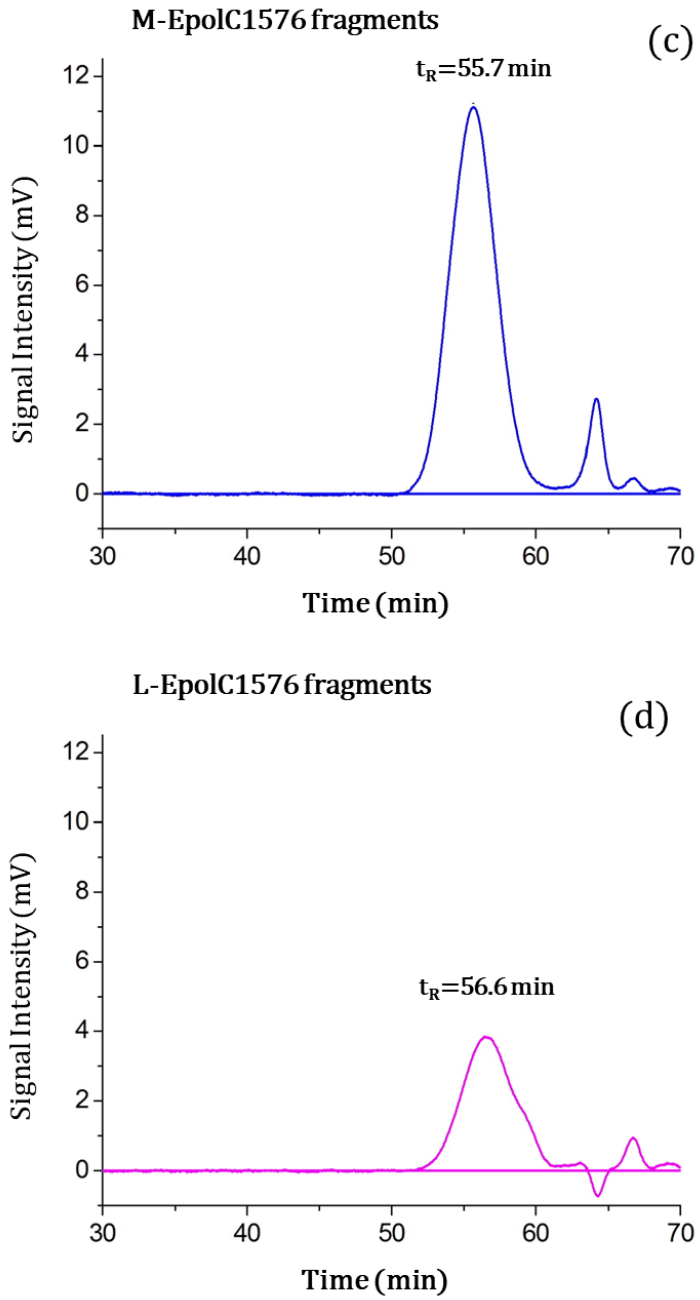

Figure 20. HP-SEC analyses of products of hydrolysis of EpolC1576 (a) and of high, medium and low molecular weight EpolC1576 fragments (b, c, d). Native EpolC1576 eluted after 42.1 min to which corresponds an apparent MW of 880 kDa (b) H-EpolC1576 fragments eluted after 54.2 min (t_R) to which corresponds an apparent MW of 18 kDa; (c) M-EpolC1576 eluted after 55.7 min (t_R) to which corresponds an apparent MW of 12 kDa, whereas (d) L-EpolC1576 fragments eluted after 56.6 min (t_R) to which corresponds an apparent MW of 10 kDa.

Due to the polydispersity of EpolC1576 fragments, the relative peak was split into three pools of fractions that were subsequently injected to determine the apparent molecular weight of each (Fig. 20 b, c and d). The three pools of fractions were named high (H),

medium (M) and low (L) molecular weight EpolC1576 fragments (H-, M- and L-EpolC1576). By using a calibration curve built-up with carbohydrate molecular weight standards (pullulans) and accordingly to their retention times (t_R), it was found that H-, M-, and L-EpolC1576 fragments had molecular weight of approximately 18, 12 and 10 kDa respectively (Fig. 20 b, c and d).

After HP-SEC analysis, each pool of fractions was analyzed resorting to NMR to see whether TFA hydrolysis affected the structure of EpolC1576 fragments. Figure 21 shows that NMR spectra of native EpolC1576 (a), high (b), medium (c) and low (d) molecular weight fragments of EpolC1576 are practically identical, suggesting that TFA had not modified the chemical structure of EpolC1576.

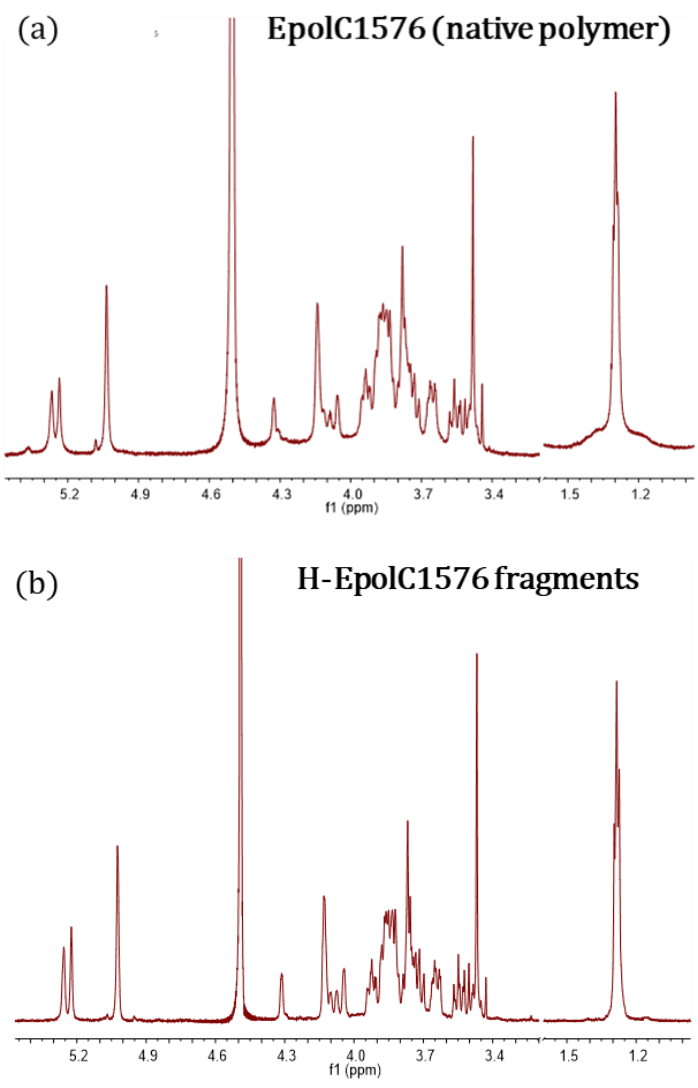

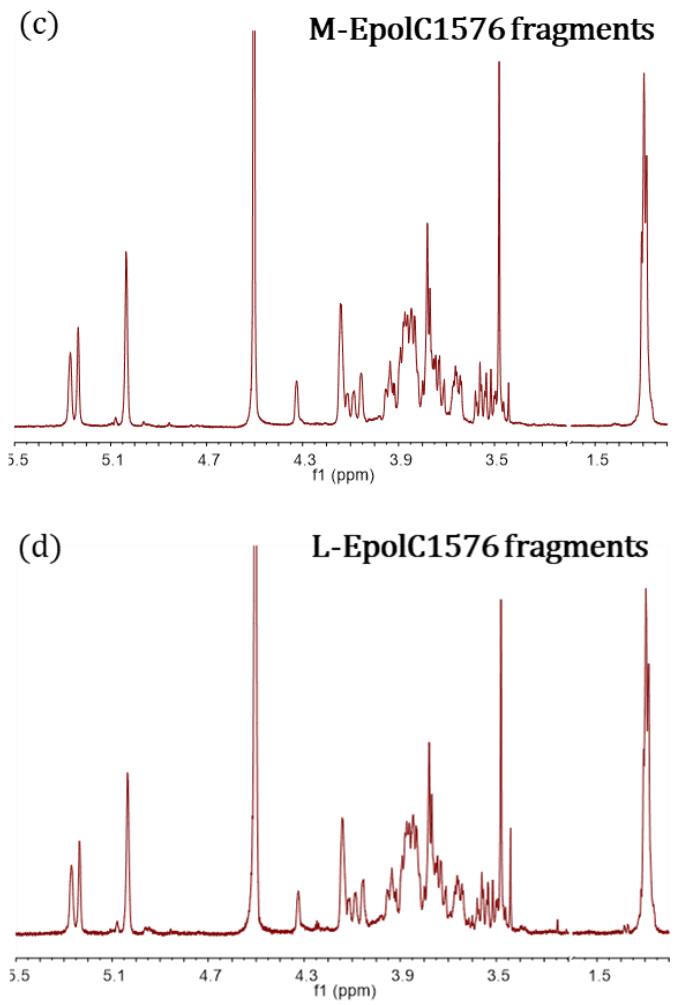

Figure 21. NMR spectra of native EpolC1576 (a) and of high (b), medium (c) and low (d) molecular weight fragments of EpolC1576 coming from the polymer chemical hydrolysis. Saccharide fragments do not show any signal differences with respect to those of the native EpolC1576.

3.3.8 Surface Plasmon Resonance (SPR) analysis of EpolC1576 interaction with a monolayer of long chain alkanes

The binding capacity of EpolC1576 to long hydrophobic alkyl chains was investigated by the Surface Plasmon Resonance (SPR) technique using an HPA sensor chip. The HPA chip presents a flat hydrophobic surface consisting of long chain alkane-thiol molecules covalently coupled to a gold film (Biacore Sensor Surface handbook page 18). Solutions of M-EpolC1576 fragments were then injected in sequence continuous flow and washing cycles, doubling the concentration at each successive run (from 5.2 to 167 µM). Dextran, chosen as negative control, was injected at the same concentrations tested for M-EpolC1576 fragments. In both cases a binding sensorgram was obtained, with resonance units (RU) increasing in a concentration-dependent manner (Fig. 22 a and b).

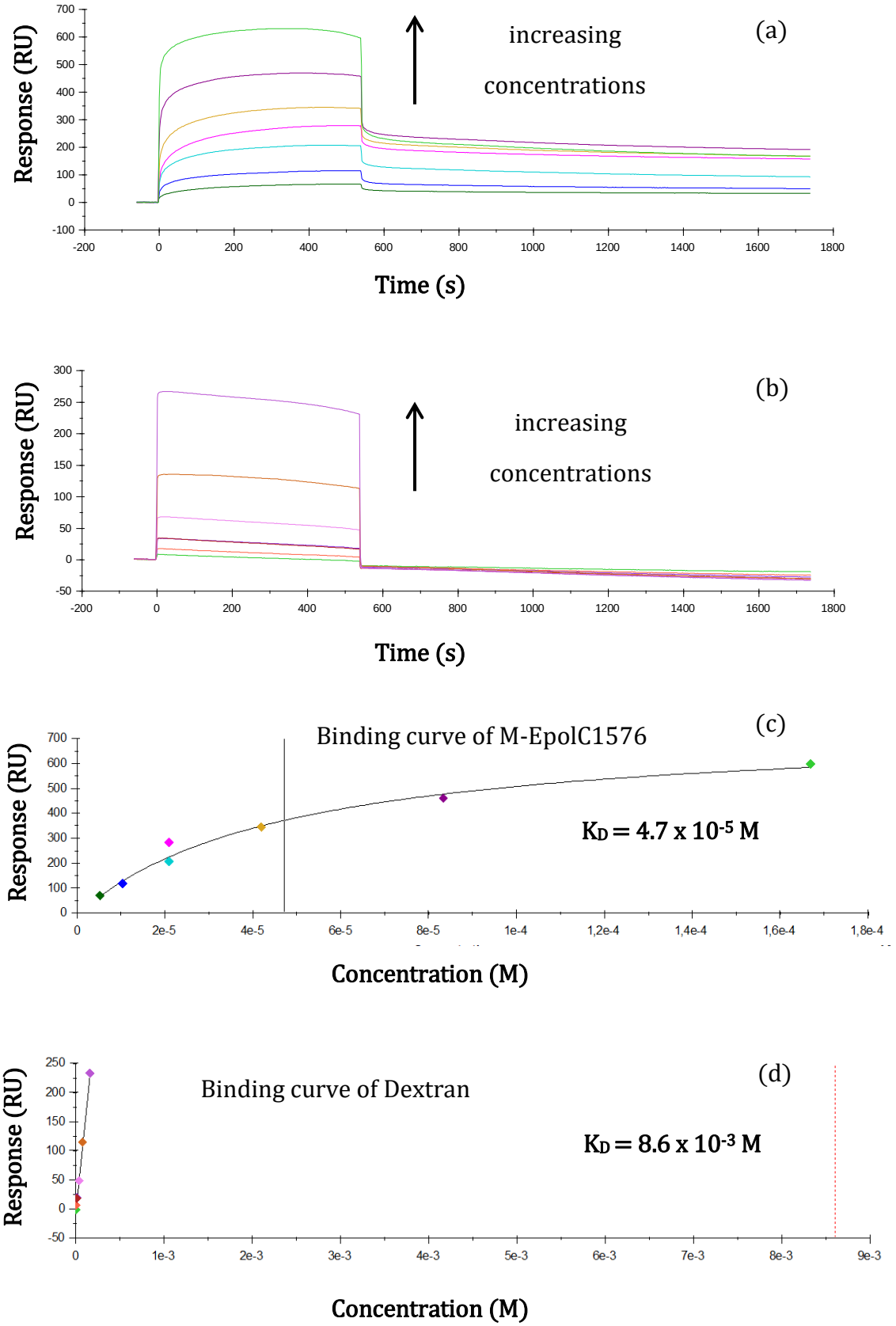

Figure 22. Binding sensorgrams (a, b) and binding curves (c, d) for M-EpolC1576 (a, c) and for Dextran (b, d). Sensorgrams were obtained flowing M-EpolC1576 fragments (12 kDa) and Dextran (12 kDa) at increasing concentrations (to each concentration corresponds a different color) over unmodified HPA sensor chip surface. Binding curves show the binding response at

the end of the injection (t: 540 s) for each concentration used. Data fitting and K_D calculation were performed using the "Affinity-Steady State" mathematical model incorporated in the BiaEvaluation software.

Interestingly, for each concentration M-EpolC1576 fragments show a marked increase in RU of binding with respect to dextran, suggesting the polymer fragments bind to alkyl chain molecules with a good affinity and better than dextran. During the dissociation phase (washing step), the binding sensorgram for M-EpolC1576 fragments did not return to the baseline (Fig. 22 a), thus indicating the formation of a stable complex between the saccharide fragments and alkyl chains. On the contrary, dextran molecules were easily washed away (Fig. 22 b) suggesting that their binding to the hydrophobic surface is very weak. This data is in good agreement with fluorescence and NMR analyses which already showed the interaction of EpolC1576 with hydrophobic compounds, including the quorum sensing signal factor cis-2-methyl-11-dodecenoic acid. SPR results suggest that EpolC1576 significantly interacts with nonpolar compounds; in this light the polymer might enhance solubility and bioavailability of hydrophobic biologically active molecules in highly hydrated environments such as the biofilm matrix. For EpolC1576 it was calculated an equilibrium dissociation constant (K_D) of 4.7 x 10^{-5} M (Fig. 22 c). Since the binding curve of dextran did not reach the saturation (Fig. 22 d), it was not possible to calculate the effective K_D; the estimated K_D for dextran was 8.6 x 10^{-3} M.

3.3.9 Visualization of conformational behavior of EpolC1576 by atomic force microscopy (AFM)

In order to elucidate the role of EpolC1576 in biofilm formation and assembly, its conformational properties and ability to aggregate were studied by means of Atomic Force Microscopy imaging. Two micro-images of the native EpolC1576 at different concentration are shown in Fig. 23 (a and b).

(a) (b)

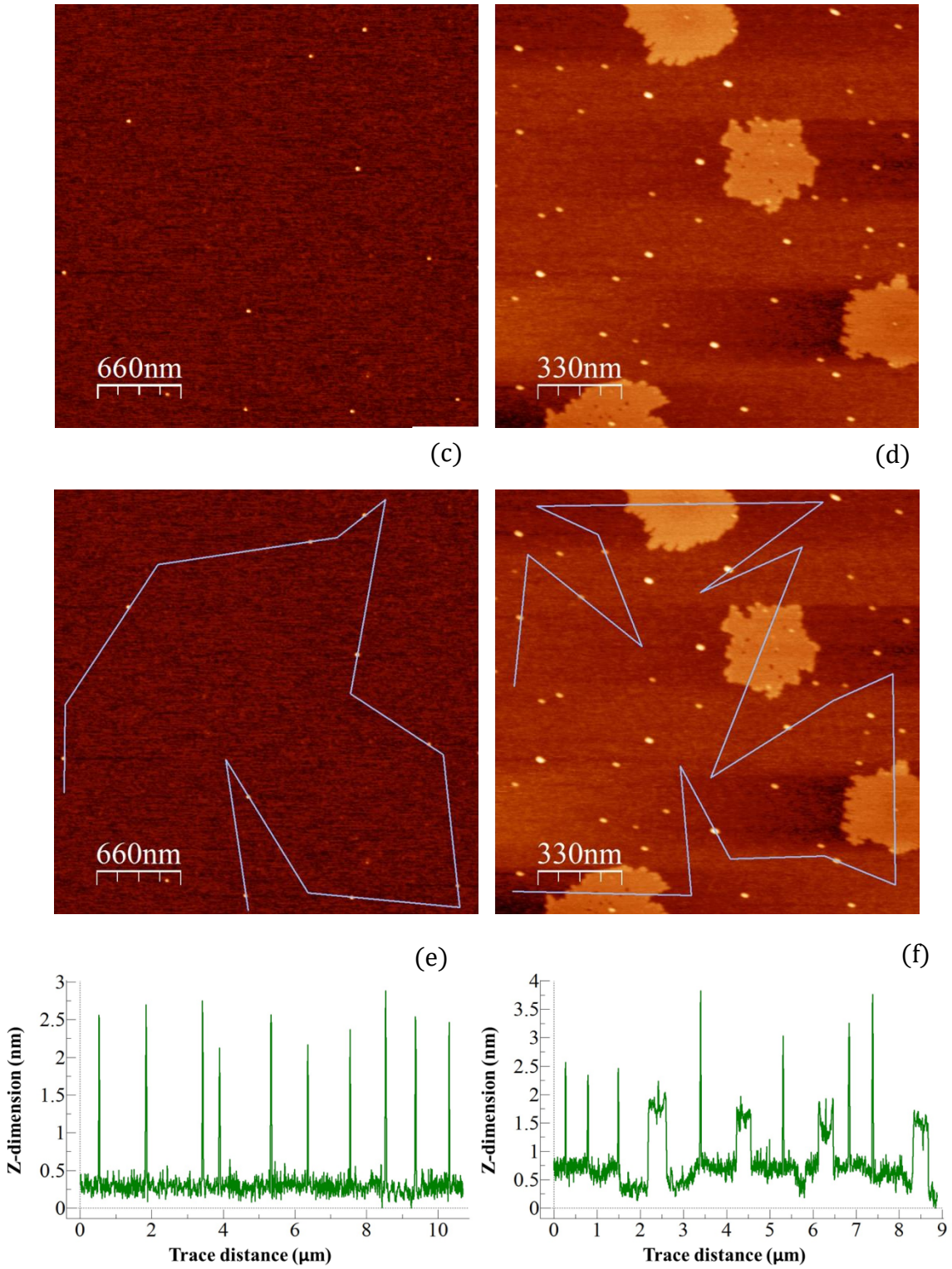

Figure 23. AFM image of native EpolC1576 recorded in tapping mode after spray-drying onto mica surface. (a and c, left) Polymer concentration 5 µg/mL in water. (b and d, right) Polymer concentration 30 µg/mL in water. (e, left) Trace through ten polymeric species showing vertical height taken from the vertical image of EpolC1576 at 5 µg/mL in water. (f, right) Trace through seven polymeric species and three aggregates formed by polymeric species showing vertical height taken from the vertical image of the polymer at 30 µg/mL in water. (Z-dimension = height).

The micro-image of the polymer at low concentration (5 µg/mL, Fig. 23 a) shows single molecular species characterized by an apparently spherical conformation. Besides single molecular species of the native polymer, the micro-image at high polymer concentration (30 µg/mL, Fig. 23 b) interestingly shows large aggregates of EpolC1576 molecules. The statistical analysis of the height of the polymeric molecules both existing as single units and forming aggregates, after subtracting the surface contribution of the mica support, revealed that single polymeric units produce objects usually larger than those giving rise to the aggregates. The average height of selected single EpolC1576 molecules (grey line, Fig. 23 c) is 22.4 $\pm$ 2.6 Å for the sample at low concentration, whereas the average height of EpolC1576 at high concentration is 23.8 $\pm$ 5.8 Å for single spheres and 11.3 $\pm$ 3.3 Å for those ones organized in aggregates (grey line, Fig. 23 d). The statistical analysis suggests that polymeric aggregates mainly consist of EpolC1576 molecules of low height values with respect to single polymer species. This might be due to the fact that packing efficiency of spherical molecules/objects increases with decreasing in size. It must be considered that polydispersity of native EpolC1576 might influence this particular distribution. In Fig. 24 a micro-image of an elongated aggregate of EpolC1576 (a, left) at high concentration and an enlargement of a section of it (b, right) are shown.

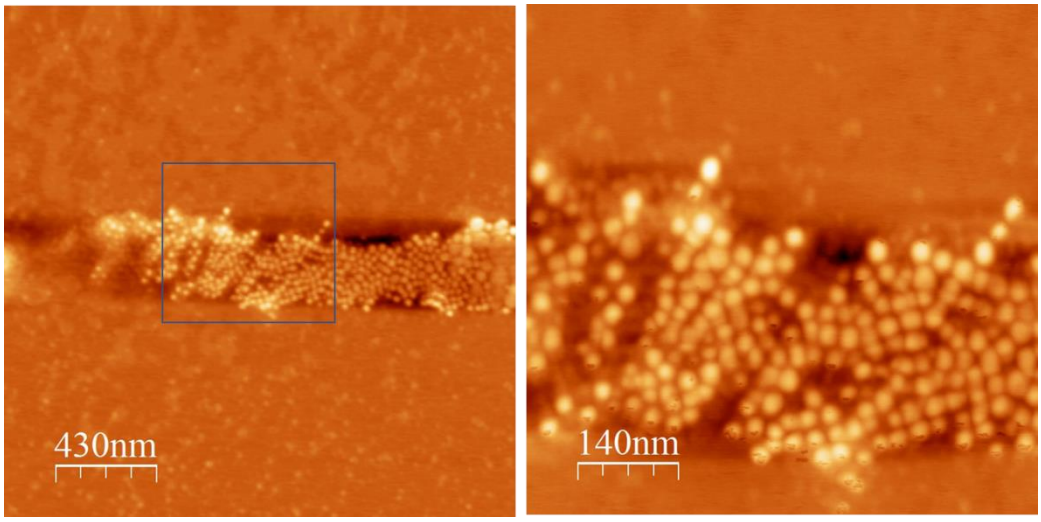

Figure 24. AFM image of native EpolC1576 recorded in tapping mode after spray-drying onto mica surface. The micro-image on the left (a) shows a long formation of clustered EpolC1576 (30 µg/mL). On the right an enlargement of the aggregate where single EpolC1576 are distinguishable from each other.

The single polymeric units forming the aggregate are clearly distinguishable from each other and they are densely-packed. Again, EpolC1576 molecules seem to adopt a

spherical conformation. It can be speculated that due to the high flexibility of EpolC1576, as water molecules evaporates during the preparation of the sample, as required for AFM analysis, hydrophobic chain segments of EpolC1576 might start interacting with each other, thus promoting the formation of a globular polymeric molecule with the most hydrophilic domains on the outside. The latter may densely pack thanks to hydrogen bonds and/or weak interactions. However, it cannot be ruled out that EpolC1576 molecules might collapse upon themselves once deprived of water molecules, thus adopting a conformation that apparently resembles a spherical one.

4 PART II - Investigation of the macromolecular matrix components of *B. multivorans* C1576 biofilm matrix

4.1 INTRODUCTION

Epols are usually the main component among EPS molecules that constitute the biofilm matrix. However, there is little knowledge about Epols synthesized by Bcc species growing under biofilm conditions since most of the data originate from genetic approaches or from polysaccharides synthesized under non-biofilm forming conditions [203]. For this reason, *B. multivorans* C1576 was grown in biofilm mode on the Synthetic Cystic Fibrosis Medium (SCFM) which mimics the nutritional environment of CF sputum to purify and characterize the exopolysaccharide component of the matrix.

In addition, Confocal Laser Scanning Microscopy (CLSM) imaging of *B. multivorans* C1576 biofilms grown on three different media (MH, YEM and SCFM) was performed to obtain further information about the morphology of biofilms and the composition of the matrix.

For many years the biofilm matrix was suggested to be primarily composed of polysaccharides, but recently it has been shown that proteins can be abundant as well [204]. For example, curli fimbriae of *E. coli* were demonstrated to be involved in colonization of abiotic surfaces and biofilm formation [205], whereas proteins TasA of *B. subtilis* assemble to form amyloid fibers that confer mechanical stability to the biofilm [206]. Interestingly, in floating activated sludge, proteins can exceed the amount of polysaccharides [207–209]. Even though the presence of proteins has been recognized in biofilms of many bacterial species, their identification and functional characterization has not yet been properly addressed. The aim of this work was to identify *B. multivorans* C1576 proteins associated with the matrix, with an interest for those potentially interacting with EpolC1576. To accomplish this goal a comprehensive proteomic approach was conducted in collaboration with Dr. Riccardo Sgarra (Dept. Life Sciences, Univ. of Trieste) to identify matrix-associated proteins of biofilm-growing *B. multivorans* C1576. The ability of *B. multivorans* C1576 to secrete outer membrane vesicles (OMVs) was also investigated resorting to transmission electron microscopy (TEM). In addition, with the aim of finding *B. multivorans* C1576 proteins able to interact with EpolC1576 a collaboration with Prof. Daniele Sblattero (Dept. Life Sciences, Univ.

of Trieste) was established. Prof. Sblattero's group constructed a phage library of genomic DNA sequences (gDNAs) of *B. multivorans* C1576 which specify for all the bacterium's proteins. Phages of the library display all the proteins of *B. multivorans* C1576 on their surface allowing to test their ability to bind EpolC1576 immobilized on a solid surface. To immobilize EpolC1576, the polymer was first hydrolyzed to obtain fragments of suitable molecular weight which were activated with sodium periodate ($NaIO_4$) and then covalently coupled to BSA, a protein whose binding properties to solid surfaces (microplates) are well-known.

4.2 MATERIAL AND METHODS

4.2.1 Biofilm production by *B. multivorans* C1576 on semipermeable cellulose membranes and exopolysaccharide purification

B. multivorans C1576 biofilm was produced using the procedures previously described (paragraph 2.2.1) with the only exception that Petri dishes were filled with SCFM agar. The exopolysaccharide was purified and analyzed by means of NMR using the same protocol previously mentioned (paragraph 2.2.1).

4.2.2 Confocal Laser Scan Microscopy (CLSM) of *B. multivorans* C1576 grown on different culture media

CLSM analysis were carried out in collaboration with Professor Cristina Lagatolla (Dept. Life Sciences, Univ. of Trieste). With the aim of obtaining structural and morphological information on biofilms, *B. multivorans* C1576 was grown in a 12-well chamber slide (ibidi GmbH, Planegg, Germany) for 6 days using the following three different media: yeast extract mannitol (YEM), Mueller-Hinton (MH) and the Synthetic Cystic Fibrosis Sputum Medium (SCFM). An overnight culture of *B. multivorans* C1576 in MH was diluted 1000 x in the three media and 3 aliquots of 250 µL of diluted cells for each medium were transferred in the wells of the 12-well chamber slide. After 3 days of static incubation at 30 °C, the culture suspensions were removed, and the wells added with 250 µL of fresh medium (3 aliquots of 250 µL for each medium). On the 6^{th} day, the culture suspensions were removed, and each well was gently rinsed with 300 µL of sterile PBS. The protein fraction was stained with 250 µL of SYPRO® Ruby (Invitrogen Corporation, NY, USA) for 30 minutes, whereas exopolysaccharides were stained with 250 µL of 100 µg/mL of Concanavalin A-Texas Red (ConA) conjugate for 30 minutes as well. Cells and eDNA were stained with 250 µL of Acridine Orange for 1 minute. After dyes removal, the wells were gently washed once with Milli-Q water. Confocal imaging was performed with the Nikon Digital Eclipse C1 Plus confocal microscope equipped with an argon laser.

Table 1. Excitation and emission settings for dyes used to stain the various macromolecular components

Target component	Excitation wavelength (nm)	Emission wavelength (nm)
Intra-and extracellular DNA	525 ± 25	523
Exopolysaccharides	590 ± 25	615
Proteins	450 ± 25	610

The image stacks collected by CSLM were analyzed with the EZ-C1 Free Viewer (Nikon Corporation, Tokyo, Japan) and the Image J 1.47 (Wayne Resband, National Institutes of Health, Bethesda, MD, USA) software. The biofilm architecture was analyzed using the COMSTAT 2.1 software package [210]. Results are the mean of three independent experiments $\pm$ standard deviation.

4.2.3 SDS-PAGE analysis of the protein content of the biofilm matrix of *B. multivorans* C1576

B. multivorans C1576 biofilm was produced using the procedures previously illustrated (paragraph 2.2.1). After 7-days of growth, the biofilm formed by *B. multivorans* C1576 was recovered with sterile NaCl 0.9% (7 mL for each membrane) and scraped from the membranes with a sterile spatula. During harvesting procedures, cell suspension was kept on ice. To reduce contamination risks with cellular proteins, the cell suspension was vortexed for 2 minutes, avoiding chemical treatment and sonication for biofilm disruption. The cell suspension was then centrifuged at 24,000 g for 30 minutes at 4 °C (Beckman J2-21 M/E Centrifuge), the supernatant was filtered first through a 0.45 µm pore size filter (Millex-HA Non-Sterile Syringe Filter) and then through 0.22 µm pore size filter (KX Sterile Syringe Filter, Kinesis) to eliminate residual bacterial cells from the supernatant. Half of the filtered supernatant was frozen at -20 °C for successive analysis. The other half filtered supernatant was ultra-centrifuged at 100,000 g for 3 hours at 4 °C and to pellet potential outer membrane vesicles (OMVs). The pellet was resuspended with water and then stored at -20 °C for successive investigation. The protein profile of both the biofilm matrix and of the pellet obtained after ultra-centrifugation were

analyzed by SDS-PAGE using a 12% Tris-Glycine polyacrylamide. 15 µL of stock solutions and of serial dilutions (1:2 and 1:5) of both samples were mixed with 6x SDS loading buffer (0.25 M Tris-HCl pH 6.8, 8 % SDS, 40% sucrose, 0.5% β-Mercaptoethanol, 0.2% bromophenol blue) and boiled for 5 minutes. The gel was electrophoresed at 80 V for 5 min and then at 120 V for 60 min in Tris-Glycine SDS buffer and stained with Coomassie Blue.

4.2.4 Transmission Electron Microscopy (TEM) imaging

Transmission electron microscopy (TEM) imaging was carried out by Dr. Paolo Bertoncin (Dept. Life Sciences, Univ. of Trieste). An aliquot of the stock solution and a 1:50 dilution of the pellet obtained after ultra-centrifugation of the biofilm matrix of *B. multivorans* C1576 were prepared for TEM imaging using the following procedure: a droplet of sample was deposited on a carbon-coated copper grid (Electron Microscopy Science, CF 200-Cu Carbon film) to allow sample adsorption and then diluted with a droplet of water. Later, the sample was negatively stained by adding a droplet of 2% uranyl acetate. After the negative staining step (2-5 minutes), liquid excess was removed with filter paper and the sample air-dried.

Sample images were acquired with an EM208 TEM (Philips, Netherlands) equipped with a Quemesa camera (Olympus Soft Imaging Solutions) using Radius software (EMSIS, Münster, Germany).

4.2.5 Protein preparations for Liquid Chromatography Coupled to Tandem Mass Spectrometry (LC-MS/MS)

Proteomic analyses were carried in collaboration with Dr. Riccardo Sgarra (Dept. Life Sciences, Univ. of Trieste). Protein content of both *B. multivorans* C1576 biofilm matrix and OMVs were concentrated by using a Millipore Microcon centrifugal filter device having a 3 kDa molecular weight cut-off. Concentrated samples were separated via SDS–PAGE and stained with Coomassie Blue. Subsequently, electrophoretic lanes were cut into five equivalent parts and proteins were processed as previously described [211]. Peptide masses and MS/MS spectra were exported as '.mgf' files and database search was performed with the MASCOT MS/MS Ion Search option (www.matrixscience.com). The parameters for the bioinformatic analyses were the following: database: NCBIprot and SwissProt; taxonomy: Bacteria (Eubacteria); enzyme: trypsin; allow up to two

missed cleavage; Fixed modification: none; variable modification: none; peptide tol.: 1.2 Da; MS/MS tol.: 0.6 Da; peptide charge: 2 and 3; mass: monoisotopic; Instrument: ESI-TRAP. On average, individual ions scores > 68 indicate identity or extensive homology ($p<0.05$).

4.2.6 Synthesis of EpolC1576 fragments-BSA conjugates

High molecular mass fragments of EpolC1576 (H-EpolC1576), which were produced following the procedures previously described (paragraph 2.2.7), were randomly activated through mild oxidation with sodium periodate ($NaIO_4$). H-EpolC1576 solution (10 mg/mL in 100 mM acetate buffer pH 5) was stirred (rotary shaker) for 2 h in the dark with 3.75 mM $NaIO_4$. The reaction was stopped by addition of ethylene glycol. The mixture was desalted using a dialysis membrane (Spectra/Por 6, MWCO 1,000 Da) and concentrated using a rotary evaporator. The activated H-EpolC1576 fragments were designated ox-H-EpolC576. For conjugation to BSA, ox-H-EpolC1576 was added to BSA in 100 mM sodium phosphate buffer pH 7.2 to give final concentrations of 10 and 5 mg/mL, respectively. $NaBH_3CN$ was added immediately after (ox-M-EpolC1576:NaBH3CN = 2:1 w/w), and the reaction mixture was stirred for 16 h at 37 °C in the dark. In addition, medium molecular mass fragments of EpolC1576 (M-EpolC1576) were also used for the preparation of the EpolC1576-BSA conjugate, and in this case the reaction between oxidized fragments (ox-M-EpolC1576) and BSA was prolonged to 72 h.

4.2.7 High performance size exclusion chromatography (HP-SEC) characterization of ox-H-EpolC1576-BSA and ox-M-EpolC1576-BSA conjugates

HP-SEC analysis was used to characterize ox-H-EpolC1576-BSA and ox-M-EpolC1576-BSA conjugates, in comparison with free H- and M-EpolC576 and free BSA. All samples were eluted on an Agilent Technologies 1200 series HPLC equipped with three TSKgel columns (Tosoh Bioscience) in series: G3000PW (< 50,000 Da), G5000PW (< 1 x 10^6 Da) and G6000PW (< 8 x 10^6 Da), with internal diameter of 7.5 mm, length of 30 cm and kept at 40 °C in a thermostated column compartment (Agilent Technologies). Calibration of the chromatographic system was done using the following standard globular proteins: ribonuclease A (13.7 kDa), chymotrypsinogen A (25.0 kDa),

ovalbumin (43.0 kDa), BSA (67.0 kDa). Elution was carried out with 0.15 M NaCl, using a flow rate of 0.5 mL/min and detected using a refractive index detector (Knauer, Labservice Analytica), interfaced with a computer via Agilent software.

4.2.8 Medium pressure size exclusion chromatography (MP-SEC) of ox-H-EpolC1576-BSA conjugate

MP-SEC was performed to purify the ox-H-EpolC1576-BSA conjugate from other component of the conjugation reaction. The glycoconjugate was eluted on a HiPrep Sephacryl S-300 HR column (GE Healthcare) connected to a Smartline 1050 pump. Elution was carried out with 0.15 M NaCl, using a flow rate of 1 mL/min and detected using a refractive index detector (Knauer, Labservice Analytica) interfaced with a computer. Fractions 27, 31 and 35-40 were desalted via dialysis to be subsequently analysed by MALDI-TOF mass spectrometry.

4.2.9 Matrix assisted laser desorption ionization-time of flight mass spectrometry (MALDI-TOF MS) analysis of ox-H-EpolC1576-BSA conjugate

MALDI-TOF analysis of ox-H-EpolC1576-BSA conjugate was carried out to prove the success of conjugation procedures. The MALDI-TOF MS data were acquired by the group of Dr. Domenico Garozzo (IPCB, CNR Catania) in the positive polarity on a 4800 Proteomic Analyzer (AB Sciex) equipped with a Nd:YAG laser operating at a wavelength of 355 nm with <500-ps pulse and 200-Hz firing rate. Each spectrum resulted from the sum of about 2000 laser shots. BSA standard (from Sigma) and ox-H-EpolC1576-BSA conjugate MS analyses were carried out in linear mode (mass range 5000-180000 Da) allowing detection of average molecular masses, with an external calibration by the CAL MIX3 standard kit (AB Sciex) [containing insulin, thioredoxin and apomyoglobin] and the "6 protein mixture" (AB Sciex) [containing BSA, α-lactalbumin, β-galactosidase, lysozyme, apotransferrin and β-lactoglobulin] affording mass accuracy better than 0.02%. GPC fractions were diluted with 50 µL of H2O/HCN/TFA 98/2/0.1% and mixed 1:1 (v/v) with a 10 g/L solution of CHCA, or sinapinic acid or DHB MALDI matrices.

4.2.10 Sodium dodecyl sulfate-polyacrylamide gel electrophoresis (SDS-PAGE) analysis of ox-M-EpolC1576-BSA conjugates

The conjugation products of the reaction between ox-M-EpolC1576 fragments and BSA were analyzed by SDS-PAGE using a 12% Tris-Glycine polyacrylamide gel to verify conjugate formation before performing purification. Samples (10-20 µL with a protein content of 4-8 µg) were mixed with 6x SDS loading buffer (0.25 M Tris-HCl pH 6.8, 8 % SDS, 40% sucrose, 0.5% β-Mercaptoethanol, 0.2% bromophenol blue) and boiled for 5 minutes. The gel was electrophoresed at 80 V for 5 min and then at 120 V for 60 min in Tris-Glycine SDS buffer and stained with Coomassie Blue.

4.2.11 Western Blot (WB) analysis of ox-M-EpolC1576-BSA conjugate

To confirm the success of the conjugation of ox-M-EpolC1576 fragments to BSA, the glycoconjugate was subjected to Western Blot analysis.

SDS-PAGE separation. The ox-M-EpolC1576-BSA conjugate (10 µg), 2 µg of BSA and the antibody to *Helicobacter pylori* (α-HPAG) were mixed with an equal volume of 6x SDS loading buffer (0.25 M Tris-HCl pH 6.8, 8% SDS, 40% sucrose, 0.5% β-Mercaptoethanol, 0.2% bromophenol blue) and boiled for 5 minutes. BSA and α-HPAG were used as negative and positive control, respectively. The protein solutions, along with 5 µL Spectra™ standard molecular weight (Multicolor Broad Range Protein Ladder, Thermo Scientific™) for comparison and size determination, were separated in a 7.5 % polyacrylamide gel and run at 120 V for 1 hour. The proteins were transferred from the gel to a nitrocellulose membrane for Western Blot analysis.

Proteins transfer on a nitrocellulose membrane. Once electrophoresis was completed, the gel was placed on pre-soaked blotting paper next to Amersham Proton 0.2 µM nitrocellulose (NC) membrane (GE Healthcare), sandwiched between foam pads, placed in a plastic cassette and loaded into the Mini-PROTEAN® Tetra Cell (Bio-Rad) filled with transfer buffer. Blotting was done using at 100 V for 1 hour. In order to visualise proteins transferred onto the nitrocellulose membrane, the latter was stained with Ponceau-S stain containing 3% trichloroacetic acid (TCA) (Sigma-Aldrich) and 0.1% Ponceau-S (Sigma-Aldrich) for 60 seconds. The membrane was then rinsed with distilled water to remove residual Ponceau-S stain. Once proteins transfer was verified, the nitrocellulose membrane was rinsed with Phosphate-Buffered Saline (PBS) containing 137 mM NaCl (Sigma), KCl 2.7 mM, Na_2HPO_4 10 mM, KH_2PO_4 and HCl pH 7.4, until the Ponceau-S stain

was completely washed away from the membrane. The latter was then blocked by incubation in PBS containing 2% (v/v) TWEEN® 20 for 2 minutes at 20°C, washed twice with PBS, and incubated in 7 mL of PBS containing 0.05 % (v/v) TWEEN 20, with 1 mM $CaCl_2$, 1 mM $MnCl_2$, 1 mM $MgCl_2$ and 2 µg/mL of Concanavalin A-peroxidase conjugate (ConA-HRP) for 16 hours at 20°C on a shaker. Concanavalin A is a lectin that has strong affinity for mannose and to less extent for glucose. The membrane was then rinsed with PBS, developed using ECL Western Blotting Substrate (Pierce, Rockford, IL) and exposed on X-ray films (Amersham Hyperfilm ECL).

4.2.12 Immobilization of ox-M-EpolC1576-BSA conjugate on a solid support and detection via an Enzyme-linked Lectin assay (ELLA)

In order to find the optimal conditions for coating a plastic solid support with ox-M-EpolC1576-BSA conjugate, a calibration curve was produced increasing conjugate concentration in serial wells. For each dilutions of ox-M-EpolC1576-BSA in 50 mM carbonate/bicarbonate buffer (CB) pH 9.6, containing from 0.5 to 10 µg/mL of conjugated BSA, 100 µL in quadruplicate were loaded on E.I.A. R.I.A. 8-well , flat bottom strips (Costar) and incubated for 16 hours at 4 °C. Dilutions of BSA (negative control) and of α-HPAG antibody (positive control) were also loaded using the same protein concentration and incubation conditions employed for ox-M-EpolC1576-BSA dilutions. After incubation, the strips were rinsed with PBS twice and incubated with 100 µL of PBS containing 0.05% (v/v) TWEEN 20, with 1 mM $CaCl_2$, 1 mM $MnCl_2$, 1 mM $MgCl_2$ and Concanavalin A-peroxidase conjugate (2 µg/mL) for 1 hour at room temperature. The strips were rinsed three times with PBS containing 0.05 % Tween 20, three times with PBS and then incubated with 70 µL of the substrate 3,3',5,5'-tetramethylbenzidine (TMB). The strips were then incubated in the dark at room temperature for 14 minutes to allow colorimetric reaction to occur (blue color), and the reaction stopped with 30 µL of 1 M H_2SO_4 (color turned from blue to yellow). Absorbance was read at 450 nm using an Infinite® 200 PRO plate reader (Tecan).

4.2.13 Phage display experiment

Production of the phage library. The frozen glycerol stock culture of *E. coli* DH5αF' (Gibco BRL) provided with the phagemid library of *B. multivorans* C1576 gDNAs was streaked out with a sterile spatula and used to inoculate 1 mL of 2xTY medium containing 100

µg/mL of ampicillin and 1% glucose (2xTY-Amp-Glu medium). Approximately 180 µL of the bacteria were used to inoculate 32 mL of 2xTY-Amp-Glu to reach an initial OD_{600} between 0.01 and 0.05. The culture was grown at 37 °C on an orbital shaker until OD_{600} reached 0.4 – 0.5 and then infected with the helper phage (ratio helper phages: bacteria 20 = 1) for 45 min at 37 °C without shaking. The bacteria were then centrifuged at 4000 rpm for 15 min at room temperature, the bacterial pellet was resuspended in 30-40 mL 2xTY-Amp-Kana and the culture incubated overnight in an orbital shaker at 28°C.

Coating of the antigen. Two Nunc Immunotubes were coated with 1 mL containing 10 µg of ox-M-EpolC1576-BSA glycoconjugate in CB 50 mM pH 9.6 overnight at 4 °C.

DH5αF' preparation. Using a sterile loop, DH5αF' bacteria were streaked out on a 2xYT agar plate for single colonies production and incubated overnight at 30°C.

DH5αF' propagation. 2 mL of 2xTY medium were inoculated with a single colony of DH5αF'. The culture was continuously diluted to reach an OD_{600} = 0.5 at the step of phage elution.

Phages preparation. The phages from the overnight culture were purified as follows: the overnight culture was centrifuged at 4000 rpm for 40 min at 10 °C. The supernatant (30 mL) was added with 1/5 of 20% PEG/NaCl 2.5 M (6 mL) to the final volume in order to precipitate the phages. The mixture was placed in ice for 1 h, gently mixed by inversion 4-5 times during the precipitation and then centrifuged for 10 min at 4000 rpm and 10 °C. The pellet containing the precipitated phages was re-suspended with 1 mL of sterile PBS. To remove residual bacteria, the solution was centrifuged for 10 min at 11000 rpm at 10 °C and the supernatant containing the phages was kept on ice.

Phages dilution preparation. To establish the "input phages", namely the number of phages used for selection, three serial dilutions of phages in PBS were prepared.

Library screening for phage selection. After the overnight coating, the two immunotubes were washed 3 times with PBST, 3 times with PBS and then blocked: one immunotube (tube A) was blocked with 4 mL of 4% (w/v) non-fat skim milk in PBST while the other one (tube B) with 4 mL of 10% (w/v) BSA in PBST. After blocking for 1 h at room temperature, both immunotubes were rinsed 2 times with PBST and 2 times with PBS before being added with the phages (input phage). Specifically, tube A was added with 1 mL phage-solution including 2% (w/v) non-fat skim milk and free BSA 100 µg/mL in PBST while tube B was added with a phage solution identical to that of tube A but

without 2% (w/v) non-fat skim milk. Tube A and B were put on a rotary shaker for 30 min shaking and then left standing for 90 min at RT.

Immunotubes washing. For the first cycle of selection, both immunotubes were rinsed 10 times with PBS-0.05% Tween 20 and 10 times with PBS. To increase selection stringency, for the second and third cycle it was added a washing step on rotation with PBS for 10 min between the 10-time-repeated washing steps with PBS-0.05% Tween 20 and PBS.

Phages elution. Elution of the selected phages was carried out by incubating both tubes A and B with 1 mL of DH5αF' cells ($OD_{600} = 0.5$) for 45 min at 37 °C in static. During the mid-log phase growth bacteria express the F pilus which is necessary for phages to attach to and enter bacteria. In parallel, 5 µL from each serial dilution of phages previously prepared were used to infect 3 aliquots of 0.5 mL of DH5αF' cells ($OD_{600} = 0.5$) for 45 min at 37 °C in static. Dilution series of these phage-infected bacteria were plated on small 2xTY-Amp-Glu agar plates and incubated at 37 °C overnight to determine the titre of both the phages used for selection ("input" phages) and eluted phages ("output phages"). Dilution series of eluted phage were also plated on small 2xTY-Amp-Glu agar plates and incubated at 37 °C overnight to allow single colony picking for PCR and ELISA characterization of eluted phages. The remaining bacteria infected by eluted phages were spread on a large 2xTY-Amp-Glu agar plate and incubated at 30 °C overnight. The following day the bacteria were rescued from the large plate using 4 mL 2xTY-10% glycerol, stored at -80 °C and successively amplified and used for a second cycle of selection. Phages eluted after the second cycle of selection were amplified and used for a third cycle of selection.

Polymerase chain reaction (PCR). The quality of the library was assessed after each selection cycle by performing a PCR screening to reveal the presence of DNA inserts of *B. multivorans* C1576 of the expected size. Selected bacterial colony infected by eluted phages were picked from 2xTY-Amp-Glu agar plates and amplified. Each selected colony should contain a single DNA sequence.

ELISA assay of eluted phages. After the second and the third round of selection, bacterial colony infected by eluted phages were randomly picked from 2xTY-Amp-Glu agar plates, amplified and superinfected with helper phages to rescue phages eluted after selection. The binding affinity of eluted phages for the saccharide portion of ox-M-EpolC1576-BSA conjugate was tested as follows: a 96-well MaxiSorp® plate was coated with 100 µL of

10 µg/mL of ox-M-EpolC1576-BSA conjugate in 50 mM CB buffer pH 9.6 and incubated overnight at 4 °C. Another a 96-well MaxiSorp® plate was coated with 100 µL of 10 µg/mL BSA in 50 mM CB buffer pH 9.6 and incubated overnight at 4 °C. BSA was used as negative control to exclude that eluted phages binding was aspecific. The wells of both microplates were washed 3 times with PBS containing 0.05% Tween 20 and 3 times with PBS. Reactive binding sites were blocked by saturating each well with 200 µL of 4% of non-fat dry milk in PBST and the microplates incubated at room temperature for 1 hour. After incubation, the microplates were rinsed 3 times with PBST and 3 times with PBS. Then, each well was loaded with 100 µL of phages and the microplates incubated at room temperature, thus allowing binding to occur between the ox-M-EpolC1576-BSA conjugate and phages. The unbound phages were washed off 3 times using PBS containing 0.05% Tween 20 and 3 times using PBS. Peroxidase conjugated anti-M13 monoclonal antibody was added and the plate incubated for 1 hour at room temperature. The plate was washed 3 times with PBS containing 0.05% Tween 20 and 3 times with PBS, then 3.3'5.5'-tetramethylbenzidine (TMB) substrate (70 µl) was added and the plate was incubated at room temperature until a blue color developed. The colorimetric reaction was blocked with 30 µL of H_2SO_4 1 M that caused color to change from blue to yellow and absorbance was measured at 450 nm using an ELISA plate reader [212].

4.2.14 Immobilization of ox-M-EpolC1576 fragments on a solid support and detection via an Enzyme-linked Lectin assay (ELLA)

In order to overcome the selection of false positives from the phage library of *B. multivorans* C1576 gDNAs, ox-M-EpolC1576 fragments were directly coupled to Costar's Carbo-BIND™ 96-well microplates. These microplates have a hydrazide surface (R_1-C(=O)-NH-NH_2) that is meant to be directly covalently coupled to $NaIO_4$-activated carbohydrates (R_2-CH=O) to form a hydrazone (R-C(=O)-NH-NH_2=CH-R_2, a Schiff base with a double bond between the carbon atom of the saccharide carbonyl group and the hydrazine nitrogen). Even though hydrazones are more stable than imines, it was decided to stabilize the N=C double bond by the addition of a reducing agent ($NaCNBH_3$). To find the optimal conditions for coating Carbo-BIND™ microplates, a calibration curve of ox-M-EpolC1576 was produced. An aliquot of 50 µL of each dilution of ox-M-EpolC1576 (1.25-20 µg/mL) in coupling buffer (100 mM CH_3COONa buffer pH

5.5) was transferred in the wells of a microplate in quadruplicate. Soon after, 50 µL of molar excess of $NaCNBH_3$ was added to each well and the microplate incubated overnight at 37 °C with shaking. The microplate was washed three times with PBS and then incubated with 100 µL of PBS containing 0.05% (v/v) Tween 20, with 1 mM $CaCl_2$, 1 mM $MnCl_2$, 1 mM $MgCl_2$ and Concanavalin A-peroxidase conjugate (2 µg/mL) for 1 hour at room temperature. The microplate was rinsed three times with PBS containing 0.05% Tween 20, three times with PBS and then incubated with 70 µL of the substrate 3,3',5,5'-tetramethylbenzidine (TMB). The microplate was then incubated in the dark at room temperature for 10 minutes and the reaction stopped with 30 µL of 1 M H_2SO_4. Absorbance was read at 450 nm using an Infinite® PRO plate reader (Tecan).

4.3 RESULTS AND DISCUSSION

4.3.1 ^{1}H-NMR spectroscopy of exopolysaccharides purified from *B. multivorans* C1576 biofilms formed on SCFM agar

B. multivorans C1576 was grown in biofilm mode on SCFM, the medium reflecting the nutritional composition of CF sputum [213], and the exopolysaccharide of the matrix purified. In Fig. 25 the ^{1}H-NMR spectra of the anomeric region of exopolysaccharides purified from the matrix of *B. multivorans* C1576 biofilms cultivated on SCFM, MH and YEM are compared.

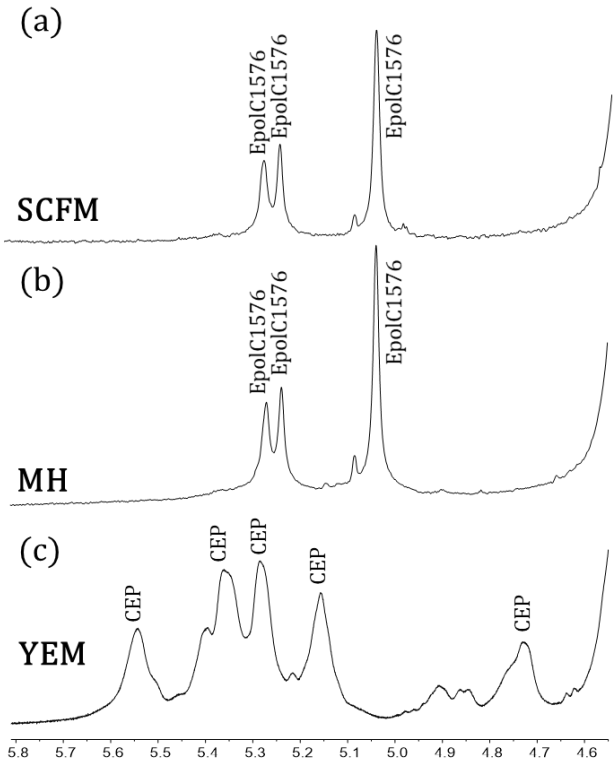

Figure 25. ^{1}H-NMR spectra of exopolysaccharides from biofilms. Anomeric regions of the ^{1}H-NMR spectra of Epols purified from biofilms of *B. multivorans* C1576 formed on cellulose membrane laid on SCFM (a), MH (b) and YEM (c) agar media. EpolC1576 and CEP indicate the resonance signals specific of the exopolysaccharides.

It is clear that SCFM stimulates only the synthesis of EpolC1576. Indeed, the anomeric region shows three resonance signals that are identical to those of EpolC1576 purified from the matrix of biofilms developed on MH, whereas YEM induces only the biosynthesis of cepacian (CEP) [49].

4.3.2 Confocal laser scanning microscopy (CLSM) imaging and quantitative analysis of matrix components of *B. multivorans* C1576 biofilms grown on three different media

The morphological aspect of the 6-days-old biofilm formed in a 12-well chamber slide by *B. multivorans* C1576 grown in three different media (MH, SCFM and YEM) was analyzed by CLSM after staining with the specific dyes for three distinct components of the matrix: Concanavalin A-Texas Red conjugate for polysaccharides, SYPRO Ruby for proteins and acridine orange for both cells and eDNA, the latter already demonstrated to be present in the biofilm matrix [214]. CLSM allowed for qualitative observation of the structural diversity of biofilms produced in the three different media. CLSM images indicate that the composition of the medium influences the morphological aspect of biofilms (Fig. 26).

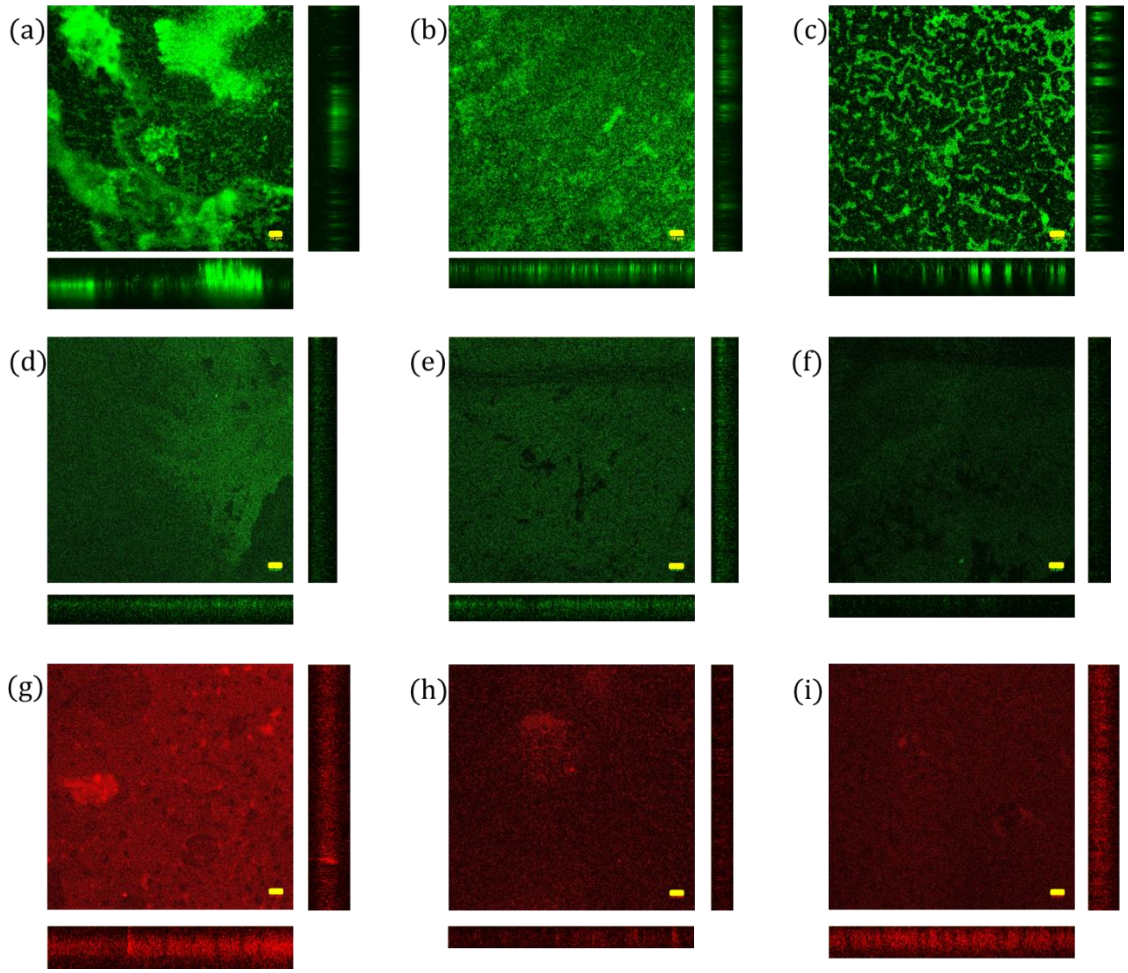

Figure 26. CLSM images of 6-days-old biofilms produced by *B. multivorans* C1576 in static conditions on the following media: MH (a, d, and g), SCFM (b, e and h) and YEM (c, f and i). Cells and eDNA were stained with acridine orange (a, b and c), exopolysaccharides with ConA-Texas Red conjugate (d, e and f) and proteins with SYPRO Ruby (g, h and i). The large panels represent the *x-y* planes in the middle of the structure, whereas the side panels and the bottom panels

represent respectively the *y-z* and *x-z* planes relative to central position of the *x-y* planes. Scale bars (yellow) are all equivalent to 20 μm.

Indeed, the stain with acridine orange shows that the biofilm grown in MH consists of huge and discontinuous formations (Fig. 26 a); the biofilm formed in SCFM appears as a homogenous dense mat (Fig. 26 b), whereas in YEM the biofilm seems to consist of several small aggregates (Fig. 26 c). These results are not surprising since it has been already shown the influence of distinct media on the biosynthetic response for other bacterial species [215–218]. CLSM images were analyzed by the COMSTAT 2.1 software, which provided quantitative evaluation of different features of the biofilm (biomass, roughness coefficient, average thickness, surface to biovolume ratio and surface coverage) in order to characterize the biofilm structures developed by *B. multivorans* C1576.

Table 2. *B. multivorans* C1576 biofilm parameters. Values represent the mean of three independent experiments ± standard deviation.

	MH (AO) (ConA) (Ruby)	SCFM (AO) (ConA) (Ruby)	YEM (AO) (ConA) (Ruby)
Biomass	55.6 ± 14.8	34.2 ± 6.2	41.8 ± 9.1
($\mu m^3/\mu m^2$)	11.0 ± 3.3	24.3 ± 3.3	3.9 ± 0.6
	23.1 ± 9.5	8.4 ± 3.6	10.2 ± 2.2
Roughness	1.0	1.0	1.0 ± 0.1
coefficient	1.0	1.0	1.2 ± 0.1
	1.0	1.1	1.0
Average thickness	34.2 ± 9.0	20.7 ± 3.0	26.6 ± 4.6
(μm)	16.6 ± 1.0	25.3 ± 3.9	7.9 ± 1.5
	31.0 ± 6.4	14.4 ± 2.4	16.3 ± 5.1
Surface to	2.0 ± 0.4	2.4 ± 0.6	2.3 ± 0.5
biovolume ratio	4.9 ± 0.4	4.3 ± 0.1	5.1 ± 0.8
($\mu m^2/\mu m^3$)	4.3 ± 0.6	4.8 ± 0.6	4.8 ± 0.8
Surface coverage	21 ± 1.7	21 ± 3.0	25 ± 7.6
(10^6 x μm^2)	8.4 ± 1.8	17 ± 2.3	3.2 ± 0.7
	18 ± 5.9	7.4 ± 2.7	8.9 ± 2.0

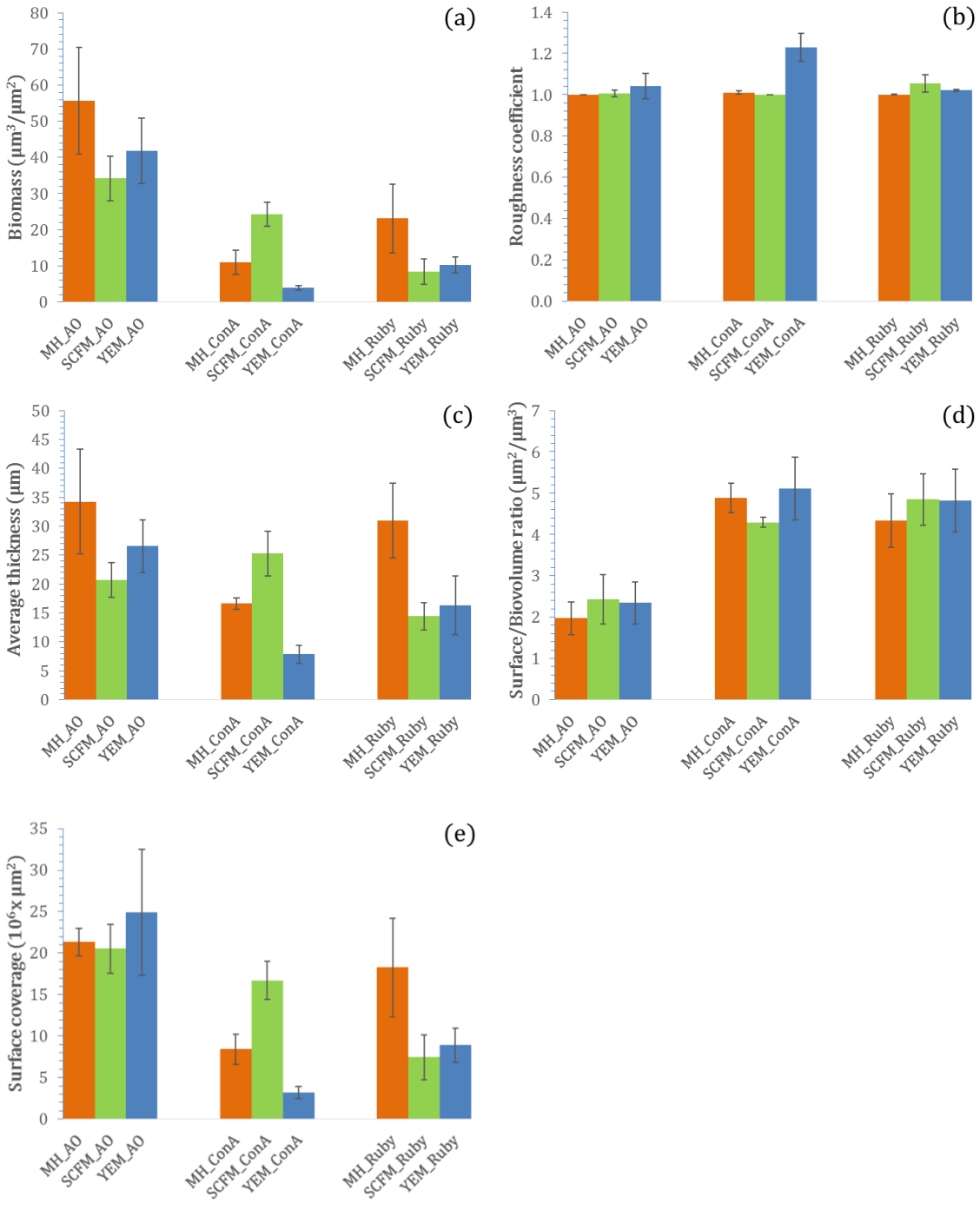

Figure 27. Analysis of the structural properties of 6-days-old biofilms of *B. multivorans* C1576 developed in MH, SCFM and YEM media. Measures of total biomass (a), roughness coefficient (b), average thickness (c), surface/biovolume ratio (d) and surface coverage (e). Acridine orange (AO), Concanavalin A-Texas Red (ConA) and SYPRO Ruby (Ruby).

Regarding the acridine orange dye (for cells and eDNA) the amount of biomass and the mean thickness of biofilms developed on MH are higher (Table 2, Fig. 27 a and c, dark orange columns) than those of biofilms formed in YEM (Table 2, Fig. 27 a and c, blue columns). Biofilms developed in SCFM shows the lowest biomass and average thickness

among the three media (Table 2, Fig. 27 a and c, green columns). The highest amount of biomass and average thickness of biofilms grown in MH can be probably ascribed to the richness in nutrients with respect to SCFM and YEM, and thus it may allow the bacteria to develop higher multilayered structures.

Interestingly, biofilms formed on SCFM and stained with Concanavalin A-Texas Red to detect the exopolysaccharide fraction of the matrix show the highest biomass and average thickness compared to those grown in MH and in YEM (Table 2, Fig. 27 a and c). These results suggest that SCFM stimulates bacteria to produce more exopolysaccharides. SCFM resembles the nutritional environment of CF sputum [213], and interestingly it has been observed that expression profile and phenotypes of *P. aeruginosa* grown in both SCFM and original CF sputum are similar [213]. In this light, it can be speculated that an *in vivo* enhanced ability to produce higher amounts of exopolysaccharides due to the nutritional support of CF sputum may favor *B. multivorans* C1576 organization in biofilm structures, thus providing bacteria with protection towards antibiotics and host immune system. It has been shown that *B. multivorans* C1576 produces biofilms on cellulose membranes deposited on SCFM agar and that the matrix contains only EpolC1576 as exopolysaccharide matrix (paragraph 3.3.1). The fact that *B. multivorans* C1576 develops biofilms on SCFM may corroborate the observation of *B. multivorans* biofilms in the sputum of a CF subject suffering from persisting lung infection [106], even though the ability of Bcc species to develop biofilms *in vivo* is still questionable [219].

Regarding the protein content of the matrix, biofilms formed in MH has the highest amount of biomass and average thickness among the three media as confirmed by visualization of CLSM images (Fig. 26 f, g and h). Biomass and average thickness measured after staining proteins with SYPRO Ruby for the three media are shown in Table 2 and Fig 27 (a and c).

The roughness coefficient, which is calculated from the thickness distribution, describes the degree of heterogeneity of the biofilm surface. The slightly high values of roughness coefficient (Table 2) for all the biofilms developed in the three media indicate (Fig. 27 b) the formation of rough and heterogeneous biofilm surfaces rather than homogenous and uniform ones.

Surface to biovolume ratio, which represents the part of the biofilm exposed to the nutrient source, is quite similar for all the biofilms formed in each medium (Fig. 27 d),

thus suggesting that bacteria maximize nutrient capture similarly, independently from the medium used.

Surface coverage measurements (Fig. 27 e) show that bacterial cells spread on the solid support with slight differences between the three media (Table 2). Interestingly, surface coverage measurement after Concanavalin A-Texas Red stain of biofilms developed in SCFM shows a value (1.7×10^7 μm^2) similar to that measured after acridine orange (2.1×10^7 μm^2) of biofilms in the same medium, thus indicating a homogenous distribution of exopolysaccharides across the biofilm sections under investigation. Similarly, the distribution of the protein fraction (1.8×10^7 μm^2) across the biofilm structures formed in MH seems to reflect the one showed by cells and eDNA (2.1×10^7 μm^2).

In general, CLSM images and quantification of structural parameters indicate that *B. multivorans* C1576 produces biofilms with a high variety of structures that also differentiate for the relative content and distribution of different EPS matrix molecules. This morphological and qualitative variability may be partly ascribed to the nutrient availability on which bacteria can count to produce biofilms. In addition, the preferential biosynthesis of exopolysaccharides over other EPS matrix on the medium reflecting the nutritional environment of CF sputum (SCFM) may support the thesis of the ability to form biofilms *in vivo* for Bcc species, at least for *B. multivorans.*

4.3.3 Investigation of the protein component of the biofilm matrix of *B. multivorans* C1576

With the aim of studying the proteinaceous fraction of the biofilm matrix of *B. multivorans* C1576, various analyses were carried out. In Fig. 28 it is shown the workflow followed:

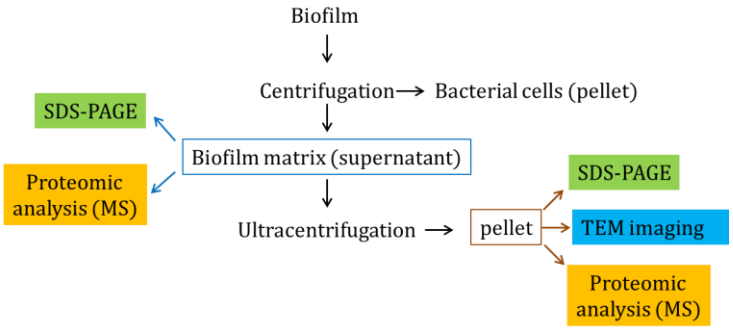

Figure 28. Schematic representation of the procedures followed to characterize the protein content of the biofilm matrix of *B. multivorans* C1576. SDS-PAGE (sodium dodecyl sulfate polyacrylamide gel electrophoresis), TEM (transmission electron microscopy), MS (mass spectrometry).

4.3.4 SDS-PAGE analysis of matrix-associated proteins of *B. multivorans* C1576

The protein profile of the biofilm matrix of *B. multivorans* C1576 was analyzed by SDS-PAGE (Fig. 29). To better characterize its macromolecular constituents, the biofilm matrix of by *B. multivorans* C1576 was also subjected to ultracentrifugation, the pellet obtained resuspended in water and investigated through SDS-PAGE. In Fig. 29 the protein profiles of both the biofilm matrix before and after ultracentrifugation are compared.

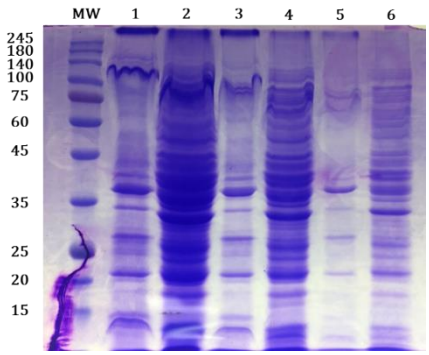

Figure 29. SDS-PAGE protein profile of biofilm matrix before and after ultracentrifugation: MW (protein markers); lane 1 and 2, biofilm matrix after and before ultracentrifugation, respectively (stock solutions); lane 3 and 4, biofilm matrix after and before ultracentrifugation (1:2 dilutions); lane 5 and 6, biofilm matrix after and before ultracentrifugation (1:5 dilutions).

With the aim of giving an identity to the pellet obtained after ultracentrifugation, the sample was observed by means of transmission electron microscopy (TEM).

4.3.5 Visualization of biofilm matrix after ultracentrifugation by Transmission Electron Microscopy (TEM)

Transmission Electron Microscopy (TEM) was performed to visualize the presence of structures of bacterial origin in the biofilm matrix. Fig. 30 shows that biofilm-growing *B. multivorans* C1576 produces OMVs that thus can be included as components of the biofilm matrix.

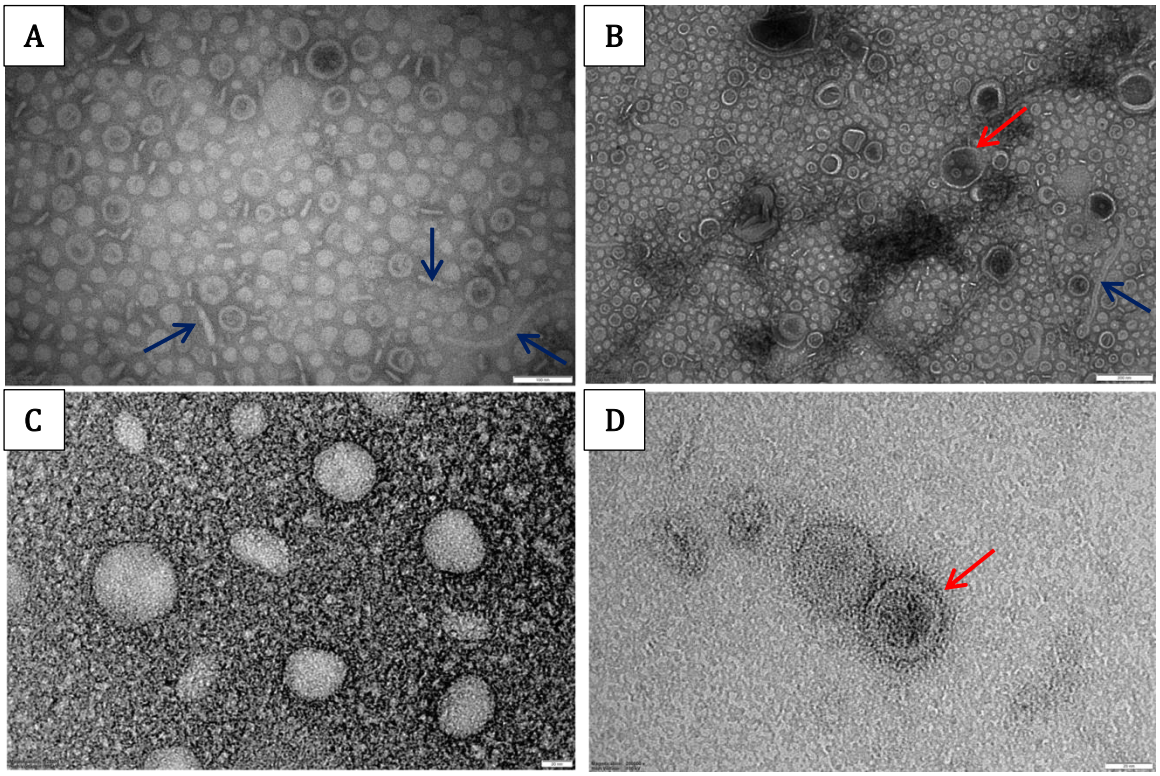

Figure 30. Negative staining micrograph of outer membrane vesicles (OMVs) purified from the biofilm matrix produced by *B. multivorans* C1576: (A, B) large amount of OMVs with elongated structures (blue arrows) of different length that may represent contamination with pili and flagella (white bars in the lower right corner = 100 nm); (C, D) magnified views of some OMVs belonging to the diluted sample (white bars in the lower right corner = 20 nm and 50 nm, respectively). Both concentrated and diluted sample show that some outer membrane vesicles are clearly surrounded by a double membrane (red arrows).

It is well-established that many metabolically active Gram-negative species release OMVs during bacterial growth [220,221]. They are spherical bilayered structures whose

diameter varies from 30 to 220 nm [221]. OMVs originate from the outer membrane of bacteria and their cargo includes lipopolysaccharides (LPS), proteins usually localized in the periplasm, proteins belonging to the outer membrane, cytoplasmic proteins, nucleic acids, metabolites and signaling molecules [222–224]. Among Bcc species, only *B. cepacia* was proven to synthesize OMVs [221] which range in size 30-220 nm and whose cargo can comprise virulence factors such as proteases and lipases. The majority of OMVs produced by *B. multivorans* C1576 have a diameter that varies from 25 to 70 nm, but the bacteria occasionally synthesize OMVs whose diameter exceeds 150 nm. For some of these spherical formations synthesized by *B. multivorans* C1576 it is possible to notice the double-membrane (Fig. 30 B and D, red arrows) that surrounds the structures. To obtain highly purified OMVs, ultracentrifugation is usually followed by OMVs purification via density gradient centrifugation. This step was not performed, and it probably explains the presence of elongated structures that may represent contaminations with pili and flagella (Fig. 30 A and B, blue arrows).
In order to better characterize OMVs, they were also analyzed by means of LC-MS/MS to investigate the proteins they contained.

4.3.6 Identification of *B. multivorans* C1576 Matrix Proteome

To determine the identity of matrix-associated proteins of biofilm-growing *B. multivorans* C1576, the soluble fraction of the biofilm was separated from the cell component and analyzed by using 1D-SDS-PAGE in combination with LC-MS/MS. In parallel, proteins associated with OMVs were also identified. It was found that proteins associated with the matrix are 163, whereas those identified from OMVs are 65. Matrix-associated proteins seem to be mainly of cytoplasm origin and involved in metabolic processes such as the tricarboxylic acid cycle (TCA) and fatty acid biosynthesis (Table 3). Furthermore, the biofilm matrix shows to be enriched in proteins belonging to the translation machinery, proteins involved in cell redox homeostasis, chaperonins and membrane-bound proteins, thus suggesting that cell lysis may be an important source of proteins for the biofilm matrix of *B. multivorans* C1576. It has already been shown that cell death usually accompanies biofilm production and development [225], thus contributing to the composition of the extracellular matrix proteome. Moreover, the presence of both membrane-bound and cytosolic proteins in biofilms matrix has already been demonstrated for several bacterial species [226–230]. Another source of

intracellular proteins for the biofilm matrix may be represented by OMVs. For example, OMVs have been found to be integral part of the biofilm matrix produced *P. aeruginosa* as much as EPS molecules [231]. *B. multivorans* C1576 produces OMVs and proteomic data reveals that 29% of OMVs-associated proteins (19 out of 65) are in common with the biofilm matrix proteome (Fig. 31 and Table 5).

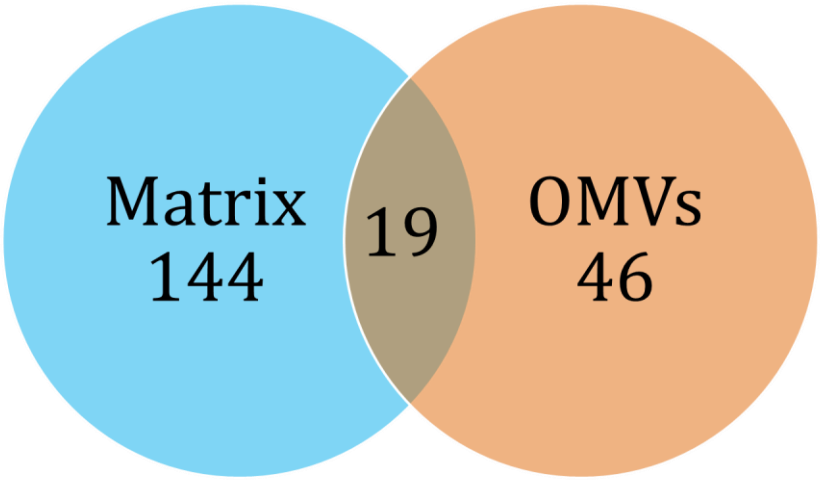

Sample	Number of identified proteins
Matrix	163
OMVs	65

Figure 31. Venn diagram of proteins that overlap between the biofilm matrix and OMVs. The table on the right indicates for each sample the number of proteins identified on the base of a peptide with a score beyond the threshold for identity or extensive homology.

Table 3. Top 20 of most prevalent matrix-associated proteins

Protein	Accession number	Number of matches	Subcellular localization
Acyl carrier protein	ACP_BURCA	35	cytoplasm
thiol peroxidase	WP_006400399.1	30	cell
carboxymuconolactone decarboxylase	EGD01850.1	22	unknown
beta-ketoacyl-ACP reductase	AOL03371.1	17	unknown
branched-chain amino acid ABC transporter substrate-binding protein	WP_006396439.1	16	unknown
thiol:disulfide interchange protein DsbA/DsbL	WP_006398112.1	15	periplasmic space
Malate dehydrogenase	WP_006399543.1	13	unknown
ABC transporter substrate-binding protein	WP_006397294.1	13	outer membrane-bounded periplasmic space
$Fe^{(3+)}$ ABC transporter substrate-binding protein	WP_035953191.1	11	unknown
glutamate/aspartate ABC transporter substrate-binding protein	WP_006408338.1	10	unknown
RNA chaperone Hfq	WP_063496600.1	10	unknown
thioredoxin	ABC39250.1	9	cell
ribosomal protein S1	EJO59460.1	9	unknown
Protein-export protein SecB	SECB_BURCA	8	cytoplasm
hypothetical protein	SAK23673.1	8	unknown
5-methyltetrahydropteroyltriglutamate-homocysteine S-methyltransferase	WP_060098089.1	8	unknown
NADP-dependent phosphogluconate dehydrogenase	WP_006399510.1	8	unknown
Endoribonuclease L-PSP	WP_006398680.1	7	unknown
NADP-dependent isocitrate dehydrogenase	WP_006398523.1	7	unknown
superoxide dismutase	WP_006398503.1	6	unknown

Table 4. Top 20 of most prevalent OMVs-associated proteins

OMVs protein	Accession number	Number of matches	Subcellular localization
porin	WP_054315301.1	30	outer membrane
OmpA-like protein	WP_006400736.1	17	outer membrane
chaperonin GroEL	WP_006400973.1	16	cytoplasm
porin	WP_059451674.1	15	outer membrane
iron complex outer membrane receptor protein	BAG43570.1	12	outer membrane
glutamate/aspartate ABC transporter, periplasmic glutamate/aspartate-binding protein	EED98255.1	10	membrane
hypothetical OmpA-like protein	WP_059451674.1	9	outer membrane
putative lipoprotein	WP_006402280.1	7	unknown
TonB-dependent hemoglobin/transferrin/lactoferrin family receptor	WP_048804300.1	7	outer membrane
aspartate/tyrosine/aromatic aminotransferase	WP_038714441.1	4	unknown
adenosylhomocysteinase	EEE03553.1	5	cytoplasm
phenylalanine--tRNA ligase beta subunit	OUX12435.1	5	cytoplasm
malate dehydrogenase	MDH_BURCJ	4	unknown
putative outer membrane protein	OJD05646.1	4	unknown
enolase	ENO_BURM1	4	cytoplasm, cell surface
aldehyde dehydrogenase family protein	WP_054317513.1	4	unknown
citrate synthase	OJD04157.1	3	cytoplasm
redoxin family protein	KOS88719.1	3	unknown
phasin protein	GAU01187.1	3	unknown
bacterioferritin	ABO01605.1	2	unknown

Table 5. Proteins associated with both the matrix and OMVs

Protein	Accession	Subcellular localization
porin	WP_054315301.1	membrane
chaperonin GroEL	WP_006400973.1	cytoplasm
citrate (Si)-synthase	OJD04157.1	cytoplasm
aldehyde dehydrogenase family protein	WP_054317513.1	unknown
aldehyde dehydrogenase	KQZ56053.1	unknown
leucine ABC transporter subunit substrate-binding protein LivK	OJD03740.1	unknown
Glycine dehydrogenase	GCSP_BURM1	unknown
beta-ketoacyl-ACP reductase	AOL03371.1	unknown
2,3,4,5-tetrahydropyridine-2,6-dicarboxylate N-succinyltransferase	DAPD_BURCA	cytoplasm
ATP-dependent Clp protease, proteolytic subunit ClpP	EED97471.1	cytoplasm
YceI family protein	EED98206.1	unknown
thiol:disulfide interchange protein DsbA/DsbL	WP_006398112.1	periplasmic space
redoxin family protein	KOS88719.1	unknown
hypothetical protein CA831_04455 partial	OXH91981.1	inner membrane
acyl carrier protein	ACP_BURCA	cytoplasm
thioredoxin	ABC39250.1	cell
conserved hypothetical protein	EBA48742.1	unknown
Endoribonuclease L-PSP	WP_006398680.1	unknown
50S ribosomal protein	RL7_BURM1	ribosome

However, only 4 proteins out of the 20 most abundant matrix-associated proteins are found in OMVs, thus suggesting that OMVs do not represent an important source of proteins for the biofilm matrix of *B. multivorans* C1576. In addition, the fact that the other 46 proteins identified in the OMVs sample of *B. multivorans* C1576 are not found in the biofilm matrix can be ascribable to the higher complexity of the matrix sample with respect to that of OMVs. Indeed, the more complex the sample, the lower the rate of success in protein identification. It cannot be also excluded that the probable low amount of OMVs presents in the matrix sample have prevented many OMVs proteins from being detected.

The proteome profile of purified OMVs shows that they are particularly enriched in outer membrane (OM) proteins (18 proteins out of 65), thus confirming findings of previous investigations [232–235]. Among these proteins are porins, receptors involved in iron uptake and ABC transporters (Table 4) that might play a role in multidrug resistance. To sum up, this data suggests that the most probable source of proteins for the matrix may be cell lysis and to less extent OMVs release. The matrix of bacterial pathogens can contain lytic enzymes that might damage host tissues, thus acting as virulence factors that promotes microbial infection [236]. Interestingly, among the matrix proteome of *B. multivorans* C1576 these lytic enzymes have been found: a serine-type carboxypeptidase (WP_006402861.1), an endoribonuclease belonging to the RidA family (WP_006398680.1) and a protease inhibitor named ecotin (WP_006405712.1). Ecotin produced by *P. aeruginosa* has been shown to inhibit the serine protease elastase synthesized by neutrophils, thus severely compromising the bactericidal efficiency of this enzyme. In the same way, ecotin produced by *B. multivorans* C1576 might protect the bacteria from killing activity of elastase secreted by neutrophils, thus enhancing bacterial tolerance towards the innate immune system. A second relevant finding is that among OMVs-associated proteins a bacteriocin (WP_006398867.1) has been found. Bacteriocins are powerful toxins with antibacterial activity that influence competition among bacterial species [237]. Since Bcc species and *P. aeruginosa* usually coinfect CF patients [238], bacteriocins might help *B. multivorans* C1576 in shaping and defining the relationship with *P. aeruginosa* within CF lungs.

Proteins responsible for detoxification of reactive oxygen species (ROS) have been shown to be a relevant fraction of both matrix- and OMVs-associated proteins (Table 3 and 4). Proteins found to be involved in oxidative stress are four thiol peroxidases (SMG02352.1, WP_006400399.1, WP_057926826.1, WP_059465341.1), a superoxide dismutase (EGD01013.1), catalase HPII (katE, CATE_ECOLI), a peroxidase (OJD07310.1) and a thioredoxin (ABC39250.1). Since some of these detoxifying enzymes have been found associated with OMVs, it may be speculated that *B. multivorans* C1576 releases them via OMVs to cope with oxidative stresses. For example, the presence of matrix-associated enzymes that inactivate ROS might allow bacteria to resist to those attacks from phagocytes based on hydrogen peroxide production [239]. The biological role of the intracellular proteins associated with both the biofilm matrix and OMVs of *B. multivorans* C1576 is not known. There is experimental evidence that some intracellular

proteins may have a function also outside the cell and for this reason they have been named moonlighting proteins [240]. Among these proteins there is the elongation factor Tu which has been localized on the surface of *P. aeruginosa* where it helps bacteria to evade the human complement attack via interactions with host regulatory proteins [241]. The matrix proteome of *B. multivorans* C1576 has been found to contain various elongation factors (G, Ts, GreAB), but not the elongation factor Tu. The latter together with chaperonin GroEL have been also shown to enable lactobacilli to bind to mucin and epithelial cells of the human gastrointestinal tract [242,243].

Since eDNA has been recognized as a prominent constituent of the bacterial biofilm matrix [37,244], it has not been unexpected to find DNA-binding proteins in the proteome of the biofilm matrix of *B. multivorans* C1576. The DNA-binding protein HU-alpha (DBHA_BURPS), which is a histone-like protein involved in DNA wrapping, has been found associated with OMVs whereas the DNA-binding protein Bv3F (POM19719.1) and a single-stranded DNA-binding protein (SMG01792.1) has been shown to be part of the matrix. Even though DNA-binding proteins affect DNA compactness and transcription [245], it is unknown whether they influence structural and functional properties of eDNA in the context of the biofilm matrix. The presence of DNA-binding proteins is in good agreement with CLSM data that shows the presence of eDNA in the matrix of biofilms produced by *B. multivorans* C1576.

In the search for proteins that may interact with EpolC1576, no known carbohydrate binding protein has been found. However, 23 out of 209 predicted proteins by proteomic analyses are hypothetical proteins whose function is still unknown. Some of these might bind to EpolC1576 and yet be unknown considering the unique structure of the polysaccharide. For this reason, potential protein binders of EpolC1576 were searched by means of the phage display technology.

4.3.7 Characterization of ox-EpolC1576-BSA conjugate via HP-SEC, MALDI-TOF mass spectrometry, SDS-PAGE and Western Blot

In order to immobilize EpolC1576 on a solid support, preliminary to screening the phage library of gDNAs of *B. multivorans* C1576, high (H) molecular weight fragments of EpolC1576 (18 kDa) were mildly activated using $NaIO_4$ and coupled to BSA during a 16 hours reaction. To prove the success of the coupling of $NaIO_4$-activated H-EpolC1576 fragments to BSA, the products of conjugation reaction were analyzed by HP-SEC. The

chromatogram of the conjugation products (Fig. 31 b, blue arrow) showed the presence of a distribution of molecular masses shifted towards higher molecular masses with respect to that of free BSA (Fig. 32 a) and the signal relative to the unconjugated ox-H-EpolC1576 fragments (Fig. 32 b, red arrow).

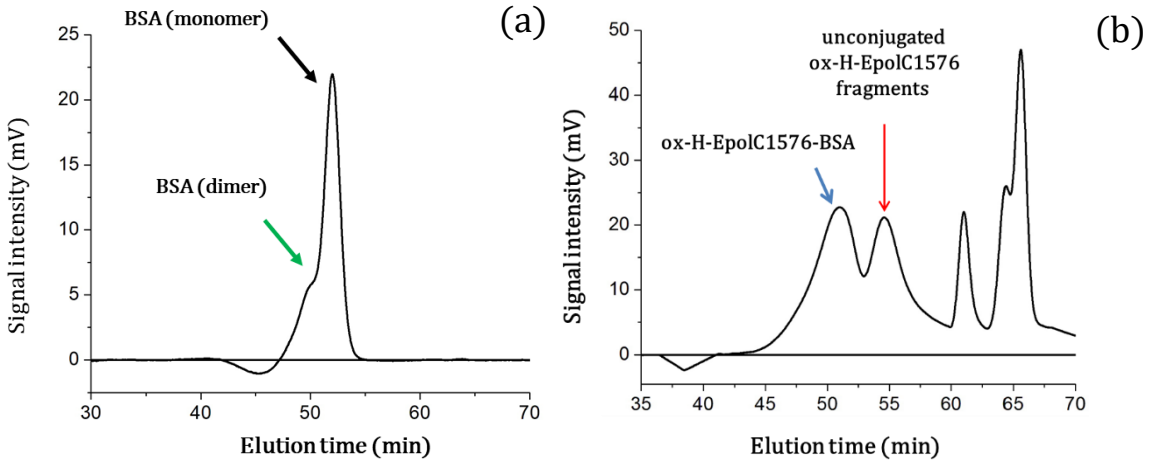

Figure 32. HP-SEC analysis of BSA alone (a) and of the products of conjugation reaction between ox-H-EpolC1576 fragments and BSA (b). BSA eluted after 52 min. The conjugation reaction was incubated for 16 h and produced a distribution of molecular masses (blue arrow) with a retention time (t_R) of 51 min that corresponds to an apparent molecular weight of 81 kDa. As expected, conjugation of ox-H-EpolC1576 fragments to BSA was not complete (red arrow).

As expected, the ox-H-EpolC1576-BSA conjugate produced a distribution of molecular masses eluting after 51 min, while free BSA eluted after 52 min. According to a calibration curve built with standards molecular mass globular proteins, the apparent molecular mass of the ox-H-EpolC1576-BSA conjugate was estimated to be about 81 kDa. The peak relative to unconjugated ox-H-EpolC1576 fragments eluted after 54.6 min which is almost identical to the retention time showed by H-EpolC1576 fragments (t_R= 54.2 min) before oxidation with $NaIO_4$ (see paragraph 2.2.7 for HP-SEC characterization of EpolC1576 fragments). The coupling of ox-H-EpolC1576 fragments to BSA was unambiguously demonstrated via MALDI-TOF analysis of selected chromatographic fractions (Fig. 33) of the glycoconjugate peak. MALDI-TOF spectra (Fig. 34 shows only the spectrum of fraction 27) confirmed that the conjugation reaction produced a distribution of molecular masses with about 1 or 2 ox-H-EpolC1576 fragments linked to BSA. Moreover, a small fraction of BSA remained unconjugated (Fig. 34, red arrows).

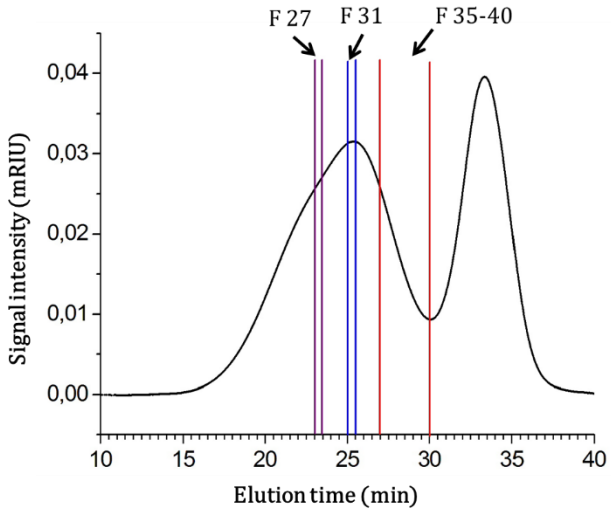

Figure 33. MPLC separation of ox-H-EpolC1576-BSA conjugate. Fractions 27, 31 and 35-40 were selected for MALDI-TOF MS investigation to confirm that covalent coupling between the two species occurred.

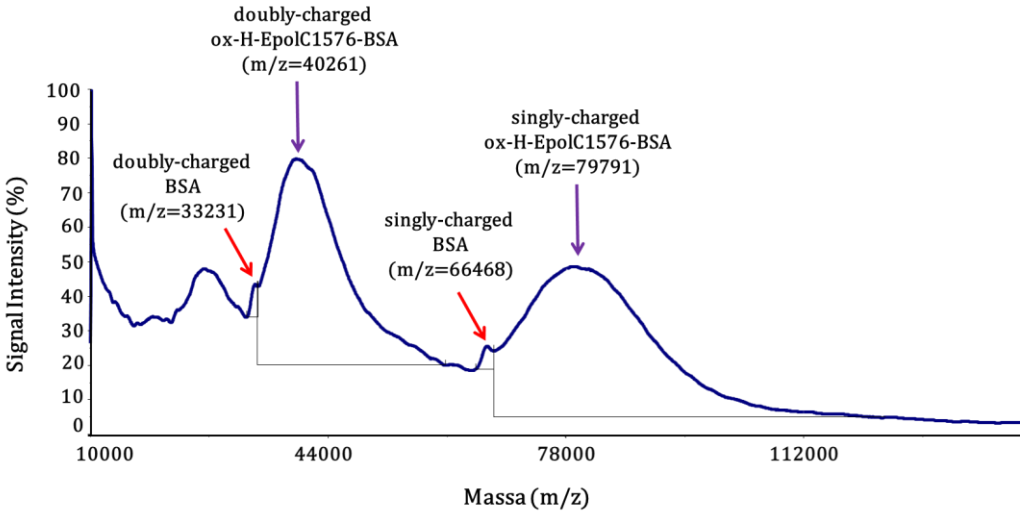

Figure 34. MALDI mass spectrum of ox-H-EpolC1576-BSA conjugate (Fraction 27).
Peak broadening characterizing singly- and doubly-charged glycoconjugate species (purple arrows) can be ascribed to the polydispersity of ox-H-EpolC1576 fragments and the randomness of the coupling process with BSA. The *m/z* value is indicated between brackets for each species.

With the aim of increasing the yield of BSA conjugation, the reaction was extended from 16 to 72 h and medium (M) molecular weight fragments (12 kDa) of EpolC1576 were used. HP-SEC analysis of the products of the reaction incubated for 72 h (Fig. 35) showed that the ox-M-EpolC1576-BSA conjugate eluted before the one synthesized over 16 h of incubation (49.6 min vs 51 min), thus indicating an increase in molecular mass.

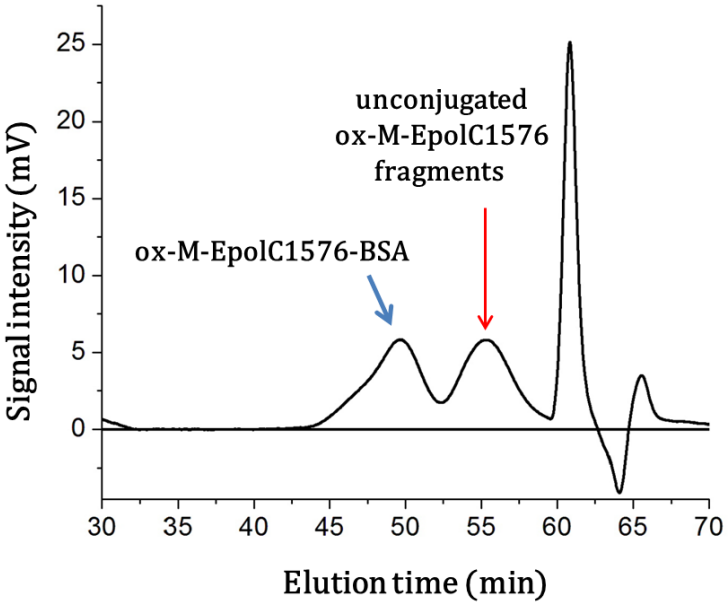

Figure 35. HP-SEC analysis of the conjugation products of the reaction between ox-M-EpolC1576 fragments and BSA. The reaction lasted 72 h and produced a distribution of molecular masses (blue arrow) with a retention time (t_R) of 49.6 min that corresponds to an apparent MW of 100 kDa. As expected, not all the activated EpolC1576 fragments coupled to BSA (red arrow).

Indeed, the apparent molecular mass of ox-M-EpolC1576-BSA was estimated to be about 100 kDa. SDS-PAGE analysis of the conjugation products confirmed that ox-M-fragments of EpolC1576 were covalently coupled to BSA, thus producing a distribution of glycoconjugates having a wide range of molecular weights. For this reason, ox-M-EpolC1576-BSA conjugate appeared on the gel as a smear rather than a discrete band (Fig. 36). This was not surprising as EpolC1576 fragments were polydisperse and the conjugation was random.

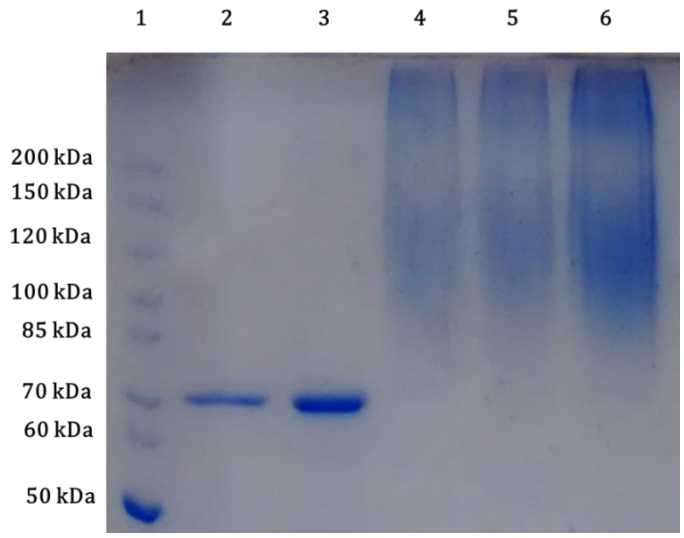

Figure 36. SDS-PAGE analysis of the products of the conjugation reaction (72 h) in comparison with unconjugated BSA. Lane 1: standard markers; lane 2 and 3: unconjugated BSA (2 and 4 µg,

respectively); lane 4, 5 and 6: conjugation mixture products (4, 4 and 8 µg respectively). Since the reaction produced a distribution of molecular masses, the glycoconjugate produced smears.

The covalent binding of ox-M-EpolC1576 fragments to BSA was also verified resorting to Western Blot analysis (Fig. 37). Coupled fragments were detected using the lectin Concanavalin A conjugated to horseradish peroxidase (Con A-HRP). BSA and the antibody α-HPAG were used as negative and positive control, respectively.

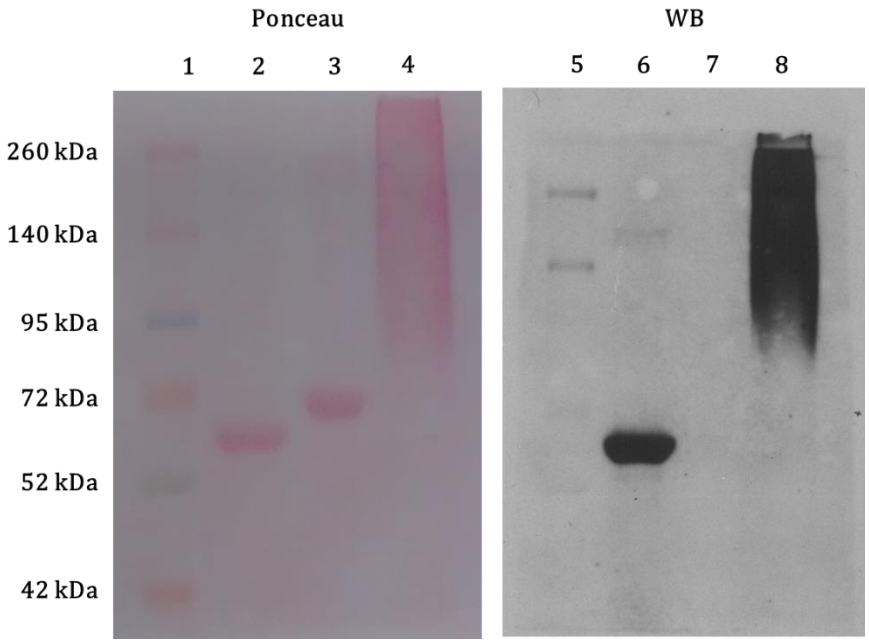

Figure 37. Ponceau S staining and Western Blot analysis of ox-M-EpolC1576-BSA conjugate. Ponceau S staining (left) was performed to verify that proteins previously separated by SDS-PAGE were transferred to a nitrocellulose membrane. Lane 1: standard markers; lane 2: α-HPAG antibody (glycoprotein); lane 3: unconjugated BSA; lane 4: ox-M-EpolC1576-BSA conjugate. Western Blot (right) with the ox-M-EpolC1576-BSA conjugate (lane 8). Unconjugated BSA (lane 7) gave no signal, while ConA-HRP also allowed to detect the antibody α-HPAG (lane 6). Lane 5: standard markers.

4.3.8 Detection of ox-M-EpolC1576-BSA conjugate immobilized on the solid support

Once the ox-M-EpolC1576-BSA conjugate was produced, its ability to bind to the plastic surface of a solid support (the wells of E.I.A. R.I.A. strips) was demonstrated using an Enzyme-linked Lectin Assay (ELLA) which is a type of ELISA assay where carbohydrates immobilization is detected after incubation with carbohydrates-binding proteins (lectins) conjugated with an enzyme that converts a substrate into a colored product. In this case it was used Concanavalin A (ConA) that possesses high affinity for mannose

residues, one of the two monosaccharides in EpolC1576. ConA is conjugated with the horseradish peroxidase (HRP) that by reacting with the substrate 3,3',5,5'-tetramethylbenzidine (TMB) produces a colored product only in the presence of immobilized carbohydrate molecules. Fig. 38 a shows the relationship between increasing concentrations of ox-M-EpolC1576-BSA and the relative absorbance intensity. The increase of absorbance intensity in a dependent-concentration manner clearly indicates that the ox-M-EpolC1576-BSA conjugate bound to the solid support and that 1 µg of the glycoconjugate was enough to saturate the wells surface. For comparison purposes, the glycosylated antibody α-HPAG was used as positive control (Fig. 37 b).

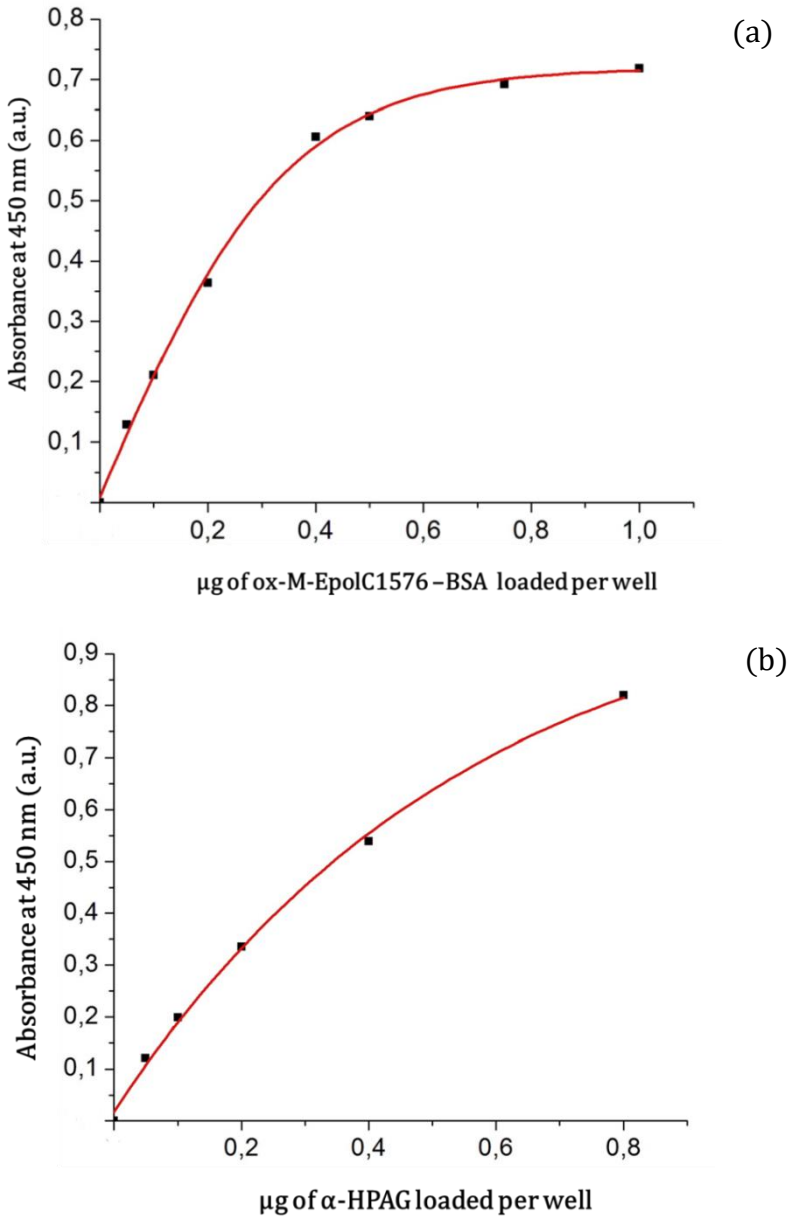

Figure 38. Standard curve for ELLA assay of the ox-M-EpolC1576-BSA (a) conjugate and antibody α-HPAG (b). The plot of absorbance at 450 nm vs ox-M-EpolC1576-BSA and α-HPAG concentration (µg).

4.3.9 Screening of the phage displayed *B. multivorans* C1576 gDNAs library

The phage display technology has been used to select proteins expressed by *B. multivorans* C1576 able to bind EpolC1576. For this reason, a library of genomic DNA sequences (gDNAs) obtained from the fragmentation of *B. multivorans* C1576 genome was constructed. Specifically, each gDNA sequence of *B. multivorans* C1576 was inserted into a phagemid vector upstream of gene pIII which codes for the minor coat protein pIII. In this way, each bacterial protein of the library is displayed on the surface of phage particles as pIII fusion. The phage library was then screened to select potential protein binders of EpolC1576 immobilized in the form of the protein-conjugate (ox-M-EpolC1576-BSA) on a solid support (the scheme of the library construction and screening is reported in Fig. 39).

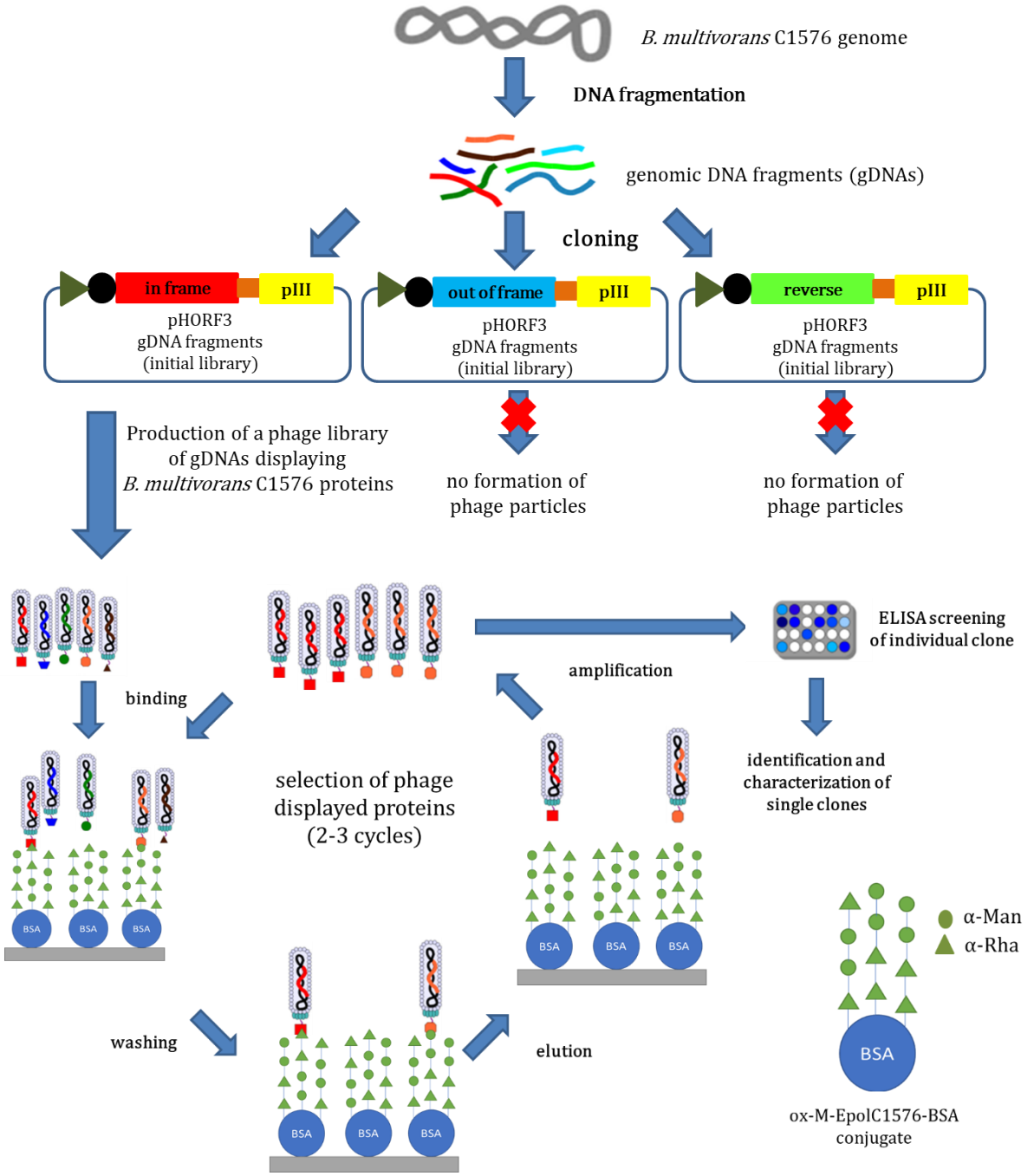

Figure 39. Schematic representation of the construction of the phage library of *B. multivorans* C1576 gDNAs, selection, enrichment and characterization of those phage particles displaying proteins that bind to EpolC1576 fragments of the ox-M-EPolC1576- BSA conjugate immobilized on the surface of ELISA microplate wells. Figure adapted from Meyer T. [246] under creative commons attribution license.

The original phage library stock was amplified to get enough quantity of viral particles to start the screening. The amplified phage library stock was titrated to determine the number of phages (input phage) used for the first round of selection. The input phage was 1.3 x 10^{10} pfu/mL. To analyse the binding specificity of *B. multivorans* C1576

displayed proteins to EpolC1576, a first round of phage selection was performed. The ox-M-EpolC1576-BSA glycoconjugate was immobilized on the surface of plastic immunotubes and incubated with the amplified phage library stock. The phage solution contained high-concentrated free BSA to reduce the number of viral particles that would have bound to the glycoconjugate due to cross-reactivity toward BSA (false positives). Unlike the one loaded in tube B, phage solution used for tube A contained 2% milk to see whether it would have positively influenced the selection procedure. The amplified phage particles from the first round of selection were again tested for their ability to bind EpolC1576, and the bound phage (output phage) were eluted from both tubes with DH5αF' cells, titrated and amplified (Table 6 and 7). A third round of selection was performed to enrich for phage particles having high affinity for EpolC1576; eluted phage (output phage) were titrated and amplified (Table 6 and 7). After the second and third round of selection, the eluted phage particles were also plated to allow for amplification and individual clones were characterize by PCR (data not shown) and investigated for their ability to bind EpolC1576 (ELISA assay). Fig. 40 illustrates the workflow of the phage library screening.

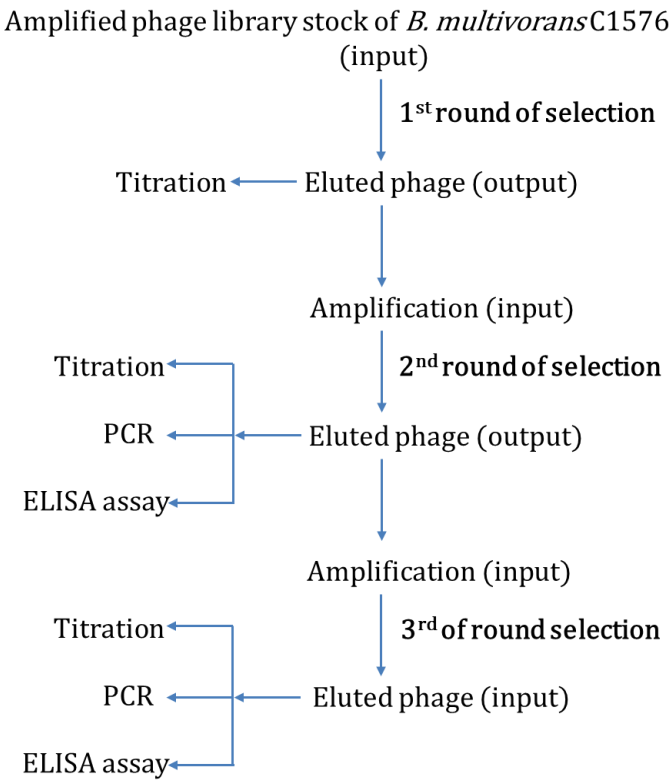

Figure 40. Schematic representation of the screening of the phage library of *B. multivorans* C1576 gDNAs. Three rounds of selection were performed to enrich for phages having high affinity for

EpolC1576 for both conditions tested (with and without 2% milk). Individual clones, randomly picked among phages eluted after the second and third round of selection, were analysed by PCR to verify that gDNA inserts had the appropriate size, whereas others were tested for their ability to specifically bind to EpolC1576.

Table 6. Phage titration during selection process in tube A (with 2% milk).

Selection round	Input phage	Output phage A
1st	1.3 x 10^{10}/mL	8 x 10^{5}/mL
2nd	3 x 10^{11}/mL	6 x 10^{3}/mL
3rd	1.5 x 10^{11}/mL	1.8 x 10^{5}/mL

Table 7. Phage titration during selection process in tube B (without milk).

Selection round	Input phage	Output phage A
1st	1.3 x 10^{10}/mL	7.5 x 10^{5}/mL
2nd	1 x 10^{11}/mL	4 x 10^{5}/mL
3rd	1.5 x 10^{11}/mL	3 x 10^{6}/mL

To test the degree of binding specificity of phages eluted from the 2nd and 3rd round of selection to EpolC1576, ELISA assays were performed. ELISA microplates (MaxiSorp®) were coated with 100 µL of ox-M-EpolC1576-BSA (10 µg/mL) and incubated with amplified single clones of phages which had been randomly chosen among eluted phages from 2nd and 3rd round of selection. Each clone virtually carried a different genomic DNA sequence of *B. multivorans* C1576 and specified for a distinct protein. Specifically, after the 2nd round of selection 24 and 60 phage clones eluted from tube A and B, respectively, were tested for binding to EpolC1576. After the 3rd round, 44 distinct phage clones for both selection conditions were screened. The same phage clones were also incubated in ELISA microplates coated with 100 µL of BSA (10 µg/mL) to see whether phage selection occurred due to non-specific binding of phage particles to BSA rather than to EpolC1576. Fig. 41 shows the results from the ELISA assay performed to analyse the binding specificity of phages eluted after the 2nd round of selection.

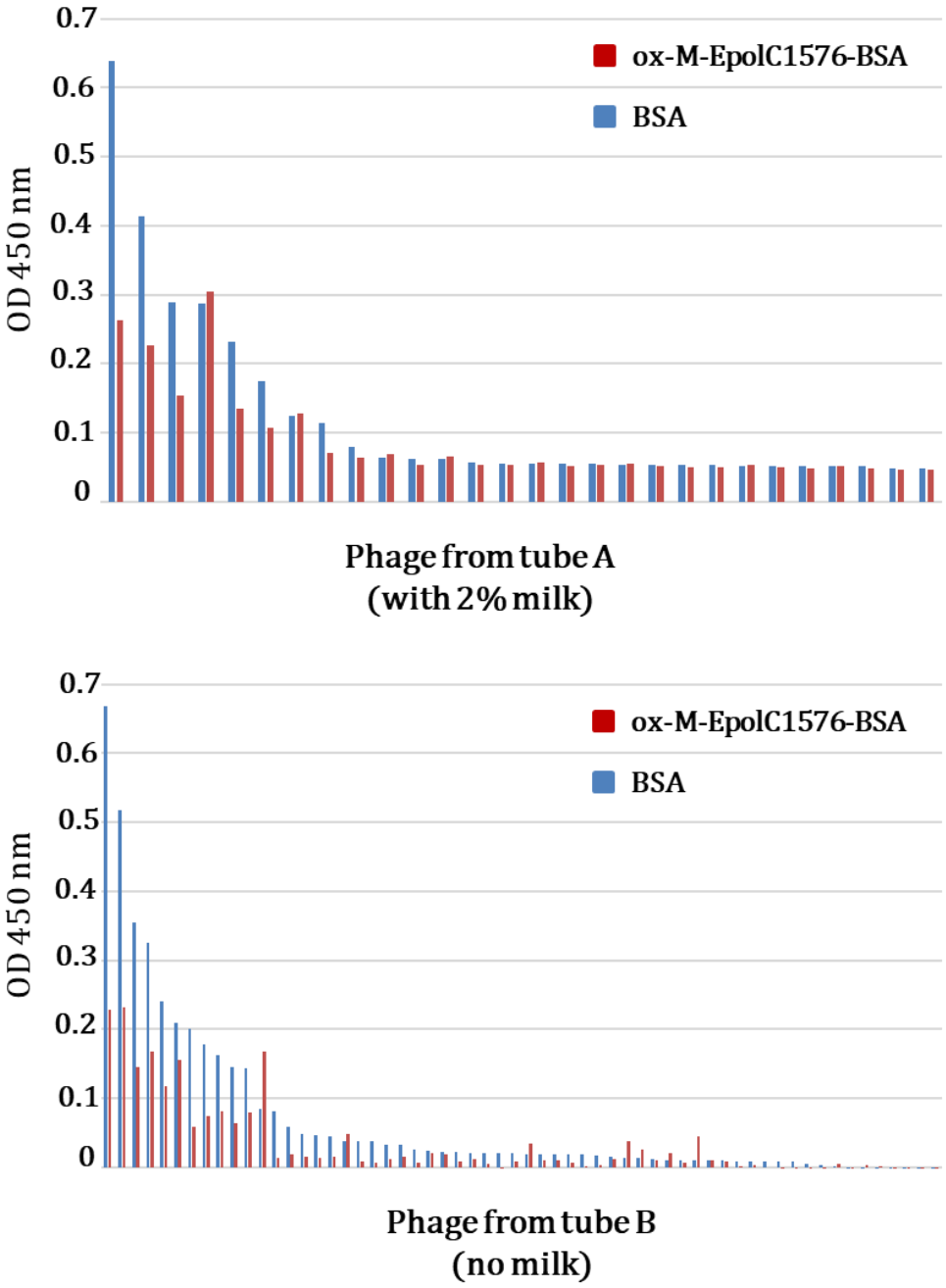

Figure 41. ELISA assay of phage displayed proteins of *B. multivorans* C1576 eluted after the second cycle of selection. ELISA signals from randomly picked phages are shown after the 2nd round of selection of the library against EpolC1576. Each phage was assayed against ox-M-EpolC1576-BSA conjugate (blue bars) and against BSA alone (red bars).

The majority of phages selected showed very low absorbance values for both conditions tested (with and without 2% milk), thus indicating a weak binding affinity for EpolC1576. However, the most important information was that the eluted phages bound to BSA alone (blue bars) with an affinity higher than the ox-M-EpolC1576-BSA conjugate

(red bars), thus suggesting that phage particles were mainly selected due to cross-reactivity toward BSA.

Fig. 42 shows the ELISA assay results for phages eluted after the 3rd round of selection.

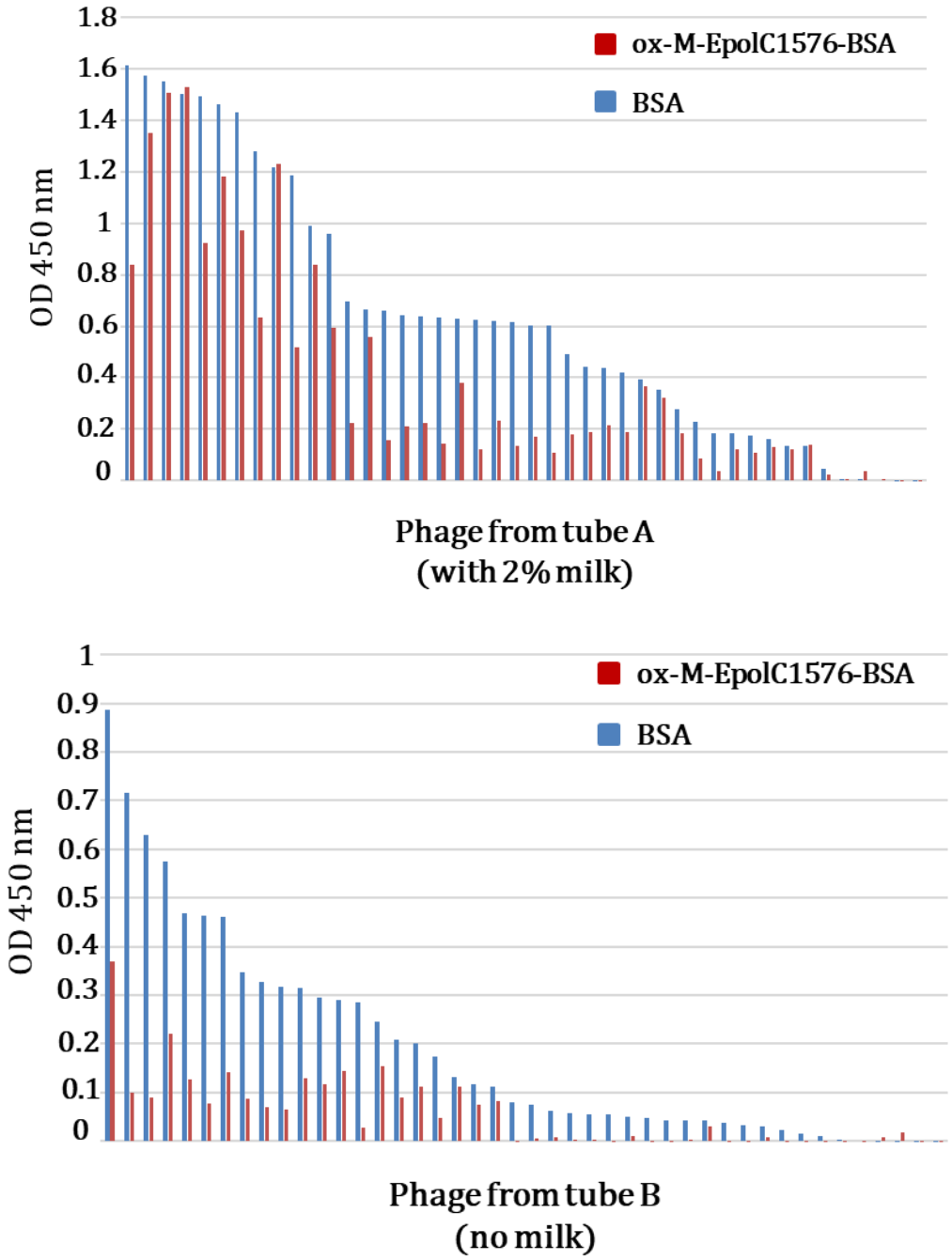

Figure 42. ELISA assay of phage displayed proteins of *B. multivorans* C1576 eluted after the third cycle of selection. ELISA signals from randomly picked phages after the 3rd round of selection of the library against EpolC1576. Each phage was assayed against ox-M-EpolC1576-BSA conjugate (red bars) and against BSA alone (blue bars).

Phages affinity for EpolC1576 increased (red bars) but it was still comparable, sometimes even lower, than that showed for BSA alone (blue bars). This data suggests

that, after the 3rd round of selection, the phage library was mainly enriched in viral particles that bound to BSA due to cross reactivity rather than affinity for EpolC1576.
To solve the problem of nonspecific binding of phage particles to BSA, ox-M-EpolC1576 fragments were directly immobilized on ELISA microplates (Corning® Carbo-BIND™ 96-well microplates) meant to be covalently coupled to sodium-periodate activated carbohydrates. The surface of these microplates presents hydrazide groups which readily react with aldehyde groups produced after mild oxidation on the carbohydrate chain.

By performing various rounds of selection of a phage library of displayed proteins, phage display usually allows to enrich the library for polypeptides having high affinity for targets immobilized on a solid surface, typically with dissociation constants (K_D) in sub to low nanomolar (nM) ranges [247]. However, interactions between carbohydrates and proteins are weak binding events, usually in the millimolar (mM) to micromolar (μM) range [248]. Lectins, which are carbohydrate-binding proteins, have been found in the biofilm matrix of various bacterial species [204]. For example, resorting to a transcriptomic analysis, Inhülsen *et al.* have found that the Bcc species *B. cenocepacia* J2315 contains 3 genes coding for three distinct lectins organized in an operon (*bcl*ACB) [162]. The synthesis of BclA, BclB and BclC seem to be linked to CepIR QS system and mutants lacking the *bcl*ACB operon produce biofilms with altered architectures with respect to those produced by the wild type counterpart [162]. The lectin-carbohydrate binding event is based on various non-covalent and reversible contacts such as hydrogen bonds, electrostatic, hydrophobic and Van der Waals interactions [249]. The binding of monovalent lectins to carbohydrates is generally weak and characterized by dissociation constants in the mM and μM range [249]. In this light, attempts to enrich the phage library of *B. multivorans* C1576 for proteins that bind to EpolC1576 may have been unsuccessful probably due to the weak affinity of potential displayed binders for the carbohydrate target. For this reason, some steps of the laborious protocol of the phage library selection need to be optimized. With the aim of finding a way to preserve weak interactions as much as possible, the phage library screening should be performed at different temperatures and the use of detergents (Tween 20) should be avoided or at least reduced as it can interfere with non-covalent interactions [250,251]. In addition, different concentrations of divalent cations should be tested during selection

procedures since the ability of some lectins to bind carbohydrates depends on the presence of divalent metal ions (Ca^{2+}, Mg^{2+}, Mn^{2+}). For example, BclA synthetized by *B. cenocepacia* J2315 is a lectin that requires two Ca^{2+} ions for binding to carbohydrates and it organizes in homodimers that have one binding site per monomer which acts cooperatively for the binding to the second site [252]. In physiologically relevant context, multivalent lectins bind to complex, branched carbohydrates displaying various binding sites with high affinities, thus showing dissociation constants in the nanomolar or even picomolar range (pM) [253]. In this light, it can be also speculated that potential lectins of *B. multivorans* C1576 are made of two or more subunits and their inability to associates into functional oligomeric and/or multimeric proteins on the surface of the phage particles may reduce their binding affinity for EpolC1576, thus making them hard to detect.

4.3.10 Detection of ox-M-EpolC1576 fragments immobilized on Carbo-BIND™ microplates

With the aim of enriching the phage library of *B. multivorans* C1576 gDNAs for proteins that bind to EpolC1576 and avoiding the selection of phage particles that show cross-reactivity toward BSA, the sodium-periodate activated fragments of EpolC1576 were covalently coupled to the Carbo-BIND™ microplates (Corning®). The binding curve of ox-M-EpolC1576 fragments showed in fig. 43 clearly indicates that the saccharide fragments have been successfully immobilized on the plastic surface of the microplates and that the binding capacity of the wells is reached with 100 µL of 10 µg/mL of ox-M-EpolC1576 fragments. The binding to Carbo-BIND™ microplates has been also demonstrated for dextran molecules (MW 20 kDa) activated with sodium periodate (data not shown).

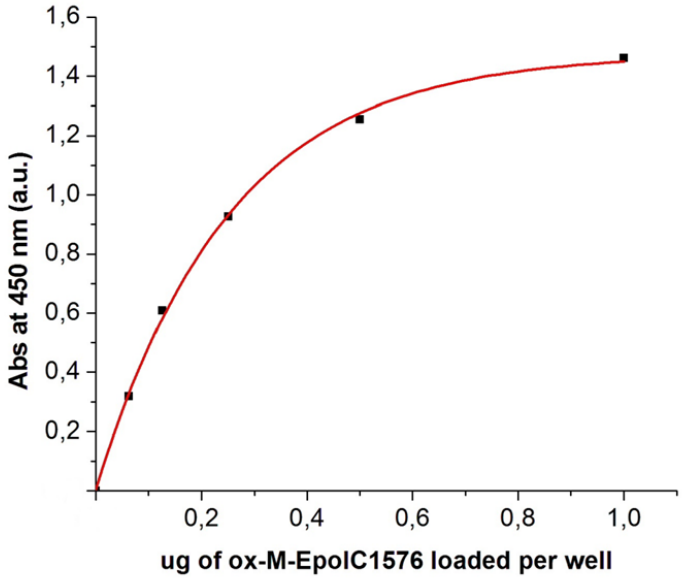

Figure 43. An ELLA binding curve of ox-M-EpolC1576 fragments that expresses the carbohydrate concentration as a function of absorbance at 450 nm.

5 CONCLUSIONS

Exopolysaccharides produced by bacteria are considered to be the matrix component mainly responsible for biofilm maintenance and mechanical stability, thus conferring them with a structural role. However, recent studies pointed at additional roles of polysaccharides such as their involvement in relevant biological/biochemical functions. Since different bacterial species produce different exopolysaccharides, it is fundamental to elucidate their physicochemical properties in order to comprehend the biological role played by the matrix within biofilm communities. Here, it has been demonstrated that the EpolC1576, purified from *B. multivorans* C1576 biofilm matrix, contains nonpolar domains that provide EpolC1576 with the ability to interact with hydrophobic molecules. Fluorescence and NMR spectroscopy data clearly indicates that EpolC1576 can form complexes with the two fluorescent aromatic probes ANS and TNS which have been previously used to identify hydrophobic pockets of proteins and cyclodextrins. Moreover, NMR data shows that in aqueous solution EpolC1576 enhances the solubility of the 11-Me-C12:Δ^2 compound which is a nonpolar signaling molecule synthesized by *B. multivorans*, thus suggesting that interactions between the two species may occur in the physiological context of the biofilm matrix. To elucidate the mechanism by which EpolC1576 interact with hydrophobic compounds, molecular modeling simulations were carried out using hexane and 11-Me-C12:Δ^2 as nonpolar guest molecules. This investigation revealed that in aqueous solution EpolC1576 has a very flexible chain that can rapidly bend and straighten. The fact that EpolC1576 has no regular conformation allows the polymer to form transient hydrophobic pockets that may accommodate nonpolar compounds, as observed for hexane and 11-Me-C12:Δ^2 during both simulations. Neighboring rhamnose residues with O-methyl substituents and the plane of the pyranose rings are mainly involved in the formation of these nonpolar pockets. Molecular modeling simulations also indicate that EpolC1576 and the two non-polar host molecules interact via both rapid local and longer interactions. The latter are localized within the hydrophobic pockets produced by the polymer along its chain, thus allowing EpolC1576 to sequester non-polar guest molecules for longer periods (few nanoseconds). STD NMR studies of the interaction between EpolC1576 and the fluorescent probes ANS and TNS further demonstrated the polymer capability to

complex these aromatic compounds. Moreover, STD NMR allowed to map on ANS and TNS structure those regions/atoms mainly involved in the binding event. When -CH_3 groups of EpolC1576 are saturated, specific rings of both aromatic compounds receive the highest magnetization, thus indicating that distinct regions of the fluorescent probes participate differently in the interactions. Another interesting finding from STD NMR studies is the observation of significant interactions between EpolC1576 and the aminoglycoside antibiotic Kanamycin. EpolC1576-Kanamycin interaction reinforces the idea that even uncharged biofilm exopolysaccharides may play a role in tolerance toward antibiotics, thus affecting their rate of penetration by transiently trapping them and/or modulate their activity throughout non-ionic interaction either of van der Waals or hydrogen bond type. SPR investigation confirmed EpolC1576 ability to interact with hydrophobic compounds, specifically long alkyl chains attached on a gold surface. It is noteworthy that EpolC1576 fragments were not completely washed away after the flowing of the solution used to regenerate the chip surface, thus indicating that EpolC1576 may bind and capture nonpolar compounds with a relatively good affinity. To sum up, all the data indicates that EpolC1576 may transiently bind hydrophobic biologically active compounds, thus favoring (quorum sensing molecules) and/or slowing down (antibiotics) their trafficking through the biofilm matrix. In this way, non-polar compounds may "reach" their target binding sites by travelling through the hydrophobic domains of EpolC1576 chains that build-up the 3D macromolecular network of the matrix that might constitute the cell-cell connections. Given the importance of both quorum sensing and tolerance to antibiotics for biofilm cells fitness, EpolC1576 production may enhance bacterial survival within the host, thus allowing *B. multivorans* C1576 infections to persist.

AFM studies of EpolC1576 conformation and ability to form a macromolecular network showed that the polymer can adopt a spherical conformation, probably due to its high flexibility, and that at high concentration it tends to form densely-packed aggregates of spherical objects. Intermolecular forces between EpolC1576 "spheres" may assist the formation of these aggregates structure, thus suggesting a possible mechanism for EpolC1576 molecules to build-up the 3D-scaffold that characterizes the biofilm matrix.

CLSM imaging of *B. multivorans* C1576 biofilms developed in three different media (MH, SCFM and YEM) revealed that the biofilm morphology is affected by the composition of the culture medium used. The morphological heterogeneity is visibly evident from one

medium to another: thick discontinuous biofilm formations are observed in MH, whereas in SCFM and YEM media biofilms appear as compact microbial mats with small cell aggregates. Besides the morphological aspect, the composition of the medium influences the relative abundance of extracellular polymeric substances (EPS) that constitute the matrix. For example, it can be observed that the matrix of biofilms developed in SCFM, which approximates the nutrient content of the CF sputum, is richer in exopolysaccharide molecules than that characterizing biofilms formed in MH and YEM media. As observed for biofilms grown on MH medium, EpolC1576 is the only exopolysaccharide purified from *B. multivorans* C157 6biofilms developed on cellulose membrane deposited on solid SCFM. The detection of biofilms of *B. multivorans* in CF sputum together with the ability of *B. multivorans* C1576 to produce biofilms on the medium that resembles the nutritional environment of CF sputum suggest that this Bcc species may develop biofilms *in vivo* where EpolC1576 is probably involved in conferring mechanical stability to the biofilm and protection to bacteria toward antibiotics, for example toward Kanamycin which has been observed to interact with the exopolysaccharide (STD NMR studies).

As for other Gram-negative bacterial species, transmission electron microscopy imaging of *B. multivorans* C1576 biofim matrix revealed the presence of outer membrane vesicles (OMVs), spherical bilayered structures with a diameter of 20-70 μm. Besides the presence of cytoplasmic and periplasmic proteins, proteomic analysis of OMVs showed that they are particularly enriched in outer membrane proteins which is not surprising as OMVs gemmate from bacterial outer membrane. However, the biological role of OMVs produced by *B. multivorans* C1576 remains elusive.

With the aim of obtaining more detail about the composition of the proteinaceous fraction of the biofilm matrix, a comprehensive proteomic analysis of the proteins associated with the matrix of *B. multivorans* C1576 was conducted. As already shown for other bacterial species, the biofilm matrix of *B. multivorans* C1576 includes several cytoplasmic, periplasmic, inner and outer membrane proteins, probably as a result of physiological cell death, thus suggesting that cell lysis is an important source of proteins for the matrix. The presence of membrane proteins can also be ascribed to the production of OMVs. Indeed, about 19 predicted proteins are common to the proteomic profile of both the matrix and OMVs. The biofilm matrix contains many enzymes for detoxification from reactive oxygen species (ROS) that may help bacteria to cope with

oxidative stresses like those experienced at sites of infection. In addition, among matrix-associated proteins some can represent virulence factors: various proteases were identified and including the protein known as ecotin which has already been shown to inhibit neutrophils elastase, thus helping bacteria to evade the neutrophil protease-mediated killing. Even though lectins had been identified in the matrix of various bacterial species, no clear carbohydrates-binding proteins were found. It cannot be ruled out that due to its peculiar chemistry and structure, EpolC1576 may interact with other types of carbohydrate-binding proteins to give structure and mechanical stability to the biofilm matrix. In addition, it cannot be excluded that among those hypothetical proteins found in the matrix one or more may be potential binders of EpolC1576.

Information about the structural and functional roles played by EpolC1576 within the biofilm matrix can be also inferred by the identification and characterization of *B. multivorans* C1576 proteins that interact with the polysaccharide. For this reason, a phage library of *B. multivorans* C1576 genomic DNA sequences (gDNAs) that displayed all the bacterium's proteins was screened to search for proteins able to bind to EpolC1576 immobilized on a solid surface. To accomplish this task, mildly oxidized fragments of EpolC1576 were covalently coupled to BSA, a protein with well-known binding properties to plastic surfaces. After various rounds of selection, it was not possible to enrich the library for phages displayed proteins that bound to EpolC1576. In this light, phage library selection procedures must be optimized by acting on those experimental conditions that can affect weak interactions such as temperature of incubation of the phage library and the use of detergents that should be avoided. In the search for lectins, it may be useful to test different concentrations of divalent metal ions since some lectins requires the presence of cations to work properly. In addition, phage particles have shown cross-reactivity toward BSA and led to the enrichment of the library for false positives. To avoid this problem, EpolC1576 fragments were directly immobilized on the surface of microplates meant to be coupled to activated carbohydrates, thus avoiding the use of BSA.

6 REFERENCES

[1] D. Dufour, V. Leung, C.M. Lévesque, Bacterial biofilm: structure , function , and antimicrobial resistance, (2012) 2–16.

[2] C.D. Nadell, B.L. Bassler, S.A. Levin, Observing bacteria through the lens of social evolution, J. Biol. 7 (2008) 27. doi:10.1186/jbiol87.

[3] H.-C. Flemming, J. Wingender, U. Szewzyk, P. Steinberg, S.A. Rice, S. Kjelleberg, Biofilms: an emergent form of bacterial life, Nat. Rev. Microbiol. 14 (2016) 563–575. doi:10.1038/nrmicro.2016.94.

[4] H.-C. Flemming, J. Wingender, The biofilm matrix, Nat. Rev. Microbiol. 8 (2010) 623–633. doi:10.1038/nrmicro2415.

[5] K. Ikuma, A.W. Decho, B.L.T. Lau, The Extracellular Bastions of Bacteria — A Biofilm Way of Life, Nat. Educ. Knowl. 4 (2013) 1–11. doi:10.1090/S0273-0979-05-01066-9.

[6] D.K. Ehrlich, H. L. & Newman, Geomicrobiology, CRC Press, 2008.

[7] R.U. Meckenstock, M. Elsner, C. Griebler, T. Lueders, C. Stumpp, J. Aamand, S.N. Agathos, H. Albrechtsen, L. Bastiaens, P.L. Bjerg, N. Boon, W. Dejonghe, W.E. Huang, S.I. Schmidt, E. Smolders, S.R. Sørensen, D. Springael, B.M. van Breukelen, Biodegradation: Updating the Concepts of Control for Microbial Cleanup in Contaminated Aquifers, Environ. Sci. Technol. 49 (2015) 7073–7081. doi:10.1021/acs.est.5b00715.

[8] B. Halan, K. Buehler, A. Schmid, Biofilms as living catalysts in continuous chemical syntheses, Trends Biotechnol. 30 (2012) 453–465. doi:10.1016/j.tibtech.2012.05.003.

[9] R.M. Donlan, Biofilms: microbial life on surfaces., Emerg. Infect. Dis. 8 (2002) 881–90. doi:10.3201/eid0809.020063.

[10] J.W. Costerton, K.J. Cheng, G.G. Geesey, T.I. Ladd, J.C. Nickel, M. Dasgupta, T.J. Marrie, Bacterial Biofilms in Nature and Disease, Annu. Rev. Microbiol. 41 (1987) 435–464. doi:10.1146/annurev.mi.41.100187.002251.

[11] E.E. Braxton, G.D. Ehrlich, L. Hall-Stoodley, P. Stoodley, R. Veeh, C. Fux, F.Z. Hu, M. Quigley, J.C. Post, Role of biofilms in neurosurgical device-related infections, Neurosurg. Rev. 28 (2005) 249–255. doi:10.1007/s10143-005-0403-8.

[12] U. Flemming, Hans-Curt, Wingender, Jost, Szewzyk, ed., Biofilm Highlights, Springer, 2011.

[13] J. Wingender, H.-C. Flemming, Biofilms in drinking water and their role as reservoir for pathogens., Int. J. Hyg. Environ. Health. 214 (2011) 417–23. doi:10.1016/j.ijheh.2011.05.009.

[14] B.J. Little, J.S. Lee, Microbiologically influenced corrosion: an update, Int. Mater. Rev. 59 (2014) 384–393. doi:10.1179/1743280414Y.0000000035.

[15] M. Balzer, N. Witt, H.-C. Flemming, J. Wingender, Faecal indicator bacteria in river biofilms, Water Sci. Technol. 61 (2010) 1105–1111. doi:10.2166/wst.2010.022.

[16] F. Morgan-Sagastume, P. Larsen, J.L. Nielsen, P.H. Nielsen, Characterization of the loosely attached fraction of activated sludge bacteria, Water Res. 42 (2008) 843–854. doi:10.1016/j.watres.2007.08.026.

[17] D. Monroe, Looking for chinks in the armor of bacterial biofilms, PLoS Biol. 5 (2007) 2458–2461. doi:10.1371/journal.pbio.0050307.

[18] D.G. Allison, The Biofilm Matrix, Biofouling. 19 (2003) 139–150. doi:10.1080/0892701031000072190.

[19] T.R. Neu, J.R. Lawrence, Innovative techniques, sensors, and approaches for imaging biofilms at different scales, Trends Microbiol. 23 (2015) 233–242. doi:10.1016/j.tim.2014.12.010.

[20] N. Billings, A. Birjiniuk, T.S. Samad, P.S. Doyle, K. Ribbeck, Material properties of biofilms – key methods for understanding permeability and mechanics, Reports Prog. Phys. 78 (2016) 36601. doi:10.1088/0034-4885/78/3/036601.Material.

[21] H.C. Flemming, A. Leis, Preface, Water Sci. Technol. 43 (2001).

[22] T.J. Battin, K. Besemer, M.M. Bengtsson, A.M. Romani, A.I. Packmann, The ecology and biogeochemistry of stream biofilms, Nat. Rev. Microbiol. 14 (2016) 251–263. doi:10.1038/nrmicro.2016.15.

[23] H. -C. & W. Späth, R., Flemming, Sorption properties of biofilms, Water Sci. Technol. 37 (1998) 207–210. doi:https://doi.org/10.2166/wst.1998.0623.

[24] M. Helm, R. F. & Potts, Ecology of Cyanobacteria II: Their Diversity in Space and Time, 2012.

[25] D. Tielker, S. Hacker, R. Loris, M. Strathmann, J. Wingender, S. Wilhelm, F. Rosenau, K.E. Jaeger, *Pseudomonas aeruginosa* lectin LecB is located in the outer membrane and is involved in biofilm formation, Microbiology. 151 (2005) 1313–1323. doi:10.1099/mic.0.27701-0.

[26] S.P. Diggle, R.E. Stacey, C. Dodd, M. Cámara, P. Williams, K. Winzer, The galactophilic lectin, LecA, contributes to biofilm development in *Pseudomonas aeruginosa*, Environ. Microbiol. 8 (2006) 1095–1104. doi:10.1111/j.1462-2920.2006.001001.x.

[27] C. Cucarella, C. Solano, J. Valle, B. Amorena, I. Lasa, J.R. Penadés, Bap, a *Staphylococcus aureus* surface protein involved in biofilm formation., J. Bacteriol. 183 (2001) 2888–96. doi:10.1128/JB.183.9.2888-2896.2001.

[28] J. Valle, C. Latasa, C. Gil, A. Toledo-Arana, C. Solano, J.R. Penadés, I. Lasa, Bap, a Biofilm Matrix Protein of *Staphylococcus aureus* Prevents Cellular Internalization through Binding to GP96 Host Receptor, PLoS Pathog. 8 (2012). doi:10.1371/journal.ppat.1002843.

[29] E.J. Van Schaik, C.L. Giltner, G.F. Audette, D.W. Keizer, D.L. Bautista, C.M. Slupsky, B.D. Sykes, R.T. Irvin, DNA Binding : a Novel Function of *Pseudomonas aeruginosa* Type IV Pili DNA Binding : a Novel Function of *Pseudomonas aeruginosa* Type IV Pili, J. Bacteriol. 187 (2005) 1455–1464. doi:10.1128/JB.187.4.1455.

[30] X. Zogaj, M. Nimtz, M. Rohde, W. Bokranz, U. Römling, The multicellular morphotypes of *Salmonella typhimurium* and *Escherichia coli* produce cellulose as the second component of the extracellular matrix, Mol. Microbiol. 39 (2001) 1452–1463. doi:10.1046/j.1365-2958.2001.02337.x.

[31] L. Ma, M. Conover, H. Lu, M.R. Parsek, K. Bayles, D.J. Wozniak, Assembly and development of the *Pseudomonas aeruginosa* biofilm matrix, PLoS Pathog. 5 (2009). doi:10.1371/journal.ppat.1000354.

[32] K. Sauer, M.C. Cullen, a H. Rickard, L. a H. Zeef, D.G. Davies, P. Gilbert, Characterization of nutrient-induced dispersion in *Pseudomonas aeruginosa* PAO1 biofilm., J. Bacteriol. 186 (2004) 7312–26. doi:10.1128/JB.186.21.7312-7326.2004.

[33] A. Pal, A.K. Paul, Microbial extracellular polymeric substances: Central elements in heavy metal bioremediation, Indian J. Microbiol. 48 (2008) 49–64. doi:10.1007/s12088-008-0006-5.

[34] L.C. Skillman, I.W. Sutherland, M. V Jones, The role of exopolysaccharides in dual species biofilm development., J. Appl. Microbiol. 85 Suppl 1 (1998) 13S–18S. doi:10.1111/j.1365-2672.1998.tb05278.x.

[35] S. Liao, M.I. Klein, K.P. Heim, Y. Fan, J.P. Bitoun, S.J. Ahn, R.A. Burne, H. Koo, L.J. Brady, Z.T. Wen, *Streptococcus mutans* extracellular DNA is upregulated during growth in biofilms, actively released via membrane vesicles, and influenced by components of the protein secretion machinery, J. Bacteriol. 196 (2014) 2355–2366. doi:10.1128/JB.01493-14.

[36] L. Yang, K.B. Barken, M.E. Skindersoe, A.B. Christensen, M. Givskov, T. Tolker-Nielsen, Effects of iron on DNA release and biofilm development by *Pseudomonas aeruginosa*, Microbiology. 153 (2007) 1318–1328. doi:10.1099/mic.0.2006/004911-0.

[37] C.B. Whitchurch, Extracellular DNA Required for Bacterial Biofilm Formation, Science (80-.). 295 (2002) 1487–1487. doi:10.1126/science.295.5559.1487.

[38] V. Dengler, L. Foulston, A.S. Defrancesco, R. Losick, An Electrostatic Net Model for the Role of Extracellular DNA in Biofilm Formation by *Staphylococcus aureus*, 197 (2015) 3779–3787. doi:10.1128/JB.00726-15.Editor.

[39] K. Schwartz, M. Ganesan, D.E. Payne, M.J. Solomon, B.R. Boles, Extracellular DNA facilitates the formation of functional amyloids in *Staphylococcus aureus* biofilms, Mol. Microbiol. 99 (2016) 123–134. doi:10.1111/mmi.13219.

[40] S. Vilain, J.M. Pretorius, J. Theron, V.S. Brözel, DNA as an adhesin: *Bacillus cereus* requires extracellular DNA to form biofilms, Appl. Environ. Microbiol. 75 (2009) 2861–2868. doi:10.1128/AEM.01317-08.

[41] A. Conrad, M. Kontro, M.M. Keinaenen, A. Cadoret, P. Faure, L. Mansuy-huault, J. Block, Fatty acids of lipid fractions in extracellular polymeric substances of activated sludge flocs, Lipids. 38 (2003) 1093–1105. doi:10.1007/s11745-006-1165-y.

[42] W. Sand, T. Gehrke, Extracellular polymeric substances mediate bioleaching/biocorrosion via interfacial processes involving iron(III) ions and acidophilic bacteria, Res. Microbiol. 157 (2006) 49–56. doi:10.1016/j.resmic.2005.07.012.

[43] T. Matsuyama, Y. Nakagawa, Surface-active exolipids: Analysis of absolute chemical structures and biological functions, J. Microbiol. Methods. 25 (1996) 165–175. doi:10.1016/0167-7012(95)00109-3.

[44] L. Bonnichsen, N.B. Svenningsen, M. Rybtke, I. de Bruijn, J.M. Raaijmakers, T. Tolker-Nielsen, O. Nybroe, Lipopeptide biosurfactant viscosin enhances dispersal of *Pseudomonas fluorescens* SBW25 biofilms, Microbiol. (United Kingdom). 161 (2015) 2289–2297. doi:10.1099/mic.0.000191.

[45] S.J. Pamp, T. Tolker-Nielsen, Multiple roles of biosurfactants in structural biofilm development by *Pseudomonas aeruginosa*, J. Bacteriol. 189 (2007) 2531–2539. doi:10.1128/JB.01515-06.

[46] A.T. Jan, Outer Membrane Vesicles (OMVs) of gram-negative bacteria: A perspective update, Front. Microbiol. 8 (2017) 1–11. doi:10.3389/fmicb.2017.01053.

[47] V.B. Gujrati, S. Jon, Bioengineered bacterial outer membrane vesicles: what is their potential in cancer therapy?, Nanomedicine. 9 (2014) 933–935. doi:10.2217/nnm.14.56.

[48] P. Cescutti, Bacterial Capsular Polysaccharides and Exopolysaccharides, in: Microb. Glycobiol., 2010: pp. 93–108. doi:10.1016/B978-0-12-374546-0.00006-7.

[49] B. Cuzzi, Y. Herasimenka, A. Silipo, R. Lanzetta, G. Liut, R. Rizzo, P. Cescutti, Versatility of the *Burkholderia cepacia* Complex for the Biosynthesis of Exopolysaccharides: A Comparative Structural Investigation, PLoS One. 9 (2014) e94372. doi:10.1371/journal.pone.0094372.

[50] J. Wingender, M. Strathmann, A. Rode, A. Leis, H.-C. Flemming, [25] Isolation and biochemical characterization of extracellular polymeric substances from *Pseudomonas aeruginosa*, in: Methods Enzymol., 2001: pp. 302–314. doi:10.1016/S0076-6879(01)36597-7.

[51] C. Ryder, M. Byrd, D.J. Wozniak, Role of polysaccharides in *Pseudomonas aeruginosa* biofilm development, Curr. Opin. Microbiol. 10 (2007) 644–648. doi:10.1016/j.mib.2007.09.010.

[52] M.S. Byrd, I. Sadovskaya, E. Vinogradov, H. Lu, A.B. Sprinkle, S.H. Richardson, L. Ma, B. Ralston, M.R. Parsek, E.M. Anderson, J.S. Lam, D.J. Wozniak, Genetic and biochemical analyses of the *Pseudomonas aeruginosa* Psl exopolysaccharide reveal overlapping roles for polysaccharide synthesis enzymes in Psl and LPS production, Mol. Microbiol. 73 (2009) 622–638. doi:10.1111/j.1365-2958.2009.06795.x.

[53] L.K. Jennings, K.M. Storek, H.E. Ledvina, C. Coulon, L.S. Marmont, I. Sadovskaya, P.R. Secor, B.S. Tseng, M. Scian, A. Filloux, D.J. Wozniak, P.L. Howell, M.R. Parsek, Pel is a cationic exopolysaccharide that cross-links extracellular DNA in the *Pseudomonas aeruginosa* biofilm matrix., Proc. Natl. Acad. Sci. U. S. A. 112 (2015) 11353–8. doi:10.1073/pnas.1503058112.

[54] D.H. Limoli, C.J. Jones, D.J. Wozniak, S. Cruz, Bacterial Extracellular Polysaccharides in Biofilm Formation and Function, Microbiol Spectr. 3 (2015) 1–30. doi:10.1128/microbiolspec.MB-0011-2014.Bacterial.

[55] K.K. Jefferson, D.A. Goldmann, G.B. Pier, Use of Confocal Microscopy To Analyze the Rate of Vancomycin Penetration through *Staphylococcus aureus* Biofilms, Antimicrob. Agents Chemother. 49 (2005) 2467–2473. doi:10.1128/AAC.49.6.2467-2473.2005.

[56] N. Høiby, T. Bjarnsholt, M. Givskov, S. Molin, O. Ciofu, Antibiotic resistance of bacterial biofilms, Int. J. Antimicrob. Agents. 35 (2010) 322–332. doi:10.1016/j.ijantimicag.2009.12.011.

[57] H.K. Kuramitsu, X. He, R. Lux, M.H. Anderson, W. Shi, Interspecies Interactions within Oral Microbial Communities, Microbiol. Mol. Biol. Rev. 71 (2007) 653–670. doi:10.1128/MMBR.00024-07.

[58] W.-L. Ng, B.L. Bassler, Bacterial Quorum-Sensing Network Architectures, Annu. Rev. Genet. (2009). doi:10.1146/annurev-genet-102108-134304.

[59] S. Heilmann, S. Krishna, B. Kerr, Why do bacteria regulate public goods by quorum sensing?-How the shapes of cost and benefit functions determine the form of optimal regulation, Front. Microbiol. 6 (2015) 1–11. doi:10.3389/fmicb.2015.00767.

[60] Y.H. Li, X.L. Tian, Quorum Sensing and Bacterial Social Interactions in Biofilms: Bacterial Cooperation and Competition, Stress Environ. Regul. Gene Expr. Adapt. Bact. 2 (2016) 1197–1205. doi:10.1002/9781119004813.ch116.

[61] H.K. Kuramitsu, X. He, R. Lux, M.H. Anderson, W. Shi, Interspecies Interactions within Oral Microbial Communities, Microbiol. Mol. Biol. Rev. 71 (2007) 653–670. doi:10.1128/MMBR.00024-07.

[62] B.A. Hense, C. Kuttler, J. Müller, M. Rothballer, A. Hartmann, J.U. Kreft, Does efficiency sensing unify diffusion and quorum sensing?, Nat. Rev. Microbiol. 5 (2007) 230–239. doi:10.1038/nrmicro1600.

[63] A. Suppiger, N. Schmid, C. Aguilar, G. Pessi, L. Eberl, Two quorum sensing systems control biofilm formation and virulence in members of the *Burkholderia cepacia* complex, Virulence. 4 (2013) 400–409. doi:10.4161/viru.25338.

[64] K. Papenfort, B. Bassler, C. Chase, Quorum sensing Signal- Rsponse Systems in Gram-Negative Bacteria, Nat Ev Microbiol. 14 (2017) 576–588. doi:10.1038/nrmicro.2016.89.Quorum-Sensing.

[65] V. Monnet, R. Gardan, Quorum-sensing regulators in Gram-positive bacteria: “cherchez le peptide”., Mol. Microbiol. 97 (2015) 181–4. doi:10.1111/mmi.13060.

[66] W.F. Yin, K. Purmal, S. Chin, X.Y. Chan, C.L. Koh, C.K. Sam, K.G. Chan, N-Acyl homoserine lactone production by *Klebsiella pneumoniae* isolated from human tongue surface, Sensors. 12 (2012) 3472–3483. doi:10.3390/s120303472.

[67] M.J. Federle, B.L. Bassler, M.J. Federle, B.L. Bassler, Interspecies communication in bacteria, 112 (2003) 1291–1299. doi:10.1172/JCI200320195.Species-specific.

[68] T. Bjarnsholt, The role of bacterial biofilms in chronic infections., Apmis. 121 (2013) 1–51. doi:10.1111/apm.12099.

[69] J.R.W. Govan, V. Deretic, Microbial pathogenesis in cystic fibrosis: mucoid *Pseudomonas aeruginosa* and *Burkholderia cepacia*., Microbiol. Rev. 60 (1996) 539–574. doi:10.1111/j.1365-2672.2007.03706.x.

[70] A. Brauner, O. Fridman, O. Gefen, N.Q. Balaban, Distinguishing between resistance, tolerance and persistence to antibiotic treatment, Nat. Rev. Microbiol. 14 (2016) 320–330. doi:10.1038/nrmicro.2016.34.

[71] I. Olsen, Biofilm-specific antibiotic tolerance and resistance, Eur. J. Clin. Microbiol. Infect. Dis. 34 (2015) 877–886. doi:10.1007/s10096-015-2323-z.

[72] P. Thuptimdang, T. Limpiyakorn, J. McEvoy, B.M. Prüß, E. Khan, Effect of silver nanoparticles on *Pseudomonas putida* biofilms at different stages of maturity, J. Hazard. Mater. 290 (2015) 127–133. doi:10.1016/j.jhazmat.2015.02.073.

[73] A.M. Königs, H.C. Flemming, J. Wingender, Nanosilver induces a non-culturable but metabolically active state in *Pseudomonas aeruginosa*, Front. Microbiol. 6 (2015) 1–11. doi:10.3389/fmicb.2015.00395.

[74] R.M. Donlan, Biofilms: Microbial life on surfaces, Emerg. Infect. Dis. 8 (2002) 881–890. doi:10.3201/eid0809.020063.

[75] I. Sutherland, Biofilm exopolysaccharides: a strong and sticky framework., Microbiology. 147 (2001) 3–9. doi:10.1099/00221287-147-1-3.

[76] W.W. Nichols, S.M. Dorrington, M.P.E. Slack, H.L. Walmsley, Inhibition of tobramycin diffusion by binding to alginate, Antimicrob. Agents Chemother. 32 (1988) 518–523. doi:10.1128/AAC.32.4.518.

[77] B. Bellich, C. Lagatolla, A. Tossi, M. Benincasa, P. Cescutti, R. Rizzo, Influence of Bacterial Biofilm Polysaccharide Structure on Interactions with Antimicrobial Peptides: A Study on *Klebsiella pneumoniae*, Int. J. Mol. Sci. 19 (2018) 1685. doi:10.3390/ijms19061685.

[78] S. Daddi Oubekka, R. Briandet, M.P. Fontaine-Aupart, K. Steenkeste, Correlative time-resolved fluorescence microscopy to assess antibiotic diffusion-reaction in biofilms, Antimicrob. Agents Chemother. 56 (2012) 3349–3358. doi:10.1128/AAC.00216-12.

[79] F. Bayer, Leading Articles, Bmj. s3-1 (1853) 497–499. doi:10.1136/bmj.s3-1.23.497.

[80] R. DE Levin BR, Non-inherited antibiotic resistance, Nat. Rev. Microbiol. Rev Microbiol. 4 (2006) 556–562.

[81] K. Driffield, K. Miller, J.M. Bostock, A.J. O'neill, I. Chopra, Increased mutability of *Pseudomonas aeruginosa* in biofilms, J. Antimicrob. Chemother. 61 (2008) 1053–1056. doi:10.1093/jac/dkn044.

[82] S. Molin, T. Tolker-Nielsen, Gene transfer occurs with enhanced efficiency in biofilms and induces enhanced stabilisation of the biofilm structure, Curr. Opin. Biotechnol. 14 (2003) 255–261. doi:10.1016/S0958-1669(03)00036-3.

[83] T.-F. Mah, Biofilm-specific antibiotic resistance., Future Microbiol. 7 (2012) 1061–72. doi:10.2217/fmb.12.76.

[84] J.S. Madsen, M. Burmølle, L.H. Hansen, S.J. Sørensen, The interconnection between biofilm formation and horizontal gene transfer, FEMS Immunol. Med. Microbiol. 65 (2012) 183–195. doi:10.1111/j.1574-695X.2012.00960.x.

[85] V.J. Savage, I. Chopra, A.J. O'Neill, *Staphylococcus aureus* biofilms promote horizontal transfer of antibiotic resistance, Antimicrob. Agents Chemother. 57 (2013) 1968–1970. doi:10.1128/AAC.02008-12.

[86] L. Cipolla, F. Rocca, C. Martinez, L. Aguerre, R. Barrios, M. Prieto, Prevalence of *Burkholderia cepacia* complex species in cystic fibrosis patients in Argentina during the period 2011-2015, Enferm. Infecc. Microbiol. Clin. (2017). doi:10.1016/j.eimc.2017.09.002.

[87] J.L. Parke, D. Gurian-Sherman, Diversity of the *Burkholderia cepacia* complex and implications for risk assessment of biological control strains., Annu. Rev. Phytopathol. 39 (2001) 225–58. doi:10.1146/annurev.phyto.39.1.225.

[88] T. Coenye, P. Vandamme, J.R.W. Govan, J.J. Lipuma, Taxonomy and identification of the *Burkholderia cepacia* complex, J. Clin. Microbiol. 39 (2001) 3427–3436. doi:10.1128/JCM.39.10.3427.

[89] W.H. Burkholder, Sour skin, a bacterial rot of Onion bulbs, Phytopathology. 40 (1950) 115–117.

[90] M. Palleroni, N.J., Kunisawa, R., Contopoulos, R., Doudoroff, Nucleic acid homologies in the genus *Pseudomonas*., Int. J. Syst. Bacteriol. (1973) 333–339.

[91] E. Yabuuchi, Y. Kosako, H. Oyaizu, I. Yano, H. Hotta, Y. Hashimoto, T. Ezaki, M. Arakawa, to the New Genus , with the Type Species *Burkholderia*, Microbiol. Immunol. 40 (1992) 1251–1275.

[92] A. Isles, I. Maclusky, M. Corey, R. Gold, C. Prober, P. Fleming, H. Levison, *Pseudomonas cepacia* infection in cystic fibrosis: an emerging problem., J. Pediatr. 104 (1984) 206–10. doi:10.1016/S0022-3476(84)80993-2.

[93] J.J. LiPuma, S.E. Dasen, D.W. Nielson, R.C. Stern, T.L. Stull, Person-to-person transmission of *Pseudomonas cepacia* between patients with cystic fibrosis., Lancet (London, England). 336 (1990) 1094–6. doi:10.1016/0140-6736(90)92571-X.

[94] R. Biddick, T. Spilker, A. Martin, J.J. LiPuma, Evidence of transmission of *Burkholderia cepacia*, *Burkholderia multivorans* and *Burkholderia dolosa* among persons with cystic fibrosis., FEMS Microbiol. Lett. 228 (2003) 57–62. doi:10.1016/S0378-1097(03)00724-9.

[95] J.R. Govan, P.H. Brown, J. Maddison, C.J. Doherty, J.W. Nelson, M. Dodd, A.P. Greening, A.K. Webb, Evidence for transmission of *Pseudomonas cepacia* by social contact in cystic fibrosis., Lancet (London, England). 342 (1993) 15–9. doi:10.1016/0140-6736(93)91881-L.

[96] E. Mahenthiralingam, T.A. Urban, J.B. Goldberg, The multifarious, multireplicon *Burkholderia cepacia* complex, Nat. Rev. Microbiol. 3 (2005) 144–156. doi:10.1038/nrmicro1085.

[97] P. Vandamme, P. Dawyndt, Classification and identification of the *Burkholderia cepacia* complex: Past, present and future, Syst. Appl. Microbiol. 34 (2011) 87–95. doi:10.1016/j.syapm.2010.10.002.

[98] T. Coenye, P. Vandamme, Diversity and significance of *Burkholderia* species occupying diverse ecological niches, Environ. Microbiol. 5 (2003) 719–729. doi:10.1046/j.1462-2920.2003.00471.x.

[99] V.P. Storms V, Van Den Vreken N, Coenye T, Mahenthiralingam E, LiPuma JJ, Gillis M, Polyphasic characterisation of *Burkholderia cepacia*-like isolates leading to the emended description of *Burkholderia pyrrocinia*, Syst. Appl. Microbiol. 27 (2004) 517–526.

[100] E. Vanlaere, J.J. Lipuma, A. Baldwin, D. Henry, E. De Brandt, E. Mahenthiralingam, D. Speert, C. Dowson, P. Vandamme, P. Vandamme, Burkholderia latens sp . nov ., *Burkholderia diffusa* sp . nov ., *Burkholderia arboris* sp . nov ., *Burkholderia seminalis* sp . nov . and *Burkholderia metallica* sp . nov ., novel species within the *Burkholderia cepacia* complex, (2018) 1580–1590. doi:10.1099/ijs.0.65634-0.

[101] E. Vanlaere, A. Baldwin, D. Gevers, D. Henry, E. De Brandt, J.J. Lipuma, E. Mahenthiralingam, D.P. Speert, C. Dowson, P. Vandamme, P. Vandamme, Taxon K , a complex within the *Burkholderia cepacia* complex , comprises at least two novel species , (2009) 102–111. doi:10.1099/ijs.0.001123-0.

[102] C. Peeters, J.E.A. Zlosnik, T. Spilker, T.J. Hird, J.J. Lipuma, P. Vandamme, *Burkholderia pseudomultivorans* sp. nov., a novel *Burkholderia cepacia* complex species from human respiratory samples and the rhizosphere, Syst. Appl. Microbiol. (2013) 1–7. doi:10.1016/j.syapm.2013.06.003.

[103] B. De Smet, M. Mayo, C. Peeters, J.E.A. Zlosnik, T. Spilker, T.J. Hird, J.J. Li Puma, T.J. Kidd, M. Kaestli, J.L. Ginther, D.M. Wagner, P. Keim, S.C. Bell, J.A. Jacobs, B.J. Currie, P. Vandamme, *Burkholderia stagnalis* sp. nov. and *Burkholderia territorii* sp. nov., two novel *Burkholderia cepacia* complex species from environmental and human sources, Int. J. Syst. Evol. Microbiol. 65 (2015) 2265–2271. doi:10.1099/ijs.0.000251.

[104] B.A. Martina P, Leguizamon M, Prieto CI, Sousa SA, Montanaro P, Draghi WO, Stämmler M, Bettiol M, de Carvalho CCCR, Palau J, Figoli C, Alvarez F, Benetti S, Lejona S, Vescina C, Ferreras J, Lasch P, Lagares A, Zorreguieta A, Leitão JH, Yantorno OM, *Burkholderia puraquae* sp. nov., a novel species of the Burkholderia cepacia complex isolated from hospital settings and agricultural soils., Int. J. Syst. Evol. Microbiol. 68 (2018) 14–20.

[105] J.R. Riordan, J.M. Rommens, B. Kerem, N. Alon, Z. Grzelczak, J. Zielenski, S. Lok, N. Plavsic, J. Chou, M.L. Drumm, M.C. Iannuzzi, F.S. Collins, L. Tsui, J.R. Riordan, J.M. Rommens, B. Kerem, N.O.A. Alon, R.R. Grzelczak, J. Zielenski, S. Lok, N. Piavsic, J. Chou, M.L. Drumm, M.C. Iannuzzi, Complementary DNA Linked references are available on JSTOR for this article : Identification of the Cystic Fibrosis Gene : Cloning and Characterization of Complementary DNA, (2017).

[106] O. Ciofu, T. Tolker-Nielsen, P.Ø. Jensen, H. Wang, N. Høiby, Antimicrobial resistance, respiratory tract infections and role of biofilms in lung infections in cystic fibrosis patients, Adv. Drug Deliv. Rev. 85 (2015) 7–23. doi:10.1016/j.addr.2014.11.017.

[107] J.C. Davies, E.W.F.W. Alton, A. Bush, Cystic fibrosis, Bmj. 335 (2007) 1255–1259. doi:10.1136/bmj.39391.713229.AD.

[108] P. Kurbatova, N. Bessonov, V. Volpert, H.A.W.M. Tiddens, C. Cornu, P. Nony, D. Caudri, Model of mucociliary clearance in cystic fibrosis lungs, J. Theor. Biol. 372 (2015) 81–88. doi:10.1016/j.jtbi.2015.02.023.

[109] J.H. Leitão, J.R. Feliciano, S.A. Sousa, T. Pita, S.I. Guerreiro, *Burkholderia cepacia* Complex Infections Among Cystic Fibrosis Patients : Perspectives and Challenges, (n.d.).

[110] J.J. LiPuma, The changing microbial epidemiology in cystic fibrosis, Clin. Microbiol. Rev. 23 (2010) 299–323. doi:10.1128/CMR.00068-09.

[111] S. Brisse, C. Cordevant, P. Vandamme, P. Bidet, C. Loukil, Species Distribution and Ribotype Diversity of *Burkholderia cepacia* Complex Isolates from French Patients with Cystic Fibrosis, Society. 42 (2004) 4824–4827. doi:10.1128/JCM.42.10.4824.

[112] K. De Boeck, A. Malfroot, L. Van Schil, P. Lebecque, C. Knoop, J.R.W. Govan, C. Doherty, S. Laevens, P. Vandamme, L. Van Schil, J.P. Ursi, K. Desager, G. Ieven, A. Mertens, I. Dab, S. Lauwers, J. Gigi, M. Struelens, H. Franckx, F. De Baets, S. Vandaele, G. Verschraegen, M. Proesmans, J. Van Eldere, F. Lebrun, F. Pauquay, E. Bodart, Y. Glupczynski, C. Sevens, Epidemiology of *Burkholderia cepacia* complex colonisation in cystic fibrosis patients, Eur. Respir. J. 23 (2004) 851–856. doi:10.1183/09031936.04.00118804.

[113] J.R. Govan, A.R. Brown, A.M. Jones, Evolving epidemiology of *Pseudomonas aeruginosa* and the *Burkholderia cepacia* complex in cystic fibrosis lung infection, Future Microbiol. 2 (2007) 153–164. doi:10.2217/17460913.2.2.153.

[114] N. Nørskov-Lauritsen, H.K. Johansen, M.G. Fenger, X.C. Nielsen, T. Pressler, H. V. Olesen, N. Høiby, Unusual distribution of *Burkholderia cepacia* complex species in danish cystic fibrosis clinics may stem from restricted transmission between patients, J. Clin. Microbiol. 48 (2010) 2981–2983. doi:10.1128/JCM.00383-10.

[115] C.E. Pope, P. Short, P.E. Carter, Species distribution of *Burkholderia cepacia* complex isolates in cystic fibrosis and non-cystic fibrosis patients in New Zealand, J. Cyst. Fibros. 9 (2010) 442–446. doi:10.1016/j.jcf.2010.08.011.

[116] M.J. Medina-Pascual, S. Valdezate, P. Villalón, N. Garrido, V. Rubio, J.A. Saéz-Nieto, Identification, molecular characterisation and antimicrobial susceptibility of genomovars of the *Burkholderia cepacia* complex in Spain, Eur. J. Clin. Microbiol. Infect. Dis. 31 (2012) 3385–3396. doi:10.1007/s10096-012-1707-6.

[117] B.A. Conway, E.P. Greenberg, Quorum-sensing signals and quorum-sensing genes in *Burkholderia vietnamiensis*, J. Bacteriol. 184 (2002) 1187–1191. doi:10.1128/jb.184.4.1187-1191.2002.

[118] L.M.M. M. V. Cunha, S. A. Sousa, J. H. Leitao, I.S.-C. P. A. Videira, Studies on the Involvement of the Exopolysaccharide Produced by Cystic Fibrosis-Associated Isolates of the *Burkholderia cepacia* Complex in Biofilm Formation and in Persistence of Respiratory Infections, J. Clin. Microbiol. 42 (2004) 3052–3058.

[119] S.I. Häussler S, Lehmann C, Breselge C, Rohde M, Classen M, Tümmler B, Vandamme P, Fatal outcome of lung transplantation in cystic fibrosis patients due to small-colony variants of the *Burkholderia cepacia* complex., Eur. J. Clin. Microbiol. Infect. Dis. 22 (2003) 249–253.

[120] C.V. Traverse CC, Mayo-Smith LM, Poltak SR, Tangled bank of experimentally evolved *Burkholderia* biofilms reflects selection during chronic infections., Proc. Natl. Acad. Sci. USA. 110 (2013) 250–259.

[121] L. Dales, W. Ferris, K. Vandemheen, S.D. Aaron, Combination antibiotic susceptibility of biofilm-grown *Burkholderia cepacia* and *Pseudomonas aeruginosa* isolated from patients with pulmonary exacerbations of cystic fibrosis, Eur. J. Clin. Microbiol. Infect. Dis. 28 (2009) 1275–1279. doi:10.1007/s10096-009-0774-9.

[122] B.D. Conway, V. Venu, D.P. Speert, Formation and Acyl Homoserine Lactone Production in the, Society. 184 (2002) 5678–5685. doi:10.1128/JB.184.20.5678.

[123] G.E. Singh PK, Schaefer AL, Parsek MR, Moninger TO, Welsh MJ, Quorum-sensing signals indicate that cystic fibrosis lungs are infected with bacterial biofilms, Nature. 407 (2000) 762–4.

[124] D.D. Sriramulu, H. Lünsdorf, J.S. Lam, U. Römling, Microcolony formation: A novel biofilm model of *Pseudomonas aeruginosa* for the cystic fibrosis lung, J. Med. Microbiol. 54 (2005) 667–676. doi:10.1099/jmm.0.45969-0.

[125] U. Sajjan, M. Corey, A. Humar, E. Tullis, E. Cutz, C. Ackerley, J. Forstner, Immunolocalisation of *Burkholderia cepacia* in the lungs of cystic fibrosis patients, J. Med. Microbiol. 50 (2001) 535–546. doi:10.1099/0022-1317-50-6-535.

[126] J. Lamothe, K.K. Huynh, S. Grinstein, M.A. Valvano, Intracellular survival of *Burkholderia cenocepacia* in macrophages is associated with a delay in the maturation of bacteria-containing vacuoles, Cell. Microbiol. 9 (2007) 40–53. doi:10.1111/j.1462-5822.2006.00766.x.

[127] M.P. Murphy, E. Caraher, Residence in biofilms allows *Burkholderia cepacia* complex (Bcc) bacteria to evade the antimicrobial activities of neutrophil-like dHL60 cells, Pathog. Dis. 73 (2015) ftv069. doi:10.1093/femspd/ftv069.

[128] A. Sage, A. Linker, L.R. Evans, T.G. Lessie, Hexose phosphate metabolism and exopolysaccharide formation in *Pseudomonas cepacia*, Curr. Microbiol. 20 (1990) 191–198. doi:10.1007/BF02091996.

[129] L. Chiarini, P. Cescutti, L. Drigo, G. Impallomeni, Y. Herasimenka, A. Bevivino, C. Dalmastri, S. Tabacchioni, G. Manno, F. Zanetti, R. Rizzo, Exopolysaccharides produced by *Burkholderia cenocepacia* recA lineages IIIA and IIIB, J. Cyst. Fibros. 3 (2004) 165–172. doi:10.1016/j.jcf.2004.04.004.

[130] P. Cescutti, G. Impallomeni, D. Garozzo, R. Rizzo, O-Acetyl location on Cepacian, the principal exopolysaccharide of *Burkholderia cepacia* complex bacteria, Carbohydr. Res. 346 (2011) 2905–2912. doi:10.1016/j.carres.2011.10.011.

[131] Y. Herasimenka, P. Cescutti, G. Impallomeni, S. Campana, G. Taccetti, N. Ravenni, F. Zanetti, R. Rizzo, Exopolysaccharides produced by clinical strains belonging to the *Burkholderia cepacia* complex, J. Cyst. Fibros. 6 (2007) 145–152. doi:10.1016/j.jcf.2006.06.004.

[132] S. Cérantola, Structural studies of the acidic exopolysaccharide produced by a mucoid strain of *Burkholderia cepacia*, isolated from cystic fibrosis, Carbohydr. Res. 285 (1996) 59–67. doi:10.1016/0008-6215(96)00014-6.

[133] P. Cescutti, G. Impallomeni, D. Garozzo, L. Sturiale, Y. Herasimenka, C. Lagatolla, R. Rizzo, Exopolysaccharides produced by a clinical strain of *Burkholderia cepacia* isolated from a cystic fibrosis patient, Carbohydr. Res. 338 (2003) 2687–2695. doi:10.1016/S0008-6215(03)00384-7.

[134] P. Cescutti, B. Cuzzi, Y. Herasimenka, R. Rizzo, Structure of a novel exopolysaccharide produced by *Burkholderia vietnamiensis*, a cystic fibrosis opportunistic pathogen, Carbohydr. Polym. 94 (2013) 253–260. doi:10.1016/j.carbpol.2013.01.047.

[135] S. Dolfi, A. Sveronis, A. Silipo, R. Rizzo, P. Cescutti, A novel rhamno-mannan exopolysaccharide isolated from biofilms of *Burkholderia multivorans* C1576, Carbohydr. Res. 411 (2015) 42–48. doi:10.1016/j.carres.2015.04.012.

[136] J.L. Burns, Antibiotic Resistance of *Burkholderia* spp, in: *Burkholderia* Mol. Microbiol. Genomics, Coenye T, Horizon Bioscience, 2007: pp. 81–91.

[137] T.F.C. Mah, G.A. O'Toole, Mechanisms of biofilm resistance to antimicrobial agents, Trends Microbiol. 9 (2001) 34–39. doi:10.1016/S0966-842X(00)01913-2.

[138] R.M. Donlan, J.W. Costerton, Biofilms: survival mechanisms of clinically relevant microorganisms., Clin.Microbiol. Rev. 15 (2002) 167–19. doi:10.1128/CMR.15.2.167.

[139] P.S. Stewart, J. William Costerton, Antibiotic resistance of bacteria in biofilms, Lancet. 358 (2001) 135–138. doi:10.1016/S0140-6736(01)05321-1.

[140] K.K. Jefferson, D.A. Goldmann, B. Gerald, G.B. Pier, Use of Confocal Microscopy To Analyze the Rate of Vancomycin Penetration through *Staphylococcus aureus* Biofilms, Antimicrob. Agents Chemother. 49 (2005) 2467–2473. doi:10.1128/AAC.49.6.2467.

[141] S.G. McNee, D.A.M. Geddes, D.A. Weetman, Diffusion of sugars and acids in human dental plaque in vitro, Arch. Oral Biol. 27 (1982) 975–979. doi:10.1016/0003-9969(82)90106-6.

[142] P.S. Stewart, Theoretical aspects of antibiotic diffusion into microbial biofilms, Antimicrob. Agents Chemother. 40 (1996) 2517–2522.

[143] P.S. Stewart, Diffusion in biofilms., J. Bacteriol. 185 (2003) 1485–91. doi:10.1128/JB.185.5.1485.

[144] A.S. Messiaen, H. Nelis, T. Coenye, Investigating the role of matrix components in protection of *Burkholderia cepacia* complex biofilms against tobramycin, J. Cyst. Fibros. 13 (2014) 56–62. doi:10.1016/j.jcf.2013.07.004.

[145] C.A. Gordon, N.A. Hodges, C. Marriott, Antibiotic interaction and diffusion through alginate and exopolysaccharide of cystic fibrosis-derived pseudomonas aeruginosa, J. Antimicrob. Chemother. 22 (1988) 667–674. doi:10.1093/jac/22.5.667.

[146] W.W. Nichols, M.J. Evans, M.P.E. Slack, H.L. Walmsley, The Penetration of Antibiotics into Aggregates of Mucoid and Non-mucoid *Pseudomonas aeruginosa*, Microbiology. 135 (1989) 1291–1303. doi:10.1099/00221287-135-5-1291.

[147] C.A. Gordon, N.A. Hodges, C. Marriott, Use of slime dispersants to promote antibiotic penetration through the extracellular polysaccharide of mucoid *Pseudomonas aeruginosa*, Antimicrob. Agents Chemother. 35 (1991) 1258–1260. doi:10.1128/AAC.35.6.1258.

[148] J. Bylund, L.-A. Burgess, P. Cescutti, R.K. Ernst, D.P. Speert, Exopolysaccharides from *Burkholderia cenocepacia* Inhibit Neutrophil Chemotaxis and Scavenge Reactive Oxygen Species, J. Biol. Chem. 281 (2006) 2526–2532. doi:10.1074/jbc.M510692200.

[149] B. Cuzzi, P. Cescutti, L. Furlanis, C. Lagatolla, L. Sturiale, D. Garozzo, R. Rizzo, Investigation of bacterial resistance to the immune system response: Cepacian depolymerisation by reactive oxygen species, Innate Immun. 18 (2012) 661–671. doi:10.1177/1753425911435954.

[150] E. Peeters, A. Sass, E. Mahenthiralingam, H. Nelis, T. Coenye, Transcriptional response of *Burkholderia cenocepacia* J2315 sessile cells to treatments with high doses of hydrogen peroxide and sodium hypochlorite, BMC Genomics. 11 (2010). doi:10.1186/1471-2164-11-90.

[151] C.M. Waters, B.L. Bassler, QUORUM SENSING: Cell-to-Cell Communication in Bacteria, Annu. Rev. Cell Dev. Biol. 21 (2005) 319–346. doi:10.1146/annurev.cellbio.21.012704.131001.

[152] G.S. Shadel, T.O. Baldwin, Positive Autoregulation of the *Vibrio fischeri* luxR Gene, J. Biol. Chem. 267 (1992) 7696–7702.

[153] P.A. Sokol, R.J. Malott, K. Riedel, L. Eberl, Communication systems in the genus *Burkholderia*, 2 (2007) 555–563.

[154] A. Gotschlich, B. Huber, O. Geisenberger, A. Togl, A. Steidle, K. Riedel, P. Hill, B. Tümmler, P. Vandamme, B. Middleton, M. Camara, P. Williams, A. Hardman, L. Eberl, Synthesis of multiple N-Acylhomoserine lactones is wide-spread among the members of the *Burkholderia cepacia* complex, Syst. Appl. Microbiol. 24 (2001) 1–14. doi:10.1078/0723-2020-00013.

[155] M. Baligh, K.E. Conway, Evaluation of *Burkholderia cepacia* Strains: Root Colonization of *Catharanthus roseus* and In-Vitro Inhibition of Selected Soil-borne Fungal Pathogens, Oklahoma Acad. Sci. 79 (1999) 19–27. doi:10.1128/IAI.72.3.1537.

[156] R.J. Malott, A. Baldwin, E. Mahenthiralingam, P.A. Sokol, Characterization of the *cciIR* quorum-sensing system in *Burkholderia cenocepacia*, Infect. Immun. 73 (2005) 4982–4992. doi:10.1128/IAI.73.8.4982.

[157] S. Uehlinger, S. Schwager, S.P. Bernier, K. Riedel, D.T. Nguyen, P.A. Sokol, L. Eberl, Identification of specific and universal virulence factors in *Burkholderia cenocepacia* strains by using multiple infection hosts, Infect. Immun. 77 (2009) 4102–4110. doi:10.1128/IAI.00398-09.

[158] E.P. O'Grady, D.F. Viteri, R.J. Malott, P.A. Sokol, Reciprocal regulation by the CepIR and CciIR quorum sensing systems in *Burkholderia cenocepacia*, BMC Genomics. 10 (2009) 441. doi:10.1186/1471-2164-10-441.

[159] R.J. Malott, E.P. O'Grady, J. Toller, S. Inhülsen, L. Eberl, P.A. Sokol, A *Burkholderia cenocepacia* orphan LuxR homolog is involved in quorum-sensing regulation, J. Bacteriol. 191 (2009) 2447–2460. doi:10.1128/JB.01746-08.

[160] J. Wopperer, S.T. Cardona, B. Huber, A. Jacobi, M.A. Valvano, L. Eberl, C.A. Jacobi, A Quorum-Quenching Approach To Investigate the Conservation of Quorum-Sensing-Regulated Functions within the *Burkholderia cepacia* Complex, 72 (2006) 1579–1587. doi:10.1128/AEM.72.2.1579.

[161] B. Huber, K. Riedel, M. Hentzer, A. Heydorn, A. Gotschlich, M. Givskov, S. Molin, L. Eberl, The *cep* quorum-sensing system of *Burkholderia cepacia* H111 controls biofilm formation and swarming motility, Microbiology. 147 (2001) 2517–2528. doi:10.1099/00221287-147-9-2517.

[162] S. Inhülsen, C. Aguilar, N. Schmid, A. Suppiger, K. Riedel, L. Eberl, Identification of functions linking quorum sensing with biofilm formation in *Burkholderia cenocepacia* H111., Microbiologyopen. 1 (2012) 225–42. doi:10.1002/mbo3.24.

[163] S.M. Hinsa, M. Espinosa-Urgel, J.L. Ramos, G.A. O'Toole, Transition from reversible to irreversible attachment during biofilm formation by *Pseudomonas fluorescens* WCS365 requires an ABC transporter and a large secreted protein, Mol. Microbiol. 49 (2003) 905–918. doi:10.1046/j.1365-2958.2003.03615.x.

[164] C. Latasa, A. Roux, A. Toledo-Arana, J.M. Ghigo, C. Gamazo, J.R. Penadés, I. Lasa, BapA, a large secreted protein required for biofilm formation and host colonization of *Salmonella enterica* serovar *Enteritidis*, Mol. Microbiol. 58 (2005) 1322–1339. doi:10.1111/j.1365-2958.2005.04907.x.

[165] Z. Rocío Suárez-Moreno, G. Devescovi, M. Myers, L. Hallack, L. Mendonça-Previato, J. Caballero-Mellado, V. Venturi, Commonalities and differences in regulation of N-acyl homoserine lactone quorum sensing in the beneficial plant-associated *Burkholderia* species cluster, Appl. Environ. Microbiol. 76 (2010) 4302–4317. doi:10.1128/AEM.03086-09.

[166] C. Boon, Y. Deng, L.H. Wang, Y. He, J.L. Xu, Y. Fan, S.Q. Pan, L.H. Zhang, A novel DSF-like signal from *Burkholderia cenocepacia* interferes with *Candida albicans* morphological transition, ISME J. 2 (2008) 27–36. doi:10.1038/ismej.2007.76.

[167] C.E. Barber, J.L. Tang, J.X. Feng, M.Q. Pan, T.J. Wilson, H. Slater, J.M. Dow, P. Williams, and MJ Daniels. 1997. A novel regulatory system required for 15 pathogenicity of *Xanthomonas campestris* is mediated by a small diffusible signal 16 molecule, Mol. Microbiol. 24 (1997) 555–566.

[168] Y.W. He, L.H. Zhang, Quorum sensing and virulence regulation in *Xanthomonas campestris*, FEMS Microbiol. Rev. 32 (2008) 842–857. doi:10.1111/j.1574-6976.2008.00120.x.

[169] Y. Deng, J. Wu, F. Tao, L.H. Zhang, Listening to a new language: DSF-based quorum sensing in Gram-negative bacteria, Chem. Rev. 111 (2011) 160–179. doi:10.1021/cr100354f.

[170] H. Bi, Q.H. Christensen, Y. Feng, H. Wang, J.E. Cronan, The *Burkholderia cenocepacia* BDSF quorum sensing fatty acid is synthesized by a bifunctional crotonase homologue having both dehydratase and thioesterase activities, Mol. Microbiol. 83 (2012) 840–855. doi:10.1111/j.1365-2958.2012.07968.x.

[171] Y. Deng, N. Schmid, C. Wang, J. Wang, G. Pessi, D. Wu, J. Lee, C. Aguilar, C.H. Ahrens, C. Chang, H. Song, L. Eberl, L.-H. Zhang, Cis-2-dodecenoic acid receptor RpfR links quorum-sensing signal perception with regulation of virulence through cyclic dimeric guanosine monophosphate turnover, Proc. Natl. Acad. Sci. 109 (2012) 15479–15484. doi:10.1073/pnas.1205037109.

[172] U. Romling, M.Y. Galperin, M. Gomelsky, Cyclic di-GMP: the First 25 Years of a Universal Bacterial Second Messenger, Microbiol. Mol. Biol. Rev. 77 (2013) 1–52. doi:10.1128/MMBR.00043-12.

[173] M. Fazli, Y. Mccarthy, M. Givskov, R.P. Ryan, T. Tolker-Nielsen, The exopolysaccharide gene cluster Bcam1330-Bcam1341 is involved in *Burkholderia cenocepacia* biofilm formation, and its expression is regulated by c-di-GMP and Bcam1349, Microbiologyopen. 2 (2013) 105–122. doi:10.1002/mbo3.61.

[174] G. Cesareni, Peptide display on filamentous phage capsids An new powerful tool to study protein-ligand interaction, FEBS Lett. 307 (1992) 66–70. doi:10.1016/0014-5793(92)80903-T.

[175] G.P.. Smith, Filamentous Fusion Phage : Novel Expression Vectors that Display Cloned Antigens on the Virion Surface, Science (80-.). 228 (1985) 1315–1317.

[176] I. Ul Haq, W.N. Chaudhry, M.N. Akhtar, S. Andleeb, I. Qadri, Bacteriophages and their implications on future biotechnology: A review, Virol. J. 9 (2012) 9. doi:10.1186/1743-422X-9-9.

[177] M. Russel, Filamentous phage assembly., Mol. Microbiol. 5 (1991) 1607–13. http://www.ncbi.nlm.nih.gov/pubmed/1943697.

[178] J.X. Huang, S.L. Bishop-Hurley, M.A. Cooper, Development of anti-infectives using phage display: Biological agents against bacteria, viruses, and parasites, Antimicrob. Agents Chemother. 56 (2012) 4569–4582. doi:10.1128/AAC.00567-12.

[179] G.P. Smith, Filamentous phages as cloning vectors., Biotechnology. 10 (1988) 61–83. http://www.ncbi.nlm.nih.gov/entrez/query.fcgi?cmd=Retrieve&db=PubMed&dopt=Citation&list_uids=3061524.

[180] M.A. Arap, Phage display technology - Applications and innovations, Genet. Mol. Biol. 28 (2005) 1–9. doi:10.1590/S1415-47572005000100001.

[181] M.D. Scholle, J.W. Kehoe, B.K. Kay, Efficient construction of a large collection of phage-displayed combinatorial peptide libraries., Comb. Chem. High Throughput Screen. 8 (2005) 545–51. doi:10.2174/1386207054867337.

[182] A. Galán, L. Comor, A. Horvatić, J. Kuleš, N. Guillemin, V. Mrljak, M. Bhide, Library-based display technologies: Where do we stand?, Mol. Biosyst. 12 (2016) 2342–2358. doi:10.1039/c6mb00219f.

[183] S. Bass, R. Greene, J.A. Wells, Hormone phage: An enrichment method for variant proteins with altered binding properties, Proteins Struct. Funct. Bioinforma. 8 (1990) 309–314. doi:10.1002/prot.340080405.

[184] C.F. Barbas, A.S. Kang, R.A. Lerner, S.J. Benkovic, Assembly of combinatorial antibody libraries on phage surfaces: the gene III site., Proc. Natl. Acad. Sci. 88 (1991) 7978–7982. doi:10.1073/pnas.88.18.7978.

[185] G.S. Waldo, B.M. Standish, J. Berendzen, T.C. Terwilliger, Rapid protein-folding assay using green fluorescent protein, Nat. Biotechnol. 17 (1999) 691–695. doi:10.1038/10904.

[186] K.L. Maxwell, A.K. Mittermaier, J.D. Forman-Kay, A.R. Davidson, A simple in vivo assay for increased protein solubility, Protein Sci. 8 (1999) 1908–1911. doi:10.1110/ps.8.9.1908.

[187] Y. Lauw, M.D. Horne, T. Rodopoulos, V. Lockett, B. Akgun, W.A. Hamilton, A.R.J. Nelson, Structure of [C 4 mpyr][NTf 2] Room-Temperature Ionic Liquid at Charged Gold Interfaces, Langmuir. 28 (2012) 7374–7381. doi:10.1021/la3005757.

[188] S. D'Angelo, N. Velappan, F. Mignone, C. Santoro, D. Sblattero, C. Kiss, A.R.M. Bradbury, Filtering "genic" open reading frames from genomic DNA samples for advanced annotation, BMC Genomics. 12 (2011). doi:10.1186/1471-2164-12-S1-S5.

[189] M.M. Kuttel, P. Cescutti, M. Distefano, R. Rizzo, Fluorescence and NMR spectroscopy together with molecular simulations reveal amphiphilic characteristics of a *Burkholderia* biofilm exopolysaccharide, J. Biol. Chem. 292 (2017) 11034–11042. doi:10.1074/jbc.M117.785048.

[190] H.-C. Flemming, EPS—Then and Now, Microorganisms. 4 (2016) 41. doi:10.3390/microorganisms4040041.

[191] P. Cescutti, M. Bosco, F. Picotti, G. Impallomeni, J.H. Leitão, J.A. Richau, I. Sá-Correia, Structural study of the exopolysaccharide produced by a clinical isolate of *Burkholderia cepacia*, Biochem. Biophys. Res. Commun. 273 (2000) 1088–1094. doi:10.1006/bbrc.2000.3059.

[192] R. Crescenzi, V., Gamini, A., Palleschi, A., and Rizzo, Physico-chemical aspects of inclusion complex formation between cycloamyloses and aromatic guest molecules in water., Gazz.Chim.Ital. 116 (1986) 435–440.

[193] W.O. McClure, G.M. Edelman, Fluorescent probes for conformational states of proteins. II. The binding of 2-p-toluidinylnaphthalene-6-sulfonate to alpha-chymotrypsin., Biochemistry. 6 (1967) 559–66. http://www.ncbi.nlm.nih.gov/pubmed/6047639.

[194] G.M. Edelman, W.O. McClure, Fluorescent Probes and the Conformation of Proteins, Acc. Chem. Res. 1 (1968) 65–70. doi:10.1021/ar50003a001.

[195] T. Coenye, Social interactions in the *Burkholderia cepacia* complex: Biofilms and quorum sensing, Future Microbiol. 5 (2010) 1087–1099. doi:10.2217/fmb.10.68.

[196] Y. Deng, J. Wu, L. Eberl, L.H. Zhang, Structural and functional characterization of diffusible signal factor family quorum-sensing signals produced by members of the *Burkholderia cepacia* complex, Appl. Environ. Microbiol. 76 (2010) 4675–4683. doi:10.1128/AEM.00480-10.

[197] H.E. Gottlieb, V. Kotlyar, A. Nudelman, NMR Chemical Shifts of Common Laboratory Solvents as Trace Impurities, J. Org. Chem. 62 (1997) 7512–7515. doi:10.1021/jo971176v.

[198] J. Angulo, P.M. Nieto, STD-NMR: application to transient interactions between biomolecules-a quantitative approach., Eur. Biophys. J. 40 (2011) 1357–69. doi:10.1007/s00249-011-0749-5.

[199] M. Beseničar, P. Maček, J.H. Lakey, G. Anderluh, Surface plasmon resonance in protein-membrane interactions, Chem. Phys. Lipids. 141 (2006) 169–178. doi:10.1016/j.chemphyslip.2006.02.010.

[200] https://www.gelifesciences.co.jp/contact/pdf/BiacoreAssayHandbook.pdf, (n.d.).

[201] J.T. Vivian, P.R. Callis, Mechanisms of tryptophan fluorescence shifts in proteins, Biophys. J. 80 (2001) 2093–2109. doi:10.1016/S0006-3495(01)76183-8.

[202] A. Poveda, J. Jiménez-Barbero, NMR studies of carbohydrate-protein interactions in solution, Chem. Soc. Rev. 27 (1998) 133–143. doi:10.1039/a827133z.

[203] D. Scaini, F. Ravalico, P. Cescutti, E. Pellizzoni, R. Rizzo, A. Delneri, Biofilms produced by *Burkholderia cenocepacia*: influence of media and solid supports on composition of matrix exopolysaccharides, Microbiology. 162 (2016) 283–294. doi:10.1099/mic.0.000214.

[204] J.N.C. Fong, F.H. Yildiz, Biofilm Matrix Proteins., Microbiol. Spectr. 3 (2015) 1–27. doi:10.1128/microbiolspec.MB-0004-2014.

[205] M.R. Chapman, L.S. Robinson, J.S. Pinkner, R. Roth, M. Hammar, S. Normark, S.J. Hultgren, NIH Public Access, 295 (2010) 851–855. doi:10.1126/science.1067484.Role.

[206] D. Romero, C. Aguilar, R. Losick, R. Kolter, Amyloid fibers provide structural integrity to *Bacillus subtilis* biofilms, Proc. Natl. Acad. Sci. 107 (2010) 2230–2234. doi:10.1073/pnas.0910560107.

[207] T. Etterer, P.A. Wilderer, Generation and properties of aerobic granular sludge, Water Sci. Technol. 43 (2001) 19–26. doi:10.1128/AEM.71.2.1051.

[208] P.H.N. B. Frølund, Ri. Palmgren, K. Keiding, Extraction of extracellular polymers from activated sludge using a cation exchange resin, Water Res. 30 (1996).

[209] V. Urban, J.C. Block, J. Manem, Bioflocculation in Activated- Sludge: an Analytic Approach., Water Res. 27 (1993) 829–838.

[210] A. Heydorn, A.T. Nielsen, M. Hentzer, Quantification of biofilm structures by the novel computer program, Image Process. 146 (2000) 2395–2407. doi:10.1099/00221287-146-10-2395.

[211] R. Sgarra, C. Furlan, S. Zammitti, A. Lo Sardo, E. Maurizio, J. Di Bernardo, V. Giancotti, G. Manfioletti, Interaction proteomics of the HMGA chromatin architectural factors., Proteomics. 8 (2008) 4721–32. doi:10.1002/pmic.200800193.

[212] D. Wu, G. Li, C. Qin, X. Ren, Phage displayed peptides to avian H5N1 virus distinguished the virus from other viruses, PLoS One. 6 (2011) 6–11. doi:10.1371/journal.pone.0023058.

[213] K.L. Palmer, L.M. Aye, M. Whiteley, Nutritional cues control *Pseudomonas aeruginosa* multicellular behavior in cystic fibrosis sputum., J. Bacteriol. 189 (2007) 8079–87. doi:10.1128/JB.01138-07.

[214] S.S. Branda, S. Vik, L. Friedman, R. Kolter, Biofilms: the matrix revisited., Trends Microbiol. 13 (2005) 20–6. doi:10.1016/j.tim.2004.11.006.

[215] J. Kives, B. Orgaz, C. Sanjosé, Polysaccharide differences between planktonic and biofilm-associated EPS from *Pseudomonas fluorescens* B52., Colloids Surf. B. Biointerfaces. 52 (2006) 123–7. doi:10.1016/j.colsurfb.2006.04.018.

[216] Y.-P. Chen, P. Zhang, J.-S. Guo, F. Fang, X. Gao, C. Li, Functional groups characteristics of EPS in biofilm growing on different carriers., Chemosphere. 92 (2013) 633–8. doi:10.1016/j.chemosphere.2013.01.059.

[217] J.-H. Jung, N.-Y. Choi, S.-Y. Lee, Biofilm formation and exopolysaccharide (EPS) production by *Cronobacter sakazakii* depending on environmental conditions., Food Microbiol. 34 (2013) 70–80. doi:10.1016/j.fm.2012.11.008.

[218] M. Moryl, A. Kaleta, K. Strzelecki, S. Różalska, A. Różalski, Effect of nutrient and stress factors on polysaccharides synthesis in *Proteus mirabilis* biofilm., Acta Biochim. Pol. 61 (2014) 133–9. http://www.ncbi.nlm.nih.gov/pubmed/24644556.

[219] U. Schwab, L.H. Abdullah, O.S. Perlmutt, D. Albert, C.W. Davis, R.R. Arnold, J.R. Yankaskas, P. Gilligan, H. Neubauer, S.H. Randell, R.C. Boucher, Localization of *Burkholderia cepacia* complex bacteria in cystic fibrosis lungs and interactions with *Pseudomonas aeruginosa* in hypoxic mucus., Infect. Immun. 82 (2014) 4729–45. doi:10.1128/IAI.01876-14.

[220] D.G. D. Mayrand, Biological activities of outer membrane vesicles, Can. J. Microbiol. 6 (1989) 607–13. doi:10.1139/m89-097.

[221] N.D. Allan, C. Kooi, P.A. Sokol, T.J. Beveridge, Putative virulence factors are released in association with membrane vesicles from *Burkholderia cepacia*, Can. J. Microbiol. 49 (2003) 613–624. doi:10.1139/w03-078.

[222] B. Lindmark, P.K. Rompikuntal, K. Vaitkevicius, T. Song, Y. Mizunoe, B.E. Uhlin, P. Guerry, S.N. Wai, Outer membrane vesicle-mediated release of cytolethal distending toxin (CDT) from *Campylobacter jejuni*, BMC Microbiol. 9 (2009) 1–10. doi:10.1186/1471-2180-9-220.

[223] K. Koeppen, T.H. Hampton, M. Jarek, M. Scharfe, S.A. Gerber, D.W. Mielcarz, E.G. Demers, E.L. Dolben, J.H. Hammond, D.A. Hogan, B.A. Stanton, A Novel Mechanism of Host-Pathogen Interaction through sRNA in Bacterial Outer Membrane Vesicles, PLoS Pathog. 12 (2016) 1–22. doi:10.1371/journal.ppat.1005672.

[224] S.K. Vanaja, A.J. Russo, B. Behl, I. Banerjee, M. Yankova, S.D. Deshmukh, V.A.K. Rathinam, Bacterial Outer Membrane Vesicles Mediate Cytosolic Localization of LPS and Caspase-11 Activation, Cell. 165 (2016) 1106–1119. doi:10.1016/j.cell.2016.04.015.

[225] S. Webb, J. S.; Thompson, L. S.; James, S.; Charlton, T.; Tolker- Nielsen, T.; Koch, B.; Givskov, M.; Kjelleberg, Cell death in Pseudomonas aeruginosa biofilm development, Society. 185 (2003) 4585–4592. doi:10.1128/JB.185.15.4585.

[226] Y. Jiao, P. D'haeseleer, B.D. Dill, M. Shah, N.C. VerBerkmoes, R.L. Hettich, J.F. Banfield, M.P. Thelen, Identification of biofilm matrix-associated proteins from an acid mine drainage microbial community, Appl. Environ. Microbiol. 77 (2011) 5230–5237. doi:10.1128/AEM.03005-10.

[227] T.K. Gallaher, S. Wu, P. Webster, R. Aguilera, Identification of biofilm proteins in non-typeable *Haemophilus influenzae*, BMC Microbiol. 6 (2006) 1–9. doi:10.1186/1471-2180-6-65.

[228] P.D. Curtis, J. Atwood, R. Orlando, L.J. Shimkets, Proteins associated with the *Myxococcus xanthus* extracellular matrix, J. Bacteriol. 189 (2007) 7634–7642. doi:10.1128/JB.01007-07.

[229] K.E. Eboigbodin, C.A. Biggs, Characterization of the extracellular polymeric substances produced by *Escherichia coli* using infrared spectroscopic, proteomic, and aggregation studies, Biomacromolecules. 9 (2008) 686–695. doi:10.1021/bm701043c.

[230] C. Park, J.T. Novak, R.F. Helm, Y.O. Ahn, A. Esen, Evaluation of the extracellular proteins in full-scale activated sludges, Water Res. 42 (2008) 3879–3889. doi:10.1016/j.watres.2008.05.014.

[231] S.R. Schooling, T.J. Beveridge, Membrane vesicles: An overlooked component of the matrices of biofilms, J. Bacteriol. 188 (2006) 5945–5957. doi:10.1128/JB.00257-06.

[232] G.Y. Lee EY, Bang JY, Park GW, Choi DS, Kang JS, Kim HJ, Park KS, Lee JO, Kim YK, Kwon KH, Kim KP, Global proteomic profiling of native outer membrane vesicles derived from *Escherichia coli*, Proteomics. 7 (2007) 3143–53.

[233] S.R. Schooling, A. Hubley, T.J. Beveridge, Interactions of DNA with Biofilm-Derived Membrane Vesicles, J. Bacteriol. 191 (2009) 4097–4102. doi:10.1128/JB.00717-08.

[234] N. Srinivas, P. Jetter, B.J. Ueberbacher, M. Werneburg, K. Zerbe, J. Steinmann, B. Van Der Meijden, F. Bernardini, A. Lederer, R.L.A. Dias, P.E. Misson, H. Henze, J. Zumbrunn, F.O. Gombert, D. Obrecht, P. Hunziker, S. Schauer, U. Ziegler, A. Käch, L. Eberl, K. Riedel, S.J. Demarco, J.A. Robinson, Peptidomimetic antibiotics target outer-membrane biogenesis in *Pseudomonas aeruginosa*, Science (80-.). 327 (2010) 1010–1013. doi:10.1126/science.1182749.

[235] D.S. Choi, D.K. Kim, S.J. Choi, J. Lee, J.P. Choi, S. Rho, S.H. Park, Y.K. Kim, D. Hwang, Y.S. Gho, Proteomic analysis of outer membrane vesicles derived from *Pseudomonas aeruginosa,* Proteomics. 11 (2011) 3424–3429. doi:10.1002/pmic.201000212.

[236] M. Toyofuku, B. Roschitzki, K. Riedel, L. Eberl, Identification of Proteins Associated with the *Pseudomonas aeruginosa* Biofilm Extracellular Matrix, J. Proteome Res. 11 (2012) 4906–4915. doi:10.1021/pr300395j.

[237] M.A. Riley, D.M. Gordon, The ecological role of bacteriocins in bacterial competition, Trends Microbiol. 7 (1999) 129–133. doi:10.1016/S0966-842X(99)01459-6.

[238] S. Bakkal, S.M. Robinson, C.L. Ordonez, D.A. Waltz, M.A. Riley, Role of bacteriocins in mediating interactions of bacterial isolates taken from cystic fibrosis patients, Microbiology. 156 (2010) 2058–2067. doi:10.1099/mic.0.036848-0.

[239] D.J. Hassett, S. Cohen, N. Carolina, Bacterial adaptation to oxidative stress : and cells implications interaction for pathogenesis with phagocytic, FASEB J. 3 (1989) 2574–2582. http://www.ncbi.nlm.nih.gov/pubmed/2556311.

[240] C.J. Jeffery, Moonlighting proteins: Old proteins learning new tricks, Trends Genet. 19 (2003) 415–417. doi:10.1016/S0168-9525(03)00167-7.

[241] A. Kunert, J. Losse, C. Gruszin, M. Huhn, K. Kaendler, S. Mikkat, D. Volke, R. Hoffmann, T.S. Jokiranta, H. Seeberger, U. Moellmann, J. Hellwage, P.F. Zipfel, Immune Evasion of the Human Pathogen *Pseudomonas aeruginosa*: Elongation Factor Tuf Is a Factor H and Plasminogen Binding Protein, J. Immunol. 179 (2007) 2979–2988. doi:10.4049/jimmunol.179.5.2979.

[242] D. Granato, G.E. Bergonzelli, R.D. Pridmore, L. Marvin, M. Rouvet, Cell Surface-Associated Elongation Factor Tu Mediates the Attachment of, Society. 72 (2004) 2160–2169. doi:10.1128/IAI.72.4.2160.

[243] G.E. Bergonzelli, D. Granato, R.D. Pridmore, L.F. Marvin-Guy, D. Donnicola, I.E. Corthésy-Theulaz, GroEL of Lactobacillus johnsonii La1 (NCC 533) is cell surface associated: Potential role in interactions with the host and the gastric pathogen *Helicobacter pylori,* Infect. Immun. 74 (2006) 425–434. doi:10.1128/IAI.74.1.425-434.2006.

[244] M. Allesen-Holm, K.B. Barken, L. Yang, M. Klausen, J.S. Webb, S. Kjelleberg, S. Molin, M. Givskov, T. Tolker-Nielsen, A characterization of DNA release in *Pseudomonas aeruginosa* cultures and biofilms, Mol. Microbiol. 59 (2006) 1114–1128. doi:10.1111/j.1365-2958.2005.05008.x.

[245] S.C. Dillon, C.J. Dorman, Bacterial nucleoid-associated proteins, nucleoid structure and gene expression, Nat. Rev. Microbiol. 8 (2010) 185–195. doi:10.1038/nrmicro2261.

[246] T. Meyer, T. Schirrmann, A. Frenzel, S. Miethe, J. Stratmann-Selke, G.F. Gerlach, K. Strutzberg-Minder, S. Dübel, M. Hust, Identification of immunogenic proteins and generation of antibodies against *Salmonella Typhimurium* using phage display., BMC Biotechnol. 12 (2012) 29. doi:10.1186/1472-6750-12-29.

[247] P. Jha, X. Wang, J. Auwerx, Analysis of Mitochondrial Respiratory Chain Supercomplexes Using Blue Native Polyacrylamide Gel Electrophoresis (BN-PAGE), in: Curr. Protoc. Mouse Biol., John Wiley & Sons, Inc., Hoboken, NJ, USA, 2016: pp. 1–14. doi:10.1002/9780470942390.mo150182.

[248] T. Christensen, E.J. Toone, Calorimetric Evaluation of Protein–Carbohydrate Affinities, in: 2003: pp. 486–504. doi:10.1016/S0076-6879(03)01032-2.

[249] J. Pohleven, B. Trukelj, J. Kos, Affinity Chromatography of Lectins, in: Affin. Chromatogr., InTech, 2012. doi:10.5772/36578.

[250] A.-C. Gingras, M. Gstaiger, B. Raught, R. Aebersold, Analysis of protein complexes using mass spectrometry, Nat. Rev. Mol. Cell Biol. 8 (2007) 645–654. doi:10.1038/nrm2208.

[251] K.A. Rashid, S. Hevi, Y. Chen, F. Le Cahérec, S.L. Chuck, A Proteomic Approach Identifies Proteins in Hepatocytes That Bind Nascent Apolipoprotein B, J. Biol. Chem. 277 (2002) 22010–22017. doi:10.1074/jbc.M112448200.

[252] C. Pifferi, D. Goyard, E. Gillon, A. Imberty, O. Renaudet, Synthesis of Mannosylated Glycodendrimers and Evaluation against BC2L-A Lectin from *Burkholderia Cenocepacia*, Chempluschem. 82 (2017) 390–398. doi:10.1002/cplu.201600569.

[253] S. Munro, Essentials of Glycobiology, Trends Cell Biol. 10 (2000) 552–553. doi:10.1016/S0962-8924(00)01855-9.

Acknowledgments

It would not have been possible to reach the goals of this research project and write the relative thesis without the work, the help, the kindness and experience of many people. The Ph.D. project has been funded by the University of Trieste.

Firstly, I am very grateful to my supervisor Dr. Paola Cescutti who heads, with Professor Roberto Rizzo, the Bacterial Polysaccharides group at the University of Trieste. I thank her for the careful guide, the help when I was stuck and proofreading all the abstracts, reports and the Ph.D. thesis. I want to thank also for sharing her research experience and to have always come up with clever solutions: I have been very lucky to work within this research group.

I am also extremely grateful to Professor Roberto Rizzo who have supervised me (not officially) and shared with me his huge research experience. He has always been willing to discuss about the project, thus widening my knowledge about topics I was not familiar with before starting my Ph.D. It has always been a pleasure for me to listen to him. I have really appreciated his availability, even though he retired from his job last year.

I am grateful to Professor Daniele Sblattero (Dept. of Life Sciences, University of Trieste). The project is the result of a partnership with his research group. He has always willing to discuss about the project, providing me with solutions to get out of research problems that arose. He has kindly proofread my annual reports and let the door of his laboratories always open. For this purpose, I want to thank all the people of his research group, especially Dr. Serena Rizzo, Dr. Marco Dal Ferro and Dr. Imma Luisi, who have been fundamental for performing SDS-PAGE and Western Blotting analysis, but also for phage display and ELISA assays. I have really appreciated the time they have dedicated to me.

I also thank Dr. Maria Felicia Soluri who performed phage display experiments during my visit at the University of Eastern Piedmont (Novara, Italy).

I am very grateful to Dr. Francesca Micoli from Gsk Vaccine Institute for Global Health whose help has been crucial to find a way to immobilize the exopolysaccharide on solid support and go on with the project.

I thank Dr. Domenico Garozzo and his group (IPCB, CNR Catania) for having performed MALDI-TOF analyses of the glycoconjugate.

I am very thankful to my external advisor Professor Neil Ravenscroft (Cape Town University, South Africa) who have read my annual reports and provided me with clever

suggestions and comments. I want also to thank Professor Tim Tolker-Nielsen (University of Copenhagen, Denmark) for kindly accepting to read this thesis.

I thank Professor Jesus Angulo and his research group (University of East Anglia, UK) who performed STD NMR analyses. I am also grateful to him as he gave me the opportunity to show the very interesting results he obtained.

I am extremely grateful to Professor Riccardo Sgarra (Dept. of Life Sciences, University of Trieste) who performed mass spectrometry analysis. A special thank goes to Dr. Sara Petrosino, Dr. Carlotta Penzo, Dr. Giovanna Gentile and Enrico Pobega (Sgarra's research group) who performed this great and laborious work.

I am grateful also to Professor Alex Tossi and Dr. Milena Guida for Surface Plasmon Resonance experiments. I am extremely grateful to Professor Cristina Lagatolla (Dept. of Life Sciences, University of Trieste) for her kind support with confocal laser scan microscopy. I thank Dr. Paolo Bertoncin who kindly performed transmission electron microscopy analysis.

I am also grateful to Dr. Zois Syrgiannis and Dr. Susanna Bosi (Dept. of Chemical and Pharmaceutical Sciences, University of Trieste) who have performed atomic force microscopy analysis.

I am very grateful to my colleague Dr.. Barbara Bellich who has been an example for me during these years with her professionality and care.

I am extremely grateful to all the people I have spent these three years with on the second floor of the C11 building. They have been kind, supportive and always willing to cheer me up and provide me with any sort of reagent, material and stuff I needed. I am talking about Professor Antonella Bandiera, Professor Federica Tramer, Dr. Odeta Kalaja, Dr. Rita De Zorzi, Dr. Laura De Stefanis, Dr. Barbara Medagli and PhD students Irene Marcovich and Caterina Deganutti. A special thank goes to Dr. Sabrina Semeraro who has always been there to get me out of my research problems during these three years.

I am also grateful to Dr. Gianluigi De Benedetto and all the people who joined our research group during the last years, particularly Jelena Loncar, Katarina Zoric and Tina Vidulin.

I'd like to thank Dr. Valentina Buemi and Dr. Bascetta Lorenzo for helping me with the thesis's proofreading and for the valuable support.

Of course, I am very grateful to my parents and my friends who have been very supportive for all these years.